Rhodes University

The creation and validation of aptamers binding to murine 3T3-L1 Preadipocytes: preliminary implications for controlled cellular attachment, differentiation and cell fate

Submitted in fulfilment of the degree Master of Science in Biotechnology

Mark Lourens Rubidge

April 2017

Supervisor: Dr Ronen Fogel

Co-Supervisor: Prof Janice Limson

RHODES UNIVERSITY
Where leaders learn

BioSENs
Research Group
Sensors ▪ Energy ▪ Nanomaterials

Abstract

The controlled seeding of a variety of stem cells *in vitro* has been reported to alter the patterns of their subsequent differentiation. This has been attributed to the control of the surface microenvironment onto which adherent stem cells are cultured, especially control of the proximal density of neighbouring cells. Simultaneously, advances in the generation of aptamers - synthetic ligand molecules developed using *in vitro* selection techniques targeting complex molecules - have aided in the production of molecules capable of selectively binding to a variety of commercial stem cell lines.

Combining the aforementioned research fields, the project reported in this thesis aimed to generate DNA-based aptamers capable of assisting with the selective binding of murine 3T3-L1 preadipocytes to a solid surface. This was performed with a view to, eventually, control the seeding densities of the adherent preadipocytes on the surface of the tissue culture dish in subsequent researchers. In the process of meeting this goal, several optimisations of the *in vitro* process by which aptamers binding to cells are generated (Cell-SELEX) were performed: an analysis into a variety of methods used for the removal of the single stranded aptamer candidate sequences attached to the surface of 3T3-L1 preadipocytes, a comparison of methods for the generation of single-stranded aptamer sequences from double-stranded DNA template molecules and a method for quantifying the removed ssDNA from the cell surface. Their use is further reported in this work.

Initially, it was determined that a fluorimetric evaluation of the unbound single stranded DNA was the optimum technique to use to evaluate the relative amounts of aptamer DNA binding to target cells during cell-SELEX; this arose from the release of DNA, and other cell lysate contaminates, which interfered UV/ Vis quantification. The evaluation into different methods of ssDNA removal from the cell surface showed that although trypsinisation of the cells demonstrated the highest level of aptamer detachment (quantified by fluorimetry), there is a decrease the number of potential targets that aptamers could attach to. The most common method for detaching bound DNA aptamer molecules from cellular targets reported in literature, the use of high temperatures, was selected for cell-SELEX to increase the variability in potential target sites on the cell surface.

Using techniques optimised in this work, fluorescently-tagged single-stranded oligonucleotide aptamers were later generated with a positive selection pressure to bind to the surface of the 3T3-L1 preadipocytes, but not to their differentiated adipocyte counterparts. After eight cycles of cell-SELEX, fluorescent spectroscopic analysis depicted a 74 % binding retention of the selection pool in the positive preadipocyte selection pool, as opposed to a 0.69 % binding of sequences to the negative differentiated preadipocytes. Following the isolation and identification of candidate sequences, seven separate sequences were identified as being successfully generated from the selection process. Bioinformatic characterisation of these placed sequenced aptamer candidates into two separate families, that were then analysed in opposition to each for their binding affinity toward each other.

Using fluorescently-tagged sequences, the binding selectivity of the generated aptamers was validated using both epifluorescent microscopy and confocal microscopy. At this stage, an aptamer sequence selected from prior in-house research to serve as a negative control also demonstrated significant binding to the extracellular matrix of both preadipocytes and mature adipocytes. 5'-thiolated aptamer sequences were used to form self-assembled monolayers on the electrode surfaces of the impedimetric Roche xCELLigence Real-Time Cell Analysis. The use of aptamer sequences to capture the seeded preadipocytes, demonstrated a slight increase in the extent of binding of the preadipocytes to the gold electrode surface and produced some preliminary indications of alterations to the pattern and rate of subsequent differentiation in the preadipocytes.

This provides preliminary evidence that aptamers developed to bind specifically to a stem cell line *in vitro* show potential to be used as to capture said cell when cast in a self-assembled monolayer assembly. This provides a future opportunity to control the seeding densities of the cells *in vitro*. The effects of cellular differentiation at a set of predefined cellular densities can be demonstrated on a desired stem cell line.

Acknowledgements

- I would like to give my deepest gratitude to my supervisor Dr Ronen Fogel for his constant support, enthusiasm and tireless patience over the duration of the project.

- I would also like to thank my co-supervisor Prof Janice Limson for her support and input into the project.

- Dr Earl Prinsloo and his research group, in particular I would like to thank Rose Kadye, Pascaline Houseman, and John Honiball for their guidance and expertise in the tissue culture facility.

- I would like to thank all the postgraduate researchers from the Rhodes University Biotechnology Innovation Centre for their input and support into the project, specifically Lance Ho, Tamika Fellows, Shane Flanagan, and the students of the BioSENs research group for their advice into the project.

- I would like to thank the NRF (Sarchi) for providing funding for tuition and living costs for financial support and sponsorship over the duration of the project.

- I would also like to thank Dr Meesbah Jiwaji for her assistance with use of the confocal microscope.

Table of Contents

List of Abbreviations

6-FAM	6-Carboxyfluorescein
ΔG	change in Gibbs free energy
ADD1-SREBP	Adipocyte Determination-Differentiation Factor 1
AMP	Ampicillin
C/EBPδ	CCAAT-Enhancer-Binding Protein
Cell Index	CI
CREB	cAMP response element-binding protein
Cy5	Cyanine-5
DAPI	4',6-diamidino-2-phenylindole
DCI	Delta Cell Index
DEX	Dexamethasone
DPBS	Dulbecco's Phosphate Buffered Saline
DMEM	Dulbecco's Modified Eagle Medium
DMSO	Dimethyl sulfoxide
dsDNA	double-stranded Deoxyribonucleic acid molecules
FACS	Fluorescence-Activated Cell Sorting
ECM	Extracellular Matrix
EDTA	Ethylenediaminetetraacetic
FCS	Foetal Calf Serum
FCS-DMEM	DMEM nutrient media supplemented with foetal calf serum
ESC	Embryonic Stem Cell
FITC	Fluorescein isothiocyanate
HSC	Hematopoietic Stem Cells
IBMX	3-isobutyl-1-methylxanthine
INS	Insulin
IVF	*in vitro* Fertilization
IPTG	Isopropyl β-D-1-thiogalactopyranoside
PCR	Polymerase Chain Reaction
PLL	poly-L-lysine
NCI	Normalised Cell Index
PBS	Phosphate Buffered Saline
PEPCK	Phosphoenolpyruvate carboxykinase
PGC1α	PPARγ co-activator-1α

PAGE	Polyacrylamide Gel Electrophoresis
PPARγ2	Peroxisome Proliferator Activated Receptor gamma 2
MAFFT	Multiple Alignment using Fast Fourier Transform
MRI	Magnetic Resonance Imaging
MSC	Mesenchymal Stem Cell
MUSCLE	Multiple Sequence Comparison by Log Expectation
MSA	Multiple Sequence Alignment
QCM-D	Quartz crystal microbalance with dissipation monitoring
RFU	Relative Fluorescent Units
RT-CES	Real Time Cell Analyser System
ROSI	Rosiglitazone
SAM	Self-Assembled Monolayer
SC	Stem Cells
ssDNA	single-stranded Deoxyribonucleic Acid
SELEX	Systematic Evolution of ligands by Exponential Enrichment
TAE	Tris-acetate-EDTA
T-Coffee	Tree-based Consistency Objective Function for Alignment Evaluation
T_m	DNA melting temperature
TE	tris-EDTA
X-GAL	5-bromo-4-chloro-3-indolyl-β-D-galactopyranoside

List of Figures

List of Tables

List of Equations

Chapter 1 : Introduction and Literature Review

1.1. Stem cells within the public space

Stem Cells (SC) were first discovered and described in the 1960's (Ehnert *et al.*, 2009). As such, they have attracted great interest, both in fundamental and applied research, for the regenerative properties these cells possess. Research into these types of cells continue despite the controversy, and ongoing discussion, regarding the ethical implication of studying these cells, particularly the embryonic stem cells, or ESCs (de Wert and Mummery, 2003; Robertson, 2010). This is further exacerbated by the fact that a number of SC research companies and clinics have taken advantage of a gap in knowledge (between scientists and the public) of SC research, and are selling treatments that have not passed clinical trials (Master and Resnik, 2011).

While SC-based treatments have promise as potential treatments in the future, there are a few challenges that need to be overcome before these SC treatments can become commercially viable. These include: the complex nature of SC differentiation, the ethical restrictions to SC research and low variability in the donor demographics available for *in vitro* SC research.

1.1.1. Donor demographics for SC research and technology development

The possibility of using SCs for the biomedical treatment of autoimmune and neurodegenerative diseases is rapidly becoming a more realistic possibility (Li and Ikehara, 2013). This is hampered by the low availability of ethnic- and demographically-diverse cell lines (Greene, 2006). A wide variety of donor cell lines is crucial to generate SC research - and any subsequent applications - that are generalizable across the entire human population. Primarily, SC donations are obtained from middle-aged, white, male donors (Greene, 2006; Laurent *et al.*, 2010).

In a demographically diverse country such as South Africa where the population is represented by 79.2 % African, 8.9 % Coloured, 8.9 % White, 2.5 % Indian/ Asian and 0.5 % Other (Statistics SA, 2012), there is a clear lack in the demographic diversity of tissues available for research purposes. This phenomenon is not only restricted to South Africa, but exists throughout the world (Greene, 2006).

SC treatments and research is dependent on the donation of viable cells from the population. The lack in demographic diversity in SC research has limited the amount of allele variability and phenotypic differences of SC in the population of researchable cell lines, limiting knowledge in SC variability studies (Laurent *et al.*, 2010). There are two methods currently in practice to harvest donated SCs from adults: bone marrow surgery, or dialysis of the stem cells from the peripheral blood system (Copelan, 2006), both performed in order to obtain haematopoietic stem cells. Bone marrow donation is an intrusive surgical procedure (Copelan, 2006; Billen *et al.*, 2014), normally requiring between one to two weeks' recovery by the donor. The donation of SCs from the peripheral blood is vastly less intrusive to that of bone marrow donation (Copelan, 2006), as the SC are separated through dialysis of the blood. Improved methods of rapidly identifying and separating SCs from other blood constituents would further increase the efficiency of this method of gathering SCs for research purposes.

1.1.3. Misunderstandings in SC and the ethics in SC research

The general ethical consensus of stem cell research amongst the public is the belief that ESC is the major source of SC for experimentation purposes (Daar *et al.*, 2004). For ESC research to take place, a viable developing embryo is needed (Daar *et al.*, 2004), this involves the eventual disposal of the developing embryonic cells. ESC have totipotent capabilities that allow for the cells to differentiate into all cell types allow for their ability to grow and differentiate into any tissue type (Dhai *et al.*, 2004).

The complex legal issues for the use of ESC for *in vitro* and *in vivo* research varies depending on the legislation of the country (Dhai *et al.*, 2004). Many countries prohibit the practise of ESC research, for the ethical reasons of disposing of a viable embryo (Dhai *et al.*, 2004), unless ethics clearance is granted for the research to take place. During *in vitro* fertilization (IVF) procedures, there are often blastocysts, made of ESC, that are not used during IVF. In many countries, permissions may be given to use these for ESC research (Carson *et al.*, 2010).

Legally speaking in South Africa (in accordance with national health act 61 of 2003, as amended by National Health Amendment Act 12 of 2013), the cloning of gametes and research on human embryos younger than 14 days, ethics may be approved by the minister of health, and by prior permissions by the donor. These cell lines need to harvested before fourteen days, following fertilisation of the zygote (de Wert and Mummery, 2003), during the

early stages in embryonic development. At this stage of development, the primitive streak begins to form on the embryo signalling the initial stages of the embryonic spinal column. (Dhai *et al.*, 2004).

Less-publicised than ESCs is the use of other sources of human stem cells found in adult tissues, which have a more limited differentiation capabilities (Pittenger *et al.*, 1999; Ding *et al.*, 2015). A prominent example of these SCs in literature are mesenchymal stem cells (MSCs). Unlike ESC, these cells only have the capacity to differentiate into certain mesodermal cell types (Pittenger *et al.*, 1999; Ding *et al.*, 2015) and are less invasive to harvest from adults than their haematopoietic counterparts (Copelan, 2006).

Due to the less-invasive methods of separating MSCs from the donor tissues, MSCs lines are ideal for regenerative research purposes. These MSC cell lines have become popular for initial *in vitro* analysis into cellular differentiation and drug development. No additional ethical clearance is required beyond the initial donor approval for the harvesting of MSC cell lines.

1.1.4. Misleading claims by companies

Increasingly, people are seeking an alternative, permanent, cure to a variety of diseases that include Alzheimer's disease, autism, and several other neurodegenerative and autoimmune-related disorders. At the current level of medical advances, most treatments for these conditions remain symptomatic, rather than curative. The treatment of many of these autoimmune diseases using SC regenerative practices is prohibited in a number of countries, owing to the potential hazards to the patient (Master and Resnik, 2011). A variety of stem cell companies - largely based in South Africa, United States of America, Russia, and China - advertise, largely online, SC-based treatments for such autoimmune disorders (DeFrancesco, 2012; Meissner-Roloff and Pepper, 2013). These treatments often have little peer-reviewed literature and clinical trials substantiating their medical claims (Lindvall and Hyun, 2009). This has allowed for what is colloquially referred to as “stem cell tourism”, where people travel abroad to receive these treatments, to other countries that offer the surgery, to receive SC treatments that are otherwise prohibited in their home countries (Master and Resnik, 2011; Meissner-Roloff and Pepper, 2013).

While there is little peer-reviewed research investigating SC tourism, it has been noted to be on the rise (Lindvall and Hyun, 2009). A particular study carried out in Australia by McLean *et al.* (2015), evaluated a number of clinics that were practising SC treatments that had not passed clinical trials. These medical practises include SC treatments for osteoarthritis, musculoskeletal pain, autism, and the treatment of a variety of neurodegenerative disorders. The costs of the treatments were reported to range between $9,000 and $70,000 (McLean *et al.*, 2015).

These treatments give hope to desperate patients, although there have been recorded short comings and potentially could cause further damage to the patient (Lindvall and Hyun, 2009). In such a case reviewed by (Amariglio *et al.*, 2009) where a child with ataxia telangiectasia, a neurodegenerative disability (Barlow *et al.*, 1996), the patient later developed a multifocal brain tumour after being treated with foetal neural stem cells.

1.1.5. Stem cell treatments that have passed clinical trials

There are on the other hand a number SC treatments, such as hematopoietic (bone marrow), transplants that have passed clinical trials and presently are practised for the treatment of leukaemia and other anaemia-related disorders (McLean *et al.*, 2015).

SC research, in particular ESC and the use of SCs for biomedical applications, have many barriers that need to be overcome before they can be used on a research and application platform. These barriers include ethical constraints and public understanding of current stem cell technologies.

SC regenerative technology holds a promising future use in the treatment of autoimmune disorders, as an alternative to the use of chronic medications to supress the side effects of the diseases. There are many challenges that need to be addressed before the SC treatments can be implicated into *in vivo* practices. For such treatments to pass clinical trials, much research is still required on SC lines. For these challenges to be overcome, the public needs to stay informed with progress in SC research, both to advance knowledge in SC treatments through donations by the public, and to educate the public to the potential hazards that come with untested technologies.

1.2. Stem cell biology

SCs are a series of non-specialized cells within both embryonic and adult tissues that functionally are able to self-renew and differentiate into other cell types (Baharvand *et al.*, 2007; Chamberlain *et al.*, 2007). SCs are crucial components in the development, maintenance and regulation of tissues in the organism (da Silva Meirelles *et al.*, 2006), and are central to tissue regeneration and wound-healing processes (Chamberlain *et al.*, 2007). In the adult body, SCs encompass a community of unspecialized cells that assist with the maintenance, development and growth of specialized tissues within multicellular organisms (Wei *et al.*, 2000). The induction and control of differentiation of SCs, as a means to effectively propagate and differentiate the SC both *in vitro* and later *in vivo* (Wong, 2011) is an ongoing focus of research in this field.

SCs are generally categorized as being either totipotent (able to differentiate into all cell types), multipotent (possessing limited differentiative capabilities), or unipotent (able to differentiate into a single cell type) (Jaenisch and Young, 2008), depending on the origin of the SC (McBeath *et al.*, 2004). The major sources of SCs that have been described *in vivo* include: ESCs, MSCs (Fuchs *et al.*, 2004), Hematopoietic stem cells (HSC) (Baharvand *et al.*, 2007).

ESCs are the derivatives of the blastula of developing embryos. These cells are totipotent in nature, and are able to divide and make up the cellular tissues that develop into the three germ layers of the adult (Marshak *et al.*, 2001). MSCs are a multipotent cell type, *in vivo* they largely execute a maintenance and regenerative role of damaged tissues of tissues derived from the mesodermal germ layer of the adult (Pittenger *et al.*, 1999). MSCs are generally described as being able to only replenish a range of specific somatic cell lines, which includes: adipocytes, chondrocytes, osteoblasts, neural tissues and myocytes (Guo *et al.*, 2007).

As such, MSCs can be found in association with a number of tissues including: adipocytes, blood tissues, spleen and a variety of other organs in multicellular organisms (Zuk *et al.*, 2002; Gomillion and Burg, 2006; Baer *et al.*, 2012).

1.2.1. Induction of differentiation in vitro for stem cell research

It has been well documented that a variety of conditions need to be met for SCs to successfully differentiate into the desired cell type (McBeath *et al.*, 2004). *In vitro* tissue engineering using SC derivatives have been prioritized in medical regenerative technology, to better understand and control the regenerative limitations of SC regeneration for both *in vivo* and *in vitro* contexts (Eberli and Atala, 2006). Studies conducted on cultured cell monolayers are the initial steps in therapeutic research; at this stage, researchers are able to control specific environmental conditions to the cultured cell monolayer. This gives an initial idea into cellular responses to changes in the culturing conditions.

In their native environment, SCs have been known to interact with a number of different elements within their surrounding extracellular matrix (ECM) including chemical, and topographical environment (at the micro- and nanoscale, such as the presence of grooves and ridges in the immediate environment), and cell-to-cell contact (Gregoire *et al.*, 1998; Kolind *et al.*, 2012). For SC differentiation to occur, a wide variety of hormones, growth factors and other signal molecules are required in the extracellular environment; in research these are frequently included in nutrient media for the *in vitro* induction of cellular differentiation during cell culture. These mixtures have been extensively studied and vary depending on the desired pathway of cellular differentiation by promoting specific signal transduction pathways in the desired cell lines (James, 2013).

Table 1.1 below details a variety of inducers commonly reported to be included in cell culture media to initiate the differentiation of MSCs *in vitro*, along with the assays employed to confirm that successful differentiation.

Table 1.1: Induction and validating tests for controlling MSC differentiation reported in the literature

Differentiation pathway	Inducer(s)	Biomarkers of differentiation	Confirmation of differentiation	Supporting Reference(s)
Adipogenic	Insulin Dexamethasone 3-isobutyl-1-methyl-xanthine Rosiglitazone Xanthine Indomethacin	lipoprotein lipase fatty acid binding protein lipase	Lipid vacuole production via Oil Red O or Nile Red fluorescence (microscopy/ fluorescence)	(Fowler and Greenspan, 1985; Ramírez-Zacarías *et al.*, 1992; Conget, 1999; Kramer *et al.*, 2014)
Osteoblast	β- glycerophosphate Dexamethasone Ascorbic acid	Alkaline phosphatase Calcium accumulation	Formation of calcium-rich aggregates/nodules (xylenol orange or calcein blue staining, microscopy)	(Conget, 1999; Chamberlain *et al.*, 2007; Wang *et al.*, 2008)
Chondrocyte	Transforming growth factor – β	Variety of glycosaminoglycans Type II collagen	Cartilage production via Toluidine blue (microscopy)	(Mackay *et al.*, 1998)
Myoblast	5-azacydine		Rhythmically beating myotube formation (microscopy)	Xu *et al.*, 2004; Chamberlain *et al.*, 2007
Neural-like cells	β – Mercaptoethanol Dimethylsulfoxide Butylated hydroxyanisole	Morphological change in the cells to dendritic like cells.	Typical mature neuron morphology formation (microscopy)	Woodbury *et al.*, 2000; Chamberlain *et al.*, 2007

Although there has been much research in the control of differentiation of SCs to different cellular types through the introduction of inducing compounds to *in vitro* culture media, there is limited understanding in the role of the density of neighbouring cells surrounding an SC to commit it to a specific cellular fate. Very little is known with regards to the optimal densities of MSCs are for the effective differentiation of the cells to adopt a specialized cellular fate (McBeath *et al.*, 2004). Additionally, recent research has shown that control of the adhesion of cells to the culturing substrate can control the differentiation properties of the SC (Curran *et al.*, 2006; Phillips *et al.*, 2010).

1.2.2. Cellular density and surface engineering research for *in vitro* SC growth and differentiation

Changing the topography of the substrate surfaces on which cells are conventionally cultured have shown that there are resultant morphological changes to the cell surface membrane, affecting the subsequent differentiation fate of the cells (Kolind *et al.*, 2012). Furthermore, alterations of the cellular seeding densities and the seeding patterns of SC have also been found to play an important role in the differentiation of SCs (Tang *et al.*, 2010; Peng *et al.*, 2011). This finding was further confirmed by McBeath *et al.* (2004), where patterning differences on the surface of poly-dimethylsiloxane stamps were used to determine differentiation fate of human MSCs at a variety of densities: more densely packed cells demonstrated preference toward adipogenic differentiation on the micro-patterned surface, while osteogenic differentiation was described with less dense packing of the MSCs (McBeath *et al.*, 2004).

Most of the density-controlled assays have been evaluated on micro-patterned surfaces such as poly-dimethylsiloxane stamps (McBeath *et al.*, 2004; Kolind *et al.*, 2012) or poly(ethylene glycol) hydrogel matrices (Tang *et al.*, 2010; Peng *et al.*, 2011), to control the binding of the cells to specific regions of the micro-patterned surfaces.

SCs traditionally have been isolated through their ability to adhere to plastic surfaces without the assistance of additional surface coatings. In mammalian cell culture, these surface coatings include: poly-L-lysine (PLL) (Mazia *et al.*, 1975), fibronectin, laminin and collagen, to assist adhering cells onto surfaces (Villa-Diaz *et al.*, 2013). Due to the nonspecific nature of these coatings, these methods provide limited control of the lateral density of attached cells and overall organisation of the cell culture (Wink *et al.*, 1997). Furthermore, the cells have a

slight change in their natural morphology once bound to these binding molecules: for example the use of PLL is reported to result in flattened cells once attached (Wink *et al.*, 1997).

To improve adhesion and propagation control of attached cells, the use of highly-organised self-assembled monolayers (SAM) between the growth substrate and the cells have been proposed and investigated (Wink *et al.*, 1997; Phillips *et al.*, 2010). The formation of a SAM assists in the controlled ordering and binding of a target ligand to the surface (Wink *et al.*, 1997). Thiol-based SAM layers, in particular, have been researched for their ability to assist with the binding of cells *in vitro* to a variety of metallic (i.e. gold) surfaces (Wink *et al.*, 1997).

1.3. Biosensors and biorecognition

Biosensor technologies make use of a wide variety of sensitive transducing devices that may be to analyte-specific ligands (Thévenot *et al.*, 2001; Castillo *et al.*, 2004). Upon the formation of a ligand-analyte complex, a measurable result is emitted as either a qualitative or quantitative outcome. This result may be conveyed either as a fluorescent, colorimetric, or electrochemical feedback response, depending on the nature of the transducing device being used (Thévenot *et al.*, 2001).

Of the more recent preferred ligands used and commercialised in biosensors (Song *et al.*, 2012), immune-derived ligands, typically antibodies, feature prominently. Monoclonal antibodies show reasonably high specificity toward their target analyte and are used for their reliable binding to the analyte surface (Mascini *et al.*, 2012; Zeng *et al.*, 2012) for biosensing purposes.

Recently, the discovery and use of selectable single-stranded oligonucleotide and oligopeptide sequences capable of specific binding to desired targets (Mascini *et al.*, 2012) - otherwise known as aptamers - have become a more popular focus and choice of ligand, rivalling monoclonal antibodies (Brody and Gold, 2000; Chen and Yang, 2015). Similar to proteins' binding mechanisms, the three-dimensional conformation that these molecules adopt, permits aptamers to bind to the target molecule (Mascini *et al.*, 2012), discussed in further detail below in Section 1.3.1. Aptamers have been generated with target recognition capabilities with high selectivity and specificity (Tan *et al.*, 2011). Furthermore, oligonucleotide aptamers may easily be modified with reporting agents on either the 5' or 3'

ends of the nucleic acid sequence, with minimal to no effect on the tertiary structure of the aptamer and the binding affinity of the aptamer / analyte complex (Tabarzad *et al.*, 2014). In addition, the production of synthetic aptamers is more affordable and scalable than the biological production of antibodies.

Aptamers, like antibodies have a wide variety of potential target analytes that include: peptides, specific nucleic acid sequences, lipids, a wide variety of small-molecule organic and inorganic compounds, viruses, bacteria and entire cells (Sefah *et al.*, 2010; Mascini *et al.*, 2012).

1.3.1. Oligonucleotide-based binding molecules and aptamers

In vivo, non-genetic oligonucleotide sequences perform many crucial roles in a variety of regulatory processes within the cell, often by performing highly specific binding reactions to other cell components. Many of these processes are integral to the standard feedback and evaluation of the regulatory processes that take place in the cells (Das *et al.*, 2006; Haller *et al.*, 2013). Some common examples of nucleic acid sequences capable of specific binding reactions in biology include: transport RNAs, ribosomal RNAs, small nuclear RNAs (Das *et al.*, 2006), and antisense riboswitch nucleic acids (Haller *et al.*, 2013). Similarly, to other biorecognition events e.g. antibody-antigen interactions, these processes rely on the ability of the oligonucleotides to fold into specific conformations inherently capable of the required binding function.

The tertiary folding structure of aptamers in their environment is a crucial step for the binding of the aptamer to the desired analyte. A combination of Watson–Crick base pairing complexations (canonical nucleic acid interactions) and a diversity of non-canonical 3D interactions between nucleotide residues combine to create the complex folding patterns of aptamers. The major determinants of these unique folding patterns are a result of the aptamer length and the primary structure of the aptamer i.e. the precise sequence of base pairs in the oligonucleotide (Batey *et al.*, 1999; Mascini *et al.*, 2012). Other strong influences on the conformation of aptamers are the environmental conditions: pH, salt concentrations (both monovalent and divalent cations) and the temperature of the solution are the most commonly-reported factors affecting the folding of the aptamers (Batey *et al.*, 1999; Tan and Chen, 2006).

Harnessing the aforementioned properties, the uses of both ribonucleic and deoxyribonucleic oligonucleotides in biosensing devices have been recognized in recent decades to provide high-affinity, target-specific, ligand/ analyte binding. The development and generation of oligonucleotide-derived binding molecules ("aptamers") that possess strong binding affinities to a desired target molecule were independently developed by Ellington and Szostak; and Tuerk and Gold in 1990. This was achieved using a method commonly refered to as the systematic evolution of ligands through exponential enrichment (SELEX). The discovery and use of aptamers have several advantages over their counterpart antibody based sensing techniques, including reduced degradation and greater specificity toward their target analyte (Zeng *et al.*, 2012).

1.4. Generation of aptamers using: SELEX and cell-SELEX

The primary structures of target-specific aptamers originate from within a pool of random single-stranded ribonucleic acids or single-stranded deoxyribonucleic acid (ssDNA) sequences, ranging between 20 – 100 nucleotides in length (Chen and Yang, 2015). These random sequences are flanked on both the 5' and 3' ends of the random sequence by specific primer-binding sequences of approximately 20 bp in length to facilitate subsequent amplification of sequences (Wilson and Szostak, 1999; Ulrich *et al.*, 2006). Individual sequences capable of binding are generated and selected for during SELEX (Stoltenburg *et al.*, 2007).

The specific generation of aptamers occurs by the selection of aptamer sequences bearing high affinity to a specific target, from an initial oligonucleotide library ranging between 10^{15} and 10^{20} random sequences (Brody and Gold, 2000). This can be readily performed using a series of artificial selection cycles that isolate and amplify those sequences capable of specific binding present within the oligonucleotide library (exemplified in Figure 1.1 below, using cells as the specific target). By doing so, the sequences of specific and high affinity to the analyte are maintained and amplified until they become the predominant members of the population of sequences. Between 8 - 22 selection cycles are reported in literature to generate aptamers specific to a particular target (Mayer *et al.*, 2010).

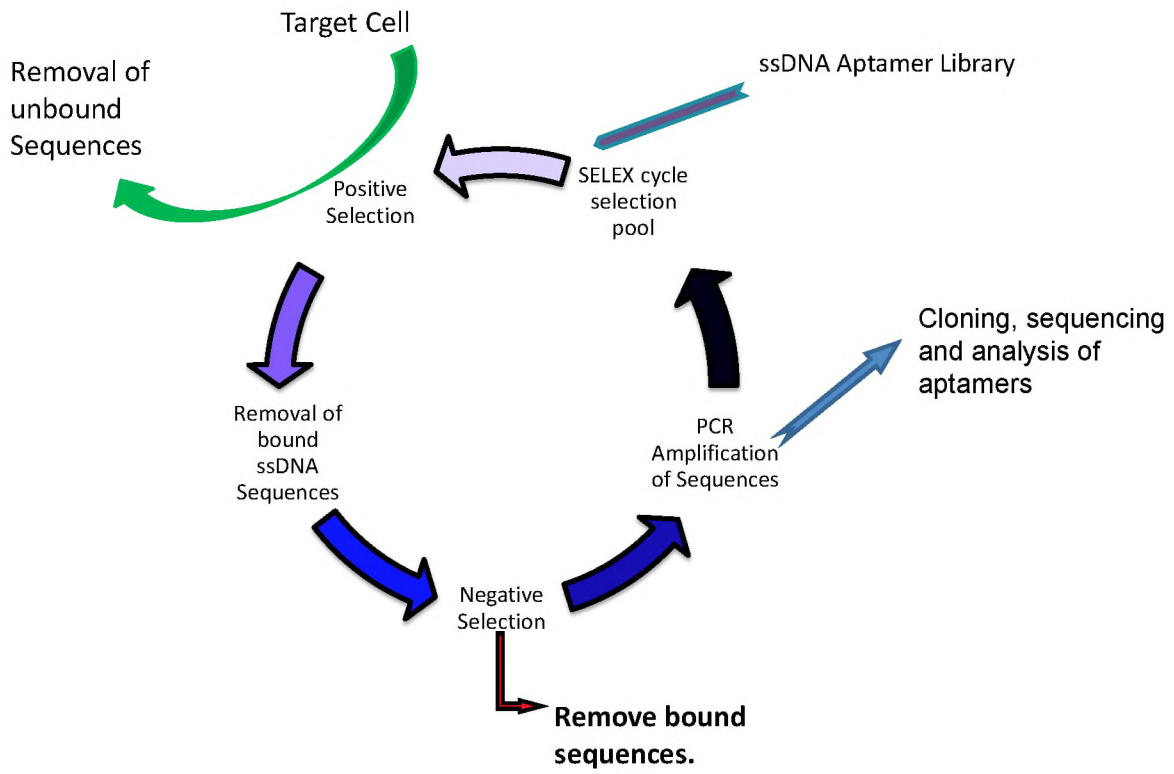

Figure 1.1: Schematic representation of cell-SELEX protocol. The random oligonucleotide sequence is selected for using the target cells; this is followed by the discarding of unbound sequences. These sequences are put through a negative selection step where the unwanted, binding oligonucleotide sequences are removed. The desired sequences are then further amplified. This cycle is repeated several times until there is minimal binding of unwanted sequences.

Since the development of SELEX, the selective protocols exemplified in Figure 1.1 have been further modified to generate aptamers for a variety of macromolecule targets that extend beyond small molecules dissolved in aqueous media. Aptamers have been generated to bind to targets present on the surfaces of entire virus capsules (Tong *et al.*, 2009), bacteria (Dwivedi *et al.*, 2013) and whole live eukaryotic cells (Sefah *et al.*, 2010), either in suspension or adhering to a surface (Stoltenburg *et al.*, 2007; Sefah *et al.*, 2010). This creates an opportunity for the bio-recognition and specific detection of select cells within a large sample (e.g. cancerous cells) in a living organism; and potential infectious diseases amongst a host of additional analytes. Furthermore, the use of aptamers has the potential to target and transport cell-specific drug treatments to a desired cell type using aptamers (Tan *et al.*, 2011). There have been a few adaptations to SELEX protocols from the conventional SELEX design (Mayer *et al.*, 2010) in order to compensate for the use of living cells as a platform of selection. This modified process is commonly referred to as cell-SELEX.

1.4.1. Cell-SELEX as a means of generating aptamers

1.4.1.a. *In* vitro tissue cultures as source of target(s) for SELEX

Cell-SELEX has the potential to generate aptamers to target individual cell proteins presented on the target cells' surfaces, as well as surface glycolipids, polysaccharides, and specific cell surface-associated protein patterns on the target cell surface (Sefah *et al.*, 2010).

In contrast to the conventional SELEX protein target binding protocols, cell-SELEX in turn captures and binds the target analyte - in its native conformation and modification(s) - at the cellular membrane, reducing the number of selective steps required in the SELEX protocol (Sefah *et al.*, 2010; Xi *et al.*, 2014). Additionally, the selection of aptamers directly to cellular-based targets could assist with cell-specific biomolecule discovery and identification expressed on the cell surface (Shangguan *et al.*, 2015): aptamers can conceivably be generated using positive selection for a given cell type, and negative selection with another, and the discriminating cell epitope(s) later identified using the aptamers as targeting agents.

Target cells may be used in suspension, or alternately SELEX may be performed directly on cells adhered on the surface of the culture dish (Sefah *et al.*, 2010). Cell-SELEX can conceivably be performed for almost all culture lines that successfully can be grown *in vitro* (Guo *et al.*, 2008). Table 1.2, below, presents a few examples of reported aptamers that have previously been generated targeting specific cell lines.

Currently, much research into cell-SELEX for aptamer generation (Table 1.2) focuses on the specific targeting of cancerous cells *in vivo* (Sefah *et al.*, 2010; Tan *et al.*, 2011; Song *et al.*, 2012; Xi *et al.*, 2014) where the healthy, tissues are used in the negative selection process. This is for the identification and eventual drug-targeting of these malignant cell states. A slightly lower focus in the literature surrounds the generation of aptamers for stem cells and cancer stem cells (Guo *et al.*, 2006; Wu *et al.*, 2013; Shangguan *et al.*, 2015).

Table 1.2: Examples of tissue-specific aptamers that have been developed using cell-SELEX in current literature

Positive Selection	Positive Cell Origin	Negative Selection	Negative Cell type	Identified target(s)	Reference(s)
PC12 (undiff.)	rat, adrenal gland	PC12 (diff.)	Neuron resemblance	Unknown	(Wang *et al.*, 2003)
RAMOS	Human Burkett's lymphoma cell line	CCRF-CEM	Human T lymphoblast	Combination of unknown cell membrane proteins and non-protein targets	(Shangguan *et al.*, 2006; Tang *et al.*, 2007)
3T3-L1 (diff.)	Mouse Fibroblast	HepG2	Human Liver	Combination of unkown cell membrane proteins and non-protein targets	(Liu *et al.*, 2012)
3T3-L1 (diff.)	Mouse Fibroblast	3T3-L1 (undiff.)	Mouse Fibroblast	Unknown cell surface expressed protein	(Kim *et al.*, 2014)
Huh7.5.1	human hepatocellular carcinoma cells	L-02	Immortal hepatic cell line	Unknown	(Ding *et al.*, 2014)
Porcine MSC	Porcine Mesenchymal Stem cells	P19	Embryonic carcinoma cell lines	Unknown protein	(Guo *et al.*, 2006)

(undiff.) - undifferentiated; (diff.) - differentiated

1.4.1.b. Major differences between cell-SELEX and conventional SELEX

Conventional SELEX targeting cells would involve the purification of specific protein targets presented on the surface of cells that could be used as a potential cell specific marker (Hicke *et al.*, 2001; Murphy *et al.*, 2003). For this method, several aspects for the selection of the protein targets need to be considered to maintain the native protein binding. Proteins after purification, or expressed recombinantly, may not retain structural or conformational identity to the native protein operating in the cellular/extracellular environment. In order to generate effective aptamers, the target analyte should conserve its native and physiological state during selection (Mayer *et al.*, 2010), which is often a challenging aspect of the SELEX process.

This may be compensated for, by rather using transformed bacterial cells to express the desired analyte and used as a target cell using SELEX (e.g. Cerchia *et al.*, 2005), but this induces other experimental challenges. The gene coding the target protein must now be inserted and stably expressed by the bacterial cell, ideally in such a manner as to overexpress the protein onto the surface membrane of the transformed cell. Additionally, post-translational modifications, such as phosphorylation and glycosylation, would affect the structure and morphology of the target protein when expressed by the recombinant bacterial cell (Schönichen *et al.*, 2013). This is especially concerning when transforming prokaryotic cells with the relevant gene due to the limited posttranslational capabilities of prokaryotic cell lines (Khow and Suntrarachun, 2012).

The third, more direct, approach of aptamer selection toward specific cell lines is to perform SELEX directly on the target living cells, by using a cell-SELEX based method. The synthetic selection of aptamers under these conditions then bind to targets on the cell surface present in their native confirmation. An additional advantage is that no prior knowledge of the targets need be known (Blank *et al.*, 2001; Stoltenburg *et al.*, 2007). This method has its own challenges: cells with reduced membrane integrity, such as those undergoing apoptosis and necrosis, have shown to non-specifically accumulate nucleic acids and may bear altered membrane surface proteins from their viable counterparts. Thus, there is a need to determine and remove damaged cells from the target sample in order to prevent non-specific target binding (Mayer *et al.*, 2010). It has also been noted that, when selection is being performed in suspension, the cellular morphology shows greater variability than selection directly on

culture plates (Sefah *et al.*, 2010) affecting the scope of potential targets presented for SELEX.

1.5. Previous research on Aptamers developed to target SC lines

Murine 3T3-L1 preadipocytes are commonly employed in research as model systems for mammalian adipocyte research (Kim and Moustaid-moussa, 2000; Storch and Thumser, 2000; Pajvani, 2003). This is further detailed in Chapter 2, section 2.1.1. Several aptamers have been developed targeting the mature adipocytes derived from 3T3-L1 cells (Liu *et al.*, 2012; Kim *et al.*, 2014), and further discussed in Chapter 3, section 3.1.1.

As stated previously, there has been some work achieved in the generation of aptamers targeting MSCs and adipocytes derived from the MSCs (Table 1.2). The uses of aptamers for the purpose of isolating MSCs from bone marrow tissues has been reviewed previously (Guo *et al.*, 2006), where it was proposed that aptamers could be used as a technique for the specific isolation of MSCs. This is opposed to the more traditional MSCs isolation methods, where MSCs would be isolated through a selection process exploiting their adhesive properties onto a plastic surface (Guo *et al.*, 2006); these methods of MSCs isolation often result in low cell densities. Additionally Wendel *et al.*, (2008) similarly proposed a project regarding MSCs isolation, using aptamers as a MSCs capture molecule.

Other relevant work was previously reported by Schäfer *et al.*, (2007), using Cell-SELEX specifically targeting MSCs using fluorescein isothicyanate (FITC) labelled ssDNA aptamers as a fluorescent biosensor to non-obtrusively target and track the migration of MSCs through vertebrate organs. This was achieved by using magnetic resonance imaging scanning, as a mechanism of tracking the directional migration of MSCs, as an attempt to understand tissue repair in the organism (Schäfer *et al.*, 2007).

Some research has been reported for the development and generation of aptamers targeting murine 3T3-L1 preadipocytes, more specifically the derivatives of differentiated 3T3-L1 preadipocytes. Liu *et al.* (2012) and Kim *et al.*, (2014), independently developed aptamers that bind mature adipocytes differentiated from 3T3-L1 preadipocytes. In both cases, undifferentiated murine 3T3-L1 preadipocytes were used as the negative selection step; Both research groups set out on different methods of selecting the aptamer sequences.

Liu *et al.* in 2012 used a more conventional protocol for cell-SELEX, where the ssDNA library, were selected from adipocytes chilled to 4 °C. It was noted that there was a minor difference in the aptamers binding abilities to the adipocytes at 4°C and 37°C. The selection preceded a negative selection with either 3T3-L1 preadipocytes or HepG2 (*Homo sapiens* liver cells) alternating between cycles. Kim *et al.* in 2014 on the other hand investigated a capillary-based SELEX method where initially the library pool was selected for with the adipocytes using conventional cell-SELEX methods, here they used the 3T3-L1 preadipocytes, undifferentiated only, for the negative selective steps. The selection of ssDNA-bound adipocytes was performed by separating the sample using a FACS cell sorter to remove the unbound ssDNA from solution after the selection steps.

1.6. Problem Statement

Previous research has highlighted that altering the microenvironment of cells during culture promotes the directed differentiation of SCs, when these are cultured as *in vitro* monolayers. Specifically, the proximity of cells to SCs undergoing differentiation has been reported to provide a means of tuning the direction and rate of differentiation of SCs.

Although aptamers have been generated to a wide variety of cell targets, and SC targets, specifically, the ability to selectively capture target cells at solid surface is under-reported. While aptamers targeting the mature (differentiated) forms of SCs are reported in literature – particularly those targeting adipocytes derived from murine model system, 3T3-L1 – no reports exist of aptamers that select for the undifferentiated form of this cell line. This represents an untapped opportunity, providing a means by which this model SC system can be selectively captured at a solid surface.

Taken together, there exists a gap in the understanding into whether aptamers can be used to control the deposition of cells onto solid surfaces, through control of the aptamer's lateral density. Furthermore, the effects of the controlled deposition on the differentiative capabilities of SC line require further investigation. Using 3T3-L1 preadipocytes as a model *in vitro* SC line, an investigation into the use of aptamers as a means of immobilising 3T3-L1 preadipocytes onto a surface monolayer would result in a surface capable of selectively binding stem cells at controlled cell densities on a solid surface to assist in the promotion of cellular differentiation to a desired cellular fate. As a means of eventually determining this, the generation and validation of aptamers targeting the undifferentiated form of 3T3-L1s

needs be tested and the ability of these aptamers to capture cells at solid surfaces must be preliminarily demonstrated.

1.7. Aim

To generate aptamer sequences as a means of controlling the seeding densities of murine 3T3-L1 preadipocytes on a surface, to test possible changes in the differentiation patterns of the preadipocytes.

1.8. Objectives

To address the above Problem Statement, ssDNA aptamers were generated through an adapted version of cell-SELEX that was proposed by (Sefah *et al.*, 2010), using cultured cells.

The developed aptamers need to display a binding preference towards the undifferentiated 3T3-L1 preadipocytes over the differentiated cells derived from this cell line. The success of preferential binding can be monitored using a Cyanine - 5 (Cy5) fluorescently - labelled aptamer pool. This necessitates the following objectives: successful culture of 3T3-L1 preadipocytes; successful differentiation of these to mature adipocytes; validation of the system's ability to monitor the selective attachment of aptamer candidates to the target samples. All these objectives required separate testing and validation prior to proceeding with SELEX.

Following cell-SELEX, the binding extent and selectivity of sampled aptamers to the two targets required testing and validation, using fluorimetric microscopy. Subsequently, the assembly of a self-assembled monolayer using a combination of both the generated aptamer and a β-mercaptohexanoic acid spacer at a variety of densities using gold/ thiol interactions between the surface and the aptamers with across the surface, the binding of the cells to the developed monolayer will be evaluated using the ACEA xCELLigence Real-time cell analyser.

1.9. Hypothesis

Novel aptamer sequences that specifically target and bind 3T3-L1 preadipocytes can be developed, using mature adipocytes as negative selection targets. Furthermore, a self-assembled monolayer containing the developed aptamer can be generated on a gold surface and be able to control the seeding densities of the preadipocytes *in vitro*.

Chapter 2 : Commonly used Methods and Materials

2.1 Introduction

2.1.1 3T3-L1 preadipocyte growth and differentiation

There are several SC lines commercially available for *in vitro* research that have been sourced from a variety of mammal species. These cell lines include MSCs from both human (Chamberlain *et al.*, 2007), porcine (Guo *et al.*, 2006), and rodent sources (Wang *et al.*, 2003).

3T3-L1 preadipocytes were originally derived from murine embryonic fibroblasts and are unipotent SCs, able to irreversibly differentiate into only adipocytes (Russell and Ho, 1976; Kaiden Student *et al.*, 1980). These have been established as a standard cell line used for adipogenic studies, due to their near-immortal capabilities and the ease of deriving adipocytes from this cell line. 3T3-L1 preadipocytes have an approximate doubling time of 12 – 15 hours (Gordeladze *et al.*, 1997; Baret *et al.*, 2013).

Irreversible differentiation of the preadipocytes can be initiated *in vitro* – usually after the preadipocytes have reached confluency – through administering a mixture of stimulating chemicals, chiefly: dexamethasone (DEX), insulin (INS), 3-isobutyl-1-methylxanthine (IBMX), and rosiglitazone (ROSI) into the nutrient culture medium of the cells (Camp *et al.*, 2002; Kramer *et al.*, 2014).

A combination of INS and IBMX are the most essential chemical stimulants for adipogenesis to occur (Reusch *et al.*, 2000; Klemm *et al.*, 2001). The activation of INS signal transduction pathways, with the addition of DEX, promotes a number of transcription factors that significantly alter gene expression in preadipocytes (Klemm *et al.*, 2001). Notably, signalling pathways that are involved with Cyclic adenosine monophosphate Response Element-Binding protein (CREB) transcription factor pathways are upregulated to promote the activation of additional signalling pathways (Klemm *et al.*, 2001). CREB in turn, activates a number of enzymes, such as peroxisome proliferator-activated receptor gamma 2 (PPARγ2) and adipocyte determination-differentiation factor 1 (ADD1-SREBP) (Reusch *et al.*, 2000). PPARγ2 is a nuclear hormone that further regulates the expression of a number of proteins including phosphoenolpyruvate carboxykinase (PEPCK) (Tontonoz *et al.*, 1995) and PPARγ co-activator-1α (PGC1α) (Rosen and MacDougald, 2006). The addition of ROSI is not essential to adipogenesis; however, this derivative of thiazolidinedione binds PPARγ. In so

doing, it increases the sensitivity of preadipocytes to INS (Albrektsen *et al.*, 2002), promoting adipogenesis (Scott *et al.*, 2011).

IBMX, along with DEX, stimulates the expression of the CCAAT-enhancer-binding protein (C/EBPδ) family, and C/EBPβ regulatory factor pathways (Pantoja *et al.*, 2008). The C/EBPβ pathway is involved with the suppression of the E2F transcription factor family, which are involved in regulatory cell cycle maintenance (Dyson, 1998; Trimarchi and Lees, 2002).

Before irreversible differentiation occurs, the cells have been reported to divide once or twice more, before cell cycle arrest occurs in the maturing adipocytes (Rosen and MacDougald, 2006). During adipogenesis, an increase in the biosynthesis of fatty acid precursors is observable (Rosen and MacDougald, 2006), resulting in a morphological change in the cells from a fibroblastic cell shape to a circularized cell morphology (Russell and Ho, 1976; Kaiden Student *et al.*, 1980). The produced triglycerides self-associate to create fatty acid vacuoles in the cytoplasm of differentiating cells; these eventually take up most of the cellular space within the mature cell (Mariman and Wang, 2010). The combination of these changes allows for rapid microscopic distinction between preadipocytes and mature adipocytes.

2.1.2 Amplification of selection pool library for SELEX

The amplification of a SELEX selection pool is a phase of SELEX (Figure 1.1) which often proceeds using the Polymerase Chain Reaction (PCR), or some variant thereof. This is a specialised instance of the conventional PCR, as it requires the amplification of a diverse population of template DNA sequences that has a large diversity in template sequences (Tombelli *et al.*, 2005). When amplifying a diverse template pool of DNA through PCR, the high diversity in the template sequences causes cross-hybridisation between the template primary sequences, which arises from incomplete complexation of template molecules to one-another during the primer-hybridisation phase of PCR (Kalle *et al.*, 2014), depicted in Figure 2.1 below.

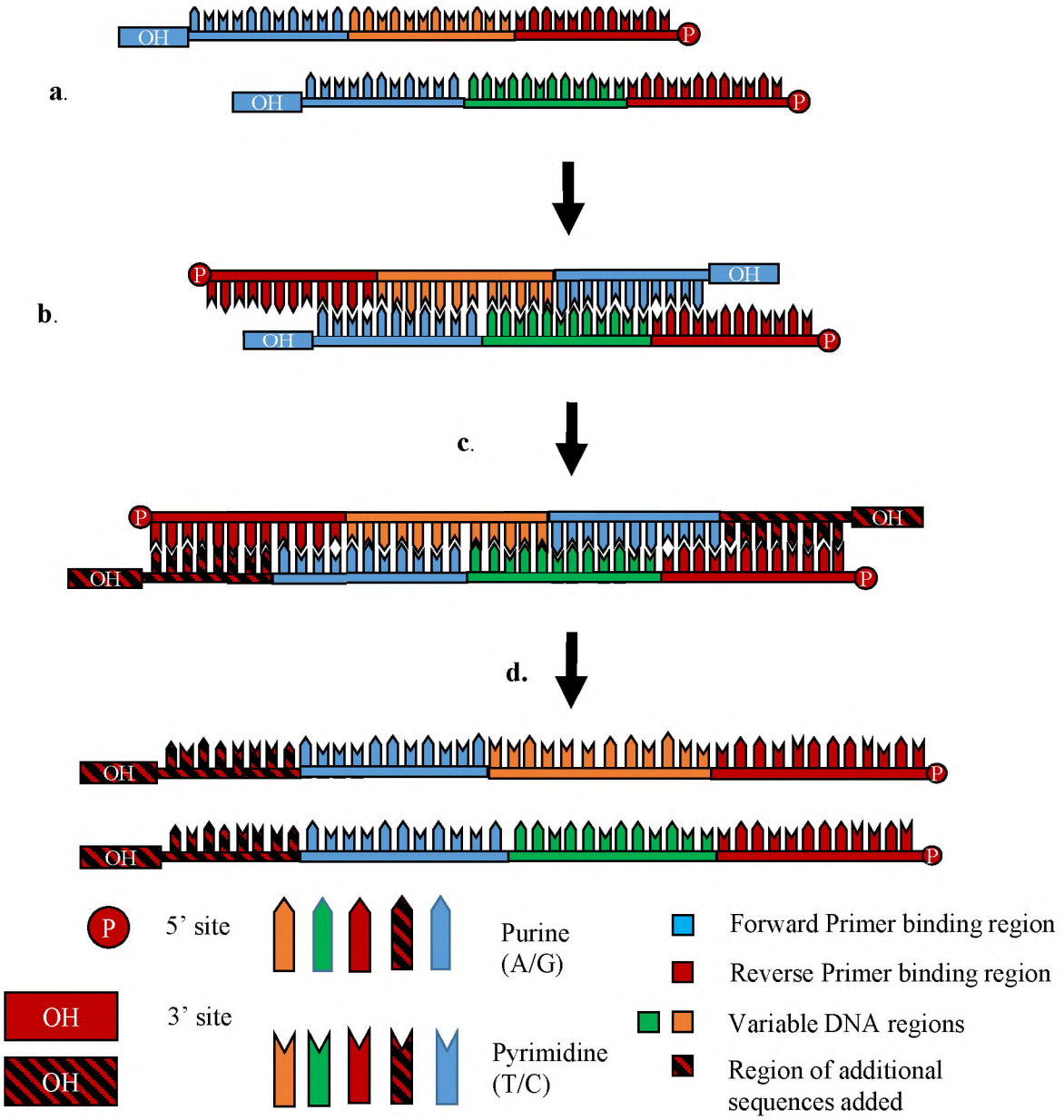

Figure 2.1: Schematic representation of mechanism of PCR Artefact formation during a ssDNA template multi-template PCR reaction, due to partial hybridisation between template molecules.

a) Original ssDNA selection library (template ssDNA). b) Hybridisation of different sequences in the library. c) Extension of the hybridised sequences. d) Denaturation of the newly synthesised concatemer sequence.

Cross-hybridisation (exemplified in Figure 2.1) causes inaccurate replication of template sequences, resulting in DNA products that are combinations of the initial template sequences (Kalle *et al.*, 2014). The hybridisation of similar sequences during multi-template PCR reaction is highlighted in (Figure 2.1.b.), where similar template sequences anneal together

improperly together. The extension of the PCR product (Figure 2.1.c.) generates an extension of the 5' primer regions on the 3' end of the product DNA strand. The continuous amplification of these high molecular weight product increases the size of the product DNA molecule, increasing the proportion of these hybrids in the amplification pool in a cycle-dependent manner. Similarly, concatemer formation also happens between primer – primer complexes, and incomplete hybridisation of primer – template complexes, which proceed and begin to dominate the amplification pool in an analogous manner to that illustrated in Figure 2.1. Collectively, these are termed as amplification artefacts.

The removal of some amplification artefacts may be controlled to a degree, where the cycle-dependent development high molecular-weight concatemer sequences are visualised through gel electrophoresis techniques and subsequent fluorescent staining of the DNA. This allows for a certain degree of quality control in the SELEX process when amplifying the selection pool, by performing a PCR cycle optimisation to amplify the maximum amounts of template DNA and minimising the formation of artefacts (Stoltenburg *et al.*, 2007; Sefah *et al.*, 2010). Due to the variability in the diversity of template sequences within the selection pool following aptamer selection, the number of optimum PCR amplification cycles changes throughout the SELEX procedure (Sefah *et al.*, 2010). This optimisation needs to take place for all selection cycles; this is due to the aforementioned dependence of cross-hybridisations on the sequence diversity of the template (Schütze *et al.*, 2009).

2.2 Methodology commonly used throughout the project

2.2.1. Commonly used reagents and apparatus

2.2.1.a. ssDNA template sequences and primers used throughout the project

A 90 bp random oligonucleotide DNA sequence library comprising of 49 random base pair sequence flanked on either side with a 16 bp forward primer and a 20 bp reverse primer binding regions (5' - GCCTGTTGTGAGCCTCCTAAC - (N_{49}) - CATGCTTATTCTTGTCT CCC - 3'), was purchased from IDT Integrated DNA Technologies, South Africa, as a formulated stock of 100 μM in a Tris-EDTA (TE) buffer (pH 8), made from a combination of 10 mM Tris-Cl with a 1 mM Ethylenediaminetetraacetic acid (EDTA) solution.

The 16 bp forward primer, either labelled on the 5' end with Cyanine-5 (Cy-5) or 6-carboxyfluorescein (6-FAM) i.e. 5' Fluorophore –GCCTGTTGTGAGCCTC -3', was purchased from IDT Integrated DNA Technologies, South Africa. The nature of the

fluorescent label differs for separate studies. These were formulated to 100 μM stock solutions in TE buffer.

The 20 bp 5' Phosphate labelled reverse primer, (5' Phos-GGGAGACAAGAATAAGC 3', was purchased from IDT Integrated DNA Technologies, South Africa). This was formulated to 100 μM stock solutions in TE buffer.

2.2.1.b. Binding and Wash buffers used for aptamer selection and binding

The binding and wash buffers were formulated similarly according to published protocols (Sefah *et al.*, 2010). To maintain similar conditions found in the DMEM nutrient media used for tissue culture (Section 2.2.2a), the binding buffer for cell-SELEX was composed of Dulbecco's phosphate buffered saline, pH 7.3, (DPBS): with $1.37x10^{-1}$ M NaCl (Sigma-Aldrich), $1.01x10^{-2}$ M $Na_2HPO_4.2H_20$ (Sigma-Aldrich), $1.01x10^{-2}$ M KH_2PO_4 (Sigma-Aldrich), and $2.68x10^{-3}$ M KCl (Sigma-Aldrich). This was supplemented with 4.5 % $^{w}/_{v}$ α - D - Glucose (Sigma-Aldrich, 96 %) (equivalent to $2.50x10^{-2}$ M), 1 % $^{w}/_{v}$ Bovine Serum Albumin (New England Biolabs) (equivalent to $1.5x10^{-5}$ M), and 5 % $^{v}/_{v}$ 1 M $MgCl_2$.

Similarly, the buffer used for washing of samples was formulated using DPBS pH 7.3, supplemented with 4.5 % $^{w}/_{v}$ glucose and 5 % $^{v}/_{v}$ 1 M $MgCl_2$ only.

2.2.1.c. Preparation of PAGE and Agarose gels

The quality of the DNA following PCR was evaluated using polyacrylamide gel electrophoresis (PAGE), the gels were comprised of a 10 % ($^{w}/_{v}$) acrylamide/bis – acrylamide (Sigma-Aldrich, from an original stock of 30 % $^{w}/_{v}$). This was added to a 1 x Tris-acetate-EDTA (TAE) buffer (40 mM Tris, 20 mM acetic acid and 1 mM EDTA, final pH 8) with 1.4 % of N,N,N′,N′-Tetramethylethylenediamine (Sigma-Aldrich) and 0.29 % ammonium persulfate (Sigma-Aldrich), and cast to a thickness of 0.75 mm.

Agarose gels were prepared at a concentration of 4 % $^{w}/_{v}$ (WhiteSci) and were dissolved through heating in a 1 X TAE buffer. Agarose gels were precast containing 1 X GelRed in distilled water solution (from an original stock of 10 000 X GelRed in water).

Gel electrophoresis was performed using 1 X TAE running buffer, with a potential difference of 80 V, for ~ 1 hour, using the BIO-RAD PowerPac™ Easy. Following electrophoresis, PAGE gels were stained with GelRed by exposure to a solution composed of 1 x TAE buffer and 1 x GelRed for 30 minutes at room temperature. Stained gels were visualised under UV

transillumination, using the BIO-RAD Gel Doc™ EZ imager, and resultant images were processed using Image Lab Version 5.0.

2.2.1.d. NucleoSpin® Gel and PCR protocol

The following buffers were used as sourced from the NucleoSpin® kit: NTI Buffer (containing guanidinium thiocyanate 30 – 60 %), NTC Buffer (potassium thiocyanate, 40 - 60 %), NT3 Buffer (with 80 % ethanol) , NE Buffer (5 mM Tris/ HCl, pH 8.5).

To purify the various forms of DNA required for the study (either ssDNA or double stranded DNA (dsDNA), depending on the study discussed), the following protocols were used. A 1: 2 ($^{v}/_{v}$) ratio of reaction buffer: DNA binding buffer (reaction buffer was NTI for dsDNA and NTC for ssDNA purification) was formulated, and 700 µl aliquots of the solution was centrifuged at 8928 x *g* for 30 seconds in the supplied column, and the waste was discarded. This step was repeated until the entire sample had passed through the column. The membrane within the column was washed using 700 µl of the NT3 wash buffer (spun through the column at 8928 x *g* for 30 seconds) and the waste discarded. The membrane was dried by centrifuging the column at 8928 x *g* for 5 minutes. The flow-through from the column was discarded, followed by a final 1 minute centrifugation at 8928 x *g*. DNA bound to the column was eluted out the column by adding 30 µl of the NE buffer and centrifuging down at 8928 x *g* for 1 minute into a sterile 1.5 ml microcentrifuge tube; the final step was repeated once more.

2.2.1.e. Fluorescent spectroscopic settings

All fluorescent spectroscopic readings took place using the Synergy™ MX microplate scanner. All samples were loaded into microtiter plate wells at 100 µl volumes prior to reading.

To normalise fluorescent spectroscopic readings (presented in RFU) to the concentration of dissolved aptamer presented in samples, all spectroscopic readings were accompanied by a standard solution of dissolved, fluorescently-tagged, aptamer. Standards used to calibrate the emission spectra of the fluorophore was prepared with a diluted stock of 9.09 $x10^{-8}$ M (9.09 pmol / 100 µl sample in well) forward primer solution in binding buffer with a total volume of 50 µl in a 96 well microtiter plate reader,

Samples containing the 6-FAM fluorophores were excited at a wavelength of 480 $\pm$ 9 nm, and an emission spectrum ranging between 500 – 700 nm, at 2 nm increments, was generated,

The peak emission RFU value of 518 nm. Fluorescent intensity was measured at a wavelength of approximately 562 nm to quantify the fluorescent emission of the sample.

Similarly, the conditions for the excitation of the Cy5-labelled samples were maintained with an excitation wavelength of 640 $\pm$ 9 nm with an emission spectrum between 500 and 800 nm, with an emission peak wavelength of 670 nm.

2.2.1.f. Epifluorescence Microscopy

Samples analysed using epifluorescent microscopy were visualised using a Zeiss Axio Vert.A1 microscope, using the Zeiss filter set 44, with an excitation waveband between 450-500 nm and the emission filters between 500 – 550 nm. Micrographs were captured using a ZEISS Axiocam MRm camera. The software used for image visualisation and processing was ZEN 2.3 lite (blue edition).

2.2.1.g. Confocal Microscopy

Confocal micrographs were generated using the Zeiss LSM 780 laser scanning confocal microscope. A 63x objective was used, using an oil immersion on the slide surface. The depth of focus for the objectives were set to 0.85 µm. The exposure and detector settings for all the channels were maintained for visualisation of all the slides, providing consistency regarding fluorescent intensity between visualised imaged. Relevant laser information is summarised in Table 2.1 below and maintained for all confocal images. Images were captured using Zen Black software and the images were processed and visualised using ZEN 2.3 lite (blue edition).

Table 2.1: Confocal microscopic analysis excitation and emission wavelength settings used during confocal microscopy

Assigned channel colour	Excitation Wavelength; % laser power	Emission Wavelength	Emission waveband	Detector gain
Red	633 nm; 0.98 %	699 nm	638-739 nm	850.0
Green	488 nm; 0.98 %	544 nm	490-597 nm	700.0
Blue	405 nm; 1.00 %	458 nm	410-505 nm	835.8

2.2.1.h. Reporting of measurement uncertainty

The quantification of dsDNA and/or ssDNA during cell-SELEX was conducted using the NanoDrop™ 2000 UV-VIS spectrophotometer (Thermo Scientific), when not fluorescently evaluated during cell-SELEX. Unless otherwise specified, all reported quantities were evaluated using three repeated measurements of the quantity of DNA found in the sample and are presented as the average ± the standard error of the sample's means.

2.2.2 3T3-L1 Tissue culture conditions

2.2.2.a. Cell growth of murine 3T3-L1 preadipocytes

Murine 3T3-L1 pre-adipocytes, Passage 24 (P24) were donated by Professor Carminita Frost at the Department of Biochemistry and Microbiology, Nelson Mandela Metropolitan University. These were maintained and grown in an adherent monolayer cultures as outlined in literature (Kramer *et al.*, 2014), using a high-glucose Dulbecco's Modified Eagle Medium (DMEM) supplemented with 5 % ($^{v}/_{v}$) foetal calf serum (FCS) (Thermo Scientific), 1 % ($^{v}/_{v}$) L-glutamine (Sigma-Aldrich), and 1 % ($^{v}/_{v}$) streptomycin (Lonza), in a humidified incubator at 37 °C and 5 % carbon dioxide. The exact protocol for subculturing and resuspension of the cells in culture is provided in further detail below (Section 2.2.2.b.)

The received cells were cultured on the surface of a T25 flask until confluent (P25) and subcultured in two T75 flasks until confluent (P26). Cryogenic stocks of the cells were formulated at P26 in 10 % $^{v}/_{v}$ Dimethyl sulfoxide (DMSO) in 3T3-L1 growth media ($^{v}/_{v}$), and stored at -80 °C.

The preadipocytes were revived and subcultured until they reached P29 for the further cell-SELEX selection cycles and cell binding assays detailed below. The P26 cryogenically frozen cells were revived in a T25 (250 mm^2) culture flask, in DMEM nutrient media and allowed to adhere and grow to the polystyrene surface of the culture flask for 24 hours. The nutrient media was replaced with fresh (prewarmed at 37 °C) DMEM preadipocyte growth media. The cells were allowed to grow (nutrient media was changed every fifth day) until the preadipocytes reached approximately 80 – 90 % confluency, by visual inspection, on the surface of the culture flask, and cultured until P29 to maintain cell passage throughout the research project.

P29 3T3-L1 preadipocytes were seeded onto 35 mm (area of ~900 mm^2) culture plates (approximately 3 x10^5 cells / plate) for aptamer generation. Alternatively, the preadipocytes were seeded onto the surfaces of 24-well plates (area of 200 mm^2) at a density of approximately 5.00 x10^4 cells/ well for aptamer binding assays.

2.2.2.b. Detailed protocol for subculturing of 3T3-L1 preadipocytes

The culture media was entirely removed from the flask. Adherent preadipocytes were washed three times with room temperature phosphate buffer solution (PBS) to remove any excess nutrient media in the flask. A solution of room temperature trypsin (Sigma-Aldrich) in PBS was added into the culture flask to make a final concentration of 0.05 % ($^v/_v$) of trypsin in PBS. The culture flask was incubated at 37 °C for two minutes, after which the PBS / Trypsin solution was placed into 2 ml of DMEM nutrient media supplemented with 5% ($^v/_v$) foetal calf serum (FCS-DMEM).

The culture flask was incubated a second time for an additional 2 minutes at 37 °C. The culture flask was removed and gently tapped to loosen up the remainder of the cells, the cells were then collected within a 2 ml wash of 5 % ($^v/_v$) FCS-DMEM nutrient media.

The cells were collected through centrifugation at 1000 x *g* for 5 minutes and then resuspended in DMEM nutrient media. The cells were counted using a haemocytometer and seeded onto the surface of new culture flasks.

2.2.2.c. Mycoplasma contamination screening

Routine tests of potential mycoplasma contamination within the culture was evaluated within both the cell media and cell lysate throughout the study.

Mycoplasma screening was conducted using a similar PCR protocol to that detailed by (Ossewaarde *et al.*, 1996). Briefly, 5 µl of the sample (either DMEM nutrient media

containing cells undergoing culturing, or cell lysate) was added to 5 µl of 10 X Taq Buffer, 3 µl of a 10 mM dNTP mixture (to a final concentration of 5.00 $x10^{-5}$ M), each from the stock of $1x10^{-4}$ M (5 µl) GPO3 (5'-GGGAGCAAACACGATAGATACCCT-3') and the reverse MGSO (5'-TGCACCATCTGTCACTCTGTTAACCTC-3') primer sequences, with 3 U Taq Polymerase. The reaction mixture was formulated to a final volume of 50 µl using autoclaved MilliQ water.

The above PCR reaction mixtures were subjected to the following thermal cycles to effect PCR: an initial denaturation of 95 °C for 3 minutes, followed by 30 cycles of 95 °C for 30 seconds, 55 °C for 30 seconds, and 72 °C for 30 seconds. A final 10 minute extension temperature at 72 °C was included. Agarose gel electrophoresis and visualisation of the amplicon was used as the basis for detecting mycoplasma infection of mammalian tissue culture

2.2.2.d. Differentiation of 3T3-L1 preadipocytes

Passage 29 3T3-L1 preadipocytes were allowed to grow on the surface of the culture flask to confluency (approximately 10^6 cells) and cultured for an additional two days before initiating differentiation in the cells. The initiation of adipogenesis was then carried out as proposed by (Kramer *et al.*, 2014):

A differentiation medium was prepared using the 3T3-L1 growth medium supplemented with $2.5x10^{-11}$ M DEX (Sigma-Aldrich), $1.67x10^{-6}$ M INS (Sigma-Aldrich), $5x10^{-11}$ M IBMX (Sigma-Aldrich) and $2x10^{-6}$ M ROSI (Sigma-Aldrich) and added to the cells.

Prior to differentiation, the wells, containing the cells, were washed 3 times with sterile PBS. Cells were cultured in the differentiation media for three days, to initiate cellular differentiation. Subsequently, the differentiation media was washed out 3 times with sterile PBS before a differentiation maintenance nutrient media was added in the place of the differentiation nutrient media. The maintenance media was comprised of DMEM supplemented only with $1.67x10^{-6}$ M INS (Sigma-Aldrich). The media of the cells was exchanged with fresh maintenance nutrient media every 4 days.

3T3-L1 preadipocytes have been shown to have differentiated into mature adipocytes within 8 - 10 days following initiation (Saito *et al.*, 2007; Pantoja *et al.*, 2008). For this study, adipocytes used for cell-SELEX were allowed to differentiate for 14 days before they were used for SELEX selection rounds.

2.2.2.e. Reagents used to test for adipogenic differentiation

Oil Red O staining of the lipid vacuoles was performed after 13 days of differentiation to ensure adipogenesis had occurred (Chapter 3, section 3.1.1.a.). A stock of 8.57×10^{-3} M Oil Red O in a 60 % isopropanol/PBS solution was stirred overnight and filter sterilized using a 0.2 µm cellulose acetate membrane syringe filter (Lasec, South Africa). From the stock solution, a working solution of 5.14×10^{-3} M solution of Oil Red O was prepared in PBS and filter sterilised using 0.2 µm cellulose acetate membrane syringe filter (Lasec, South Africa).

2.2.2.e.i. Fixing solution

4 % ($^{v}/_{v}$) formaldehyde (Merck Millipore, 35 % $^{Mr}/_{v}$) was formulated in PBS.

2.2.2.e.ii. Isopropanol working solution

60 % ($^{v}/_{v}$) isopropanol (Merck Millipore, 99 %) was formulated in PBS.

2.2.3 Amplification and generation of ssDNA library

2.2.3.a. dsDNA amplification of selection library for cell-SELEX

Prior to amplification of the aptamer pool, a PCR cycle optimisation study was required to identify the optimum amounts of PCR amplification cycles. This was performed for each SELEX cycle, using the KAPA Taq PCR kit (KAPA Biosystems), using the reaction conditions described below. The water used in all PCR reactions was purified using MilliQ filtration system and sterilized by autoclaving for 10 minutes at 121 °C.

Initially, a 200 µl stock PCR reaction was prepared using 20 µl of the 10 X Taq buffer with 15 mM Mg (at 10 X buffer), 1.00×10^{-7} M dNTP mix (Thermo Scientific, stock concentration of 1.0×10^{-2} M). Both forward and reverse primers 4.55×10^{-8} M (from diluted stock concentration of 9.09×10^{-6} M), 1.45×10^{-14} mol template ssDNA, and 5 U KAPA Taq DNA polymerase. The remainder of the 200 µl volume was made up with sterilised water. The stock was aliquoted out into ten 20 µl aliquots, in PCR tubes.

Thermocycle conditions for PCR amplification of the library was completed using a touchdown PCR protocol: starting with a 95 °C hot start for 5 minutes, 95 °C denaturing phase for 1 minute, a 1 minute annealing phase, followed by a 72 °C extension time of 1.5 minutes. To complete the PCR, a final 72 °C extension phase for 7.5 minutes was applied. The temperature of the annealing phase of PCR was decremented from an initial 59 °C to 58 °C, 56 °C, and 54 °C for cycles 2 to 4, and thereafter maintained at 54 °C for the remaining

cycles. At the end of each cycle, the thermocycler was paused and a 20 µl sample removed from the set. In this manner, a cycle-by-cycle evaluation of the PCR product was possible.

The PCR product was evaluated using a 10 % ($^{w}/_{v}$) Polyacrylamide Gel Electrophoresis (PAGE) gel to evaluate the optimum number of amplification cycles before over amplification of the dsDNA product, as outlined in section 2.2.1.c. Based on the cycle-dependent amplicon quality visualised by PAGE, a desired amount of PCR cycles was selected.

The PCR reaction was then scaled up to a 1 ml PCR stock reaction mix, using the same thermocycler conditions as mentioned in the cycle optimisation step above and the optimum cycle number in the optimisation stage used to amplify the aptamer pool. Multiple 1 ml PCR reactions were performed until 5 µg of dsDNA was generated.

Following DNA amplification, the product was purified and concentrated using the NucleoSpin® Gel and PCR Clean-up kit (purchased from Separations) as detailed in section 2.2.1.d.

2.2.3.b. ssDNA generation by Lambda exonuclease digestion

dsDNA originating from PCR amplification of candidate aptamer pools (Section 2.2.3.a.) was used to generate ssDNA for further cycles of SELEX. This proceeded as described in the product manual sheet (New England Biolabs). A 440 µl reaction was set up using 44 µl 10 X lambda exonuclease buffer, 6.6 U Lambda exonuclease (purchased from New England Biolabs, product number M0262L) and 5 µg dsDNA. The lambda exonuclease was then allowed to digest the antisense strand for 2 hours at 37 °C, the exonuclease digestion was then terminated by heating the reaction tube to 75 °C for 10 minutes.

The ssDNA product was purified from this reaction mixture by using the NucleoSpin® Gel and PCR kit, as detailed in section 2.2.1.d and the purity and quality of the single-stranded product evaluated using agarose gel electrophoresis, as mentioned in section 2.2.1.c

2.2.3.c. Fluorescent quantification of Cell-SELEX ssDNA Library recovery

For the fluorescent quantification of the selection library during cell-SELEX, the 5' end of the forward primer was labelled with a 5' Cy5 fluorophore; see section 2.2.1.e. for fluorescence spectroscopy protocol

Following the selection process, the samples collected from the selection process were purified using the NucleoSpin® Gel and PCR Clean-up system (purchased from Separations)

as per manufacturer's instruction. Section 2.2.1.e. of this Thesis details the fluorescence spectrometric settings.

Chapter 3 : Optimisation of preparative and selective steps for cell-SELEX

3.1 Introduction

Before the initiation of cell-SELEX, several screening assays are required to evaluate and confirm the quality of both the positive and negative targets. These tests include potential mycoplasma contamination of the cells and, in the case of adipogenesis, the level of adipogenesis that has occurred.

3.1.1. Murine 3T3-L1 preadipocytes and adipocytes

3T3-L1 preadipocytes have been a popular cell line in biochemical assays where the cell line is used as the primary cell line in adipogenic studies. A reported third of obesity related studies have used the cell line as the model for adipogenic studies (Ruiz-Ojeda *et al.*, 2016). This is mostly because the cell-line is affordable and easy to culture (Ruiz-Ojeda *et al.*, 2016). The cells are able to be grown at higher passages to that of other noncancerous cell lines (Poulos *et al.*, 2010; Ruiz-Ojeda *et al.*, 2016).

Although 3T3-L1 preadipocytes have been used as target ligands for the development of aptamers by (Liu *et al.*, 2012; Kim *et al.*, 2014), these reports focused specifically on developing aptamers that were targeted to selectively bind mature adipocytes derived from the 3T3-L1 preadipocyte cell line. This provides an array of control sequences with which to evaluate the potential binding of the developed aptamer sequence, with that of the adipocytes. This provides an additional control sequence for the binding of the aptamer to the preadipocytes.

3.1.2. *Mycoplasma* contamination

Biological contamination of eukaryotic tissue cell lines by *Mycoplasma* spp. is a routine concern at tissue culture facilities. *Mycoplasma* form part of the bacterial class *Mollicutes* that make up over 120 species of the bacteria (Ossewaarde *et al.*, 1996). An estimated 95 % of *Mycoplasma* contamination of tissue culture facilities results primarily from 5 *Mycoplasma* species (Ossewaarde *et al.*, 1996).

Mycoplasma are approximately 0.3 - 0.8 μm in size. As a result of the size of the bacteria the cells cannot be detected using light microscopic methods (Drexler and Uphoff, 2002). Primary hosts of *Mycoplasma* include that of porcine (*Sus scrofa*), Bovine (*Bos taurus*) and human (*Homo sapien*) species (Nikfarjam and Farzaneh, 2012).

The *Mollicutes* bacterial class is classified for the lack of a fixed cell wall (Drexler and Uphoff, 2002), increasing the flexibility of the bacteria. This allows them to pass through antibacterial sterilizing filters and other commonly practiced sterilization techniques and to enter culture media and containers. Attaching to the cellular membrane of the host, the *Mycoplasma* bacterium act as an intracellular parasite (Drexler and Uphoff, 2002). *Mycoplasma* infection competes with host cells for nutrients. Additionally *Mycoplasma* disrupts cellular processes and the normal functioning and growth of the cell by disrupting key cellular functions of the cell including gene expression patterns, inhibition of cell growth, inhibition of cell metabolism and cell death (Drexler and Uphoff, 2002; Nikfarjam and Farzaneh, 2012).

Of the number of protocols that have been developed to detect *Mycoplasma* contamination within tissue culture samples, the most commonly applied methods of *Mycoplasma* screening include fluorophore staining of the bacterial genomic DNA, and specific PCR amplification of the bacterial 16S rRNA gene. Both these methods have advantages and disadvantages when compared with each other (Drexler and Uphoff, 2002).

Fluorescent imaging of the bacterial genomic material typically proceeds using Hoechst stain, or the use of 4',6-diamidino-2-phenylindole (DAPI). This is considered a simple and rapid method for detecting the nuclear regions of the bacterial contamination surrounding the cell surface. However, it is regarded as relatively insensitive to *Mycoplasma* detection (Drexler and Uphoff, 2002), and high numbers of the contaminating bacteria are required to definitively detect their presence.

As an alternative detection method, PCR-based amplification of the 16S rRNA gene using *Mycoplasma* – specific primer sequences permit a more sensitive evaluation of biological contamination. However, the PCR amplification is a more lengthy process to undergo to that of fluorescent assays (Ossewaarde *et al.*, 1996).

3.1.3. Cell-SELEX

As detailed in Section 1.4, the SELEX process has been adapted to accommodate a wide variety of applications and targets. Current selection methods that have been developed from the conventional methods first described by Ellington and Szostak, 1990 and Tuerk and Gold, 1990, include the use of capillary electrophoresis (Mendonsa *et al.*, 2004), flow cytometry (Kim *et al.*, 2014), and capillary selection based techniques (Berezovski *et al.*, 2006). Within these methods, there have been a number of altered protocols that have been used to optimise the time and amount of reagents spent using SELEX (McKeague and DeRosa, 2014), (McKeague and DeRosa, 2014). These selection methods have also been altered to favour the intended application of the aptamers once selection has taken place.

SELEX could potentially, be divided into two major steps: the selection of the pool and the amplification of the selected pool (Xi *et al.*, 2014). Selection involves all the steps that provide target binding specificity and selectivity, including the positive, negative and counter stages of selection (Stoltenburg *et al.*, 2007). The amplification of the selected pool ensures increasing concentrations of binding sequences in the selection pool. These are discussed in greater detail below.

3.1.3.a. Generation of ssDNA from dsDNA for selection cycles

The amplification of the aptamer pool, and subsequent generation of the ssDNA pool for subsequent SELEX phases is an essential factor for successful aptamer generation (Citartan *et al.*, 2011). Several methods to generate ssDNA aptamers from dsDNA amplicons have been proposed, chiefly: biotin-streptavidin separation, asymmetric PCR and lambda exonuclease digestion. Figure 3.1 below illustrates different methods of ssDNA synthesis.

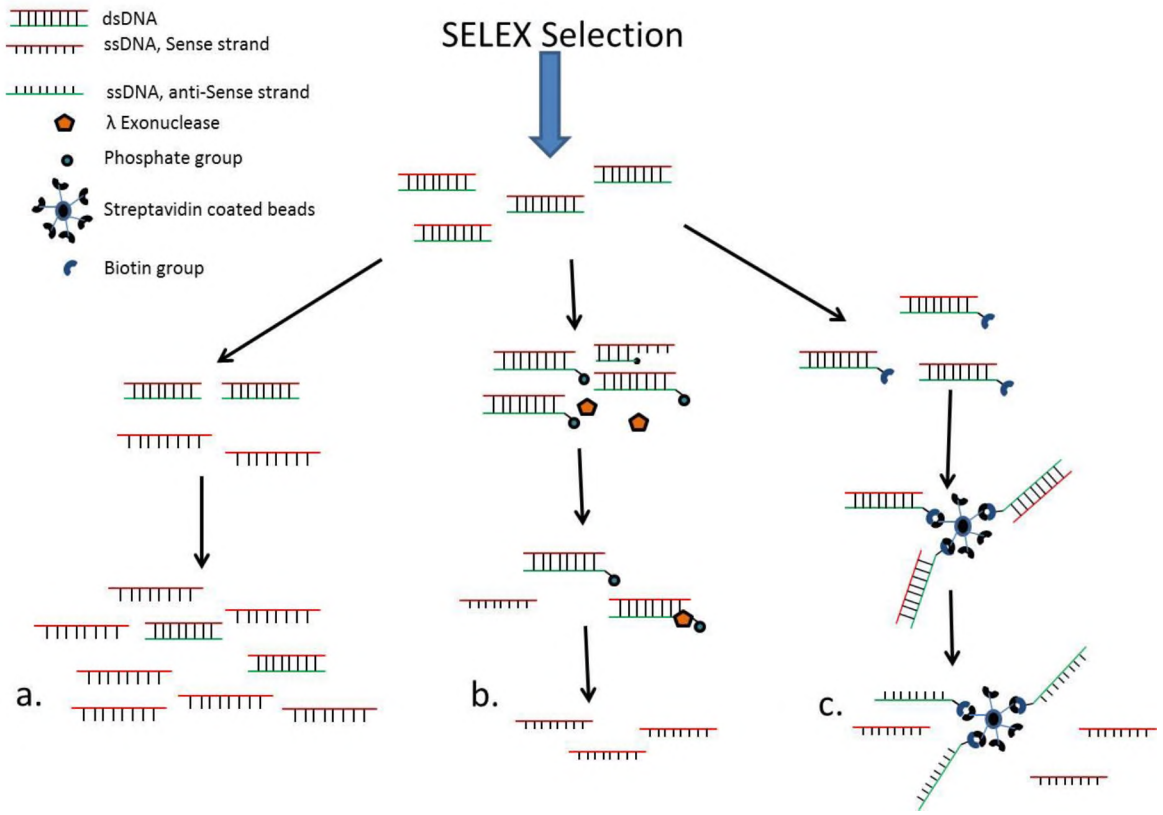

Figure 3.1: Visual representation of the different methods of ssDNA synthesis following a SELEX selection cycle.

a) Asymmetric PCR amplification. b) Lambda exonuclease digestion of the antisense strand of DNA. c) Biotin-Streptavidin separation of the strands of DNA.

Asymmetric PCR is an alternate method of PCR, where the ratios of added primer are unequal to each other, favouring the generation of the sense DNA strand. This permits the rapid synthesis of the ssDNA selection pool for additional SELEX cycles, and has been used a number of times in SELEX (Williams and Bartel, 1995; Tang *et al.*, 2006; Avci-Adali, Paul, *et al.*, 2010).

Biotinylated DNA separation involves the affinity of a 5' labelled DNA strand to streptavidin coated magnetic beads in a basic environment, allowing for the digestion and elution of the non-biotinylated DNA strand. The magnetic beads are then able to separate and capture the biotinylated DNA strand by the addition of an external magnetic field, retaining the desired ssDNA strand (Strehlitz *et al.*, 2008).

The use of lambda exonuclease as a means of ssDNA synthesis is established on the 5' → 3' exonuclease digestion, degrading the antisense strand of the dsDNA PCR product, leaving an ssDNA strand behind (Avci-Adali, Paul, *et al.*, 2010). The exonuclease activity is promoted

by labelling the 5' end of the antisense DNA strand with an additional phosphate group, favouring the exonuclease digestion (Citartan *et al.*, 2011).

3.1.3.b. Methods for the removal of bound sequences from target cells for further cycles of selection

When considering the selection phase of SELEX, much variation exists in the literature describing SELEX protocols, especially in the separation of unbound sequences from the target and the subsequent elution of bound sequences from the target (Stoltenburg *et al.*, 2007). Many protocols, especially for cell-SELEX have been proposed in literature for the elution of bound sequences from the target.

One of the most commonly used methods of removing the bound oligonucleotide sequences from the cells during cell-SELEX, is heating the sample to 95 °C for 5 – 10 minutes e.g. Sefah *et al.*, 2010, Liu *et al.*, 2012 and Kim *et al.*, 2014. While intended to detach the oligonucleotides from the surface by melting them, it lyses cells and denatures cellular proteins, releasing the debris of the cell into solution. This may result in contamination of the aptamer by cellular nucleic acids.

Simultaneous cell lysis and collection of the oligonucleotides through the use of phenol: chloroform: isoamyl alcohol extraction of the ssDNA protocols followed by ethanol precipitation, has also been applied in cell-SELEX to extract ssDNA from cell surfaces (Hicke *et al.*, 2001).

Other explored methods of ssDNA removal of the cells include the treatment of the cells with the protease enzyme, trypsin. This method detaches the extracellular proteins from the cells, allowing subsequent stages to remove the oligonucleotides bound to the proteins from the cells. This has the shortfall of preferentially allowing oligonucleotide sequences that bind to protein targets on the cell surface to be selected for. Figure 3.2 below illustrates the anticipated composition of the various oligonucleotide-rich fractions before and after the proposed methods of detaching ssDNA from the cell surface have been performed.

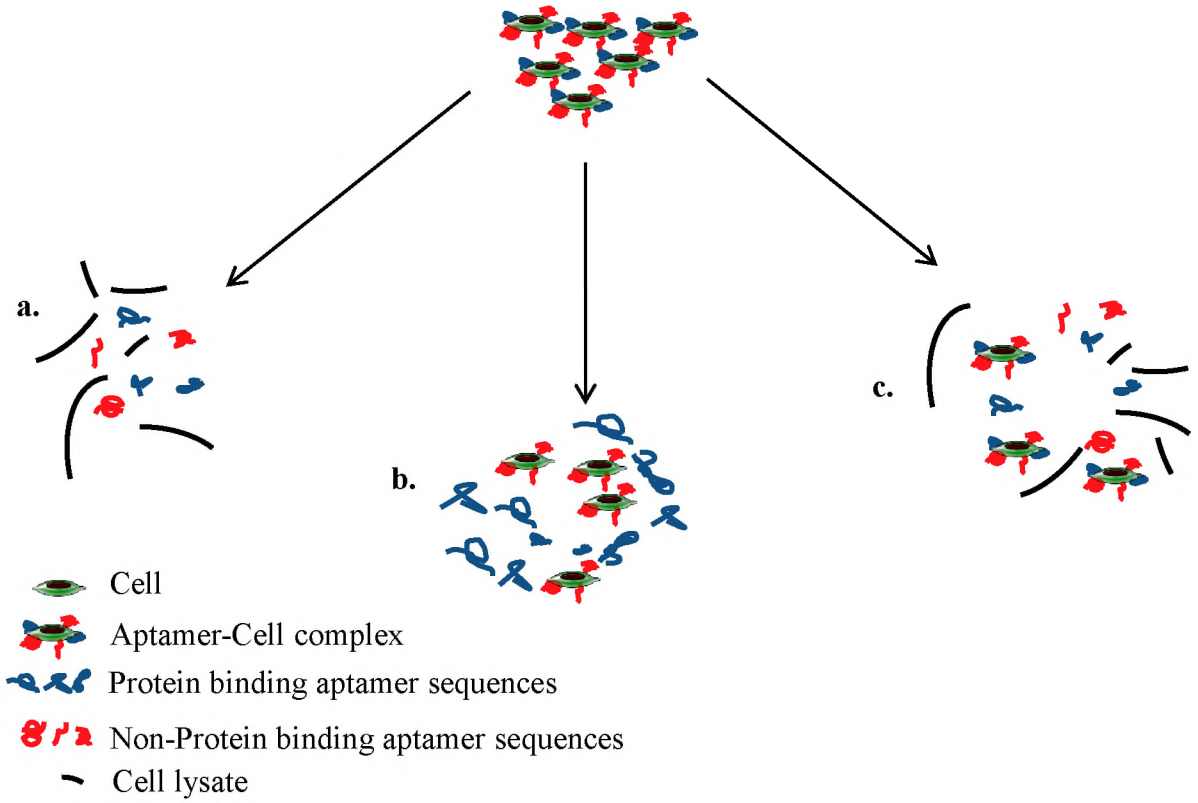

Figure 3.2; illustrative representative of the methods of commonly removing bound ssDNA during cell-SELEX.

a) Heating the cells up at 95˚C for 5-10 minutes. b) Trypsin treatment of the cells following cell-SELEX selection. c) phenol chloroform isoamyl alcohol extraction of the bound ssDNA sequences from the target cells.

As illustrated in Figure 3.2, the different methods of ssDNA removal from the target cell vary between one another by both the amount of cell lysate, and the binding sequences that are later selected as a result of the different practises for ssDNA removal from the target cell.

3.2. Objectives

The objectives of the work reported in this chapter was to report on the preparatory steps prior to initiating cell-SELEX. This included the following sub-objectives: analyse and monitor 3T3-L1 preadipocyte growth and differentiation, investigate and optimise a variety of ssDNA amplification techniques, and investigating the best method of removing the bound ssDNA library from the target cell line.

3.3. Methods and Materials

3.3.1. Tissue culture

Initially, 3T3-L1 preadipocytes were seeded and cultured in a 24 well plate, as mentioned in Chapter 2, section 2.2.2.a. where they later were differentiated, once they had reached confluence as mentioned in Chapter 2, section 2.2.2.d. Differentiation of the preadipocytes was allowed to take place for 13 days, before working with the adipocytes.

3.3.2. Tests for induced adipogenesis in 3T3-L1 preadipocytes

In order to confirm adipogenesis of the 3T3-L1 preadipocytes, Oil Red O staining of the cells induced to differentiate cells was evaluated (following 13 days, as detailed in Section 2.2.2.e) using the protocol proposed by Ramírez-Zacarías *et al.*(1992). The adipocytes were rinsed in a PBS solution and then soaked in 1 ml fixing solution (described in Chapter 2, section 2.2.2.e.i above), for 10 minutes at room temperature. The fixing solution was then replaced and the cells allowed to fix for an additional 1 hour at room temperature. Fixed cells were rinsed with two washes of distilled water. And a further wash with isopropanol working solution (described in Chapter 2, section 2.2.2.e.ii above) for 5 minutes at room temperature, to remove any excess fixative in solution.

A 10 minute exposure of the fixed cells to the Oil Red O staining solution proceeded at room temperature. The staining solution was subsequently rinsed out with four exchanges of distilled water.

Stained cells were visualised using both light microscopy and epifluorescent microscopy, as mentioned in Chapter 2, section 2.2.1.f above. The morphology of the cells was examined using phase contrast images of the adipocytes taken at 20 X magnification. Oil Red O fluorescence was visualised using the Zeiss Filter set 43 (excitation of approximately 525 - 575 nm and emission of approximately 575 - 650 nm).

3.3.3. dsDNA amplification and ssDNA synthesis optimisation for cell- SELEX optimisation

PCR amplification proceeded using the proposed protocol and apparatus detailed in Chapter 2, Section 2.2.3.a. A forward primer labelled at the 5' site with 6-FAM fluorophore was used to amplify DNA concentrations, to provide a fluorimetric means of quantifying DNA.

Two main methods to produce ssDNA were trialled: the production of dsDNA, followed by exonuclease digestion and the production of ssDNA during the PCR process, through the application of asymmetric PCR.

3.3.3.a. Lambda Exonuclease digestion

Following amplification of the candidate aptamer library for the selection assay, mentioned above, ssDNA was generated using lambda exonuclease digestion as detailed in Chapter 2, Section 2.2.3.b.

3.3.3.b. Asymmetric PCR amplification

Asymmetric PCR was adapted from the existing PCR protocol mentioned in Chapter 2, Section 2.2.3.a., and the process was briefly evaluated using a variety of different template and primer concentrations and proportions (see Table 3.1 below for alterations in the forward and reverse primer amounts), to best promote the synthesis of ssDNA, favouring the forward reaction. The denoted names of each of the asymmetric PCR reaction, relates to the type of DNA sequence (ssDNA or dsDNA), the primers (Forward, F and Reverse, R) used in the reaction and the amount of DNA used in the starting template in ng.

Table 3.1: Variations in initial template and primer amounts used during scoping study for asymmetric PCR reactions for ssDNA synthesis.

Reaction name	Template, ng (pmol)	Forward Primer (µg)	Reverse Primer (µg)
ssDNA	2.5 (0.0907)	18.2	2.00
dsDNAFR2.5	2.5(0.0907)	18.2	2.00
dsDNAF2.5	2.5 (0.0907)	18.2	0.00
dsDNAF10	10 (0.363)	18.2	0.00
dsDNAF50	50 (0.181)	72.0	0.00

All other reagents required for the PCR reactions were maintained as described in Chapter 2, Section 2.2.3.b. Optimisation of the cycle number proceeded as discussed in Chapter 2, Section 2.2.3.a. The amplification was allowed to take place for 40 amplification cycles using a MiniOpticon Real-Time PCR System. The purity and quality of amplification was evaluated by visualisation of the DNA after separation by PAGE gel electrophoresis (Chapter 2, section 2.2.1.c.).

3.3.4. Fluorescence standard curves used for ssDNA quantification

To fluorometrically quantify the relative amounts of ssDNA being released from the target cell line, a four-point standard curve was generated using known amounts of ssDNA in the binding buffer vs the RFU of the 5' 6-FAM – labelled sequences, the spectroscopic parameters were set as mentioned in Chapter 2, section 2.2.1.e, to analyse the ssDNA library extracted from the cell lysate

3.3.5. Cell-SELEX selection evaluation

Mouse 3T3-L1 preadipocytes were cultured and maintained in a 24 well plate, in the conditions mentioned above in Chapter 2, Section 2.2.2.a.

To investigate the recovery yield of oligonucleotide by various methods, a sample volume of 900 ng of the ssDNA library was diluted in binding buffer to a final concentration of 1 ng/ µl. 300 µl of the diluted library was added to three wells, with 3T3-L1 preadipocytes grown to confluency, in the 24 well plate, while 100 ng of ssDNA was set aside to act as a control.

The library was allowed to bind to the preadipocytes at 37 °C for 1 hour, on a horizontal orbital shaker at 50 rpm. The wells were washed 3 times with wash buffer.

The preadipocytes were then subjected to the varying detachment methods outlined below, in sections 3.3.5.a. to 3.3.5.d.

The extracted ssDNA was quantified using both fluorescence spectroscopy (see Chapter 2, section 2.2.1.e. above) and UV/ Vis absorption spectrophotometry, using the NanoDrop2000.

3.3.5.a. Heat bound ssDNA elution

The elution of the bound ssDNA sequences from the target cells was adapted from the methods set out by Sefah *et al.*, 2010. The selection sample was heated to 95 °C for 10 minutes, followed by centrifugation at 3100 x *g* for 5 minutes; the supernatant was removed and assayed for ssDNA.

3.3.5.b. Trypsin treatment for ssDNA elution of target cells

Following exposure of the cells to the oligonucleotide library, the 3T3-L1 cells were centrifuged at 800 x *g*, the buffer was then replaced with 100 µl 1 X trypsin solution (purchased from Sigma-Aldrich, original stock of 10 X) and incubated at 37 °C for 15 minutes. The trypsin, was deactivated by adding 100 µl DMEM (containing 5 % FCS, to discontinue the trypsin digestion) to the reaction tube.

The solution was then centrifuged at 3100 x *g* for 5 minutes, the supernatant there after separated from the cell lysate and assayed for ssDNA.

3.3.5.c. Trypsin treatment and heat denaturation of cells for ssDNA elution

3T3-L1 cells were centrifuged at 800 x *g*, the water was then replaced with 100 µl 1 X trypsin solution and incubated at 37 °C for 15 minutes. The trypsin reaction was deactivated by adding 100 µl DMEM (containing 5 % FCS).

The cells were then heated to 95°C for 10 minutes followed by centrifugation at 3100 x *g* for 5 minutes, the supernatant was then separated from the cell lysate and quantified.

3.3.5.d. Phenol: chloroform: isoamyl alcohol ssDNA (25: 24: 1 v/ v/ v) elution

3T3-L1 cells were separated from the ssDNA using the phenol: chloroform protocol proposed by (Urak *et al.*, 2016). The cells were added at a 1: 1 ratio with phenol: chloroform: isoamyl alcohol ssDNA (25: 24: 1 saturated with 100 mM Tris, pH 7.5), and vortexed until an emulsion formed. The solution was centrifuged at 7378 x *g* for 5 minutes. The aqueous layer was removed and set aside. An additional 100 µl of sterile distilled water was added into the

Eppendorf tube with the phenol: chloroform: isoamyl alcohol and centrifuged at 7378 x *g* for an additional 5min. after the removal of the aqueous layer. 1 ml pure ethanol, 30 µl 3 M Sodium acetate, and 3.3 µl 20 % Glycogen was added to the aqueous layer. The solution was then stored overnight at -20 ˚C.

Following overnight incubation, the solution was centrifuged at 7378 x *g* for 30 minutes at 4 ˚C. The supernatant was removed and 1 ml ice-cold 80 % ethanol was added, the solution was further centrifuged for 30 minutes at 7378 x *g*, at 4 ˚C. The pellet was allowed to dry for 2 – 3 hours, followed by resuspension in 30 µl sterile MiliQ water.

3.3.5.e. Standards and controls used in the removal of ssDNA from the cell surface

A standard control of 200 ng of ssDNA library was removed directly from the binding buffer and DMEM nutrient media using the NucleoSpin® Gel and PCR protocol to evaluate the efficiency of ssDNA removal techniques from the target molecule.

3.4. Results and Discussion

3.4.1. Mycoplasma screening of target cells

As mentioned in Chapter 2, section 2.2.2.c., the 3T3-L1 preadipocytes were screened for the contamination of *Mycoplasma* spp whenever the cells were sub-cultured. This was achieved using a PCR-based assay set to amplify the variable regions of the 16S rRNA gene in *Mycoplasma* spp, between base pair regions 744 - 1055. To be indicative of *Mycoplasma* contamination, an amplicon band of approximately 270 bp is expected on an agarose gel (Ossewaarde *et al.*, 1996). Figure 3.3 illustrates a typical PCR outcome for the routine screening of the cultured tissues for *Mycoplasma* contamination.

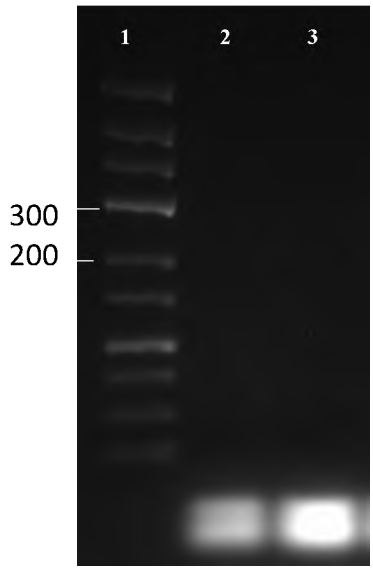

Figure 3.3: 4 % Agarose gel electrophoresis gel for evaluation of Mycoplasma contamination within a sample of cultured 3L3-L1 preadipocytes.

Lane 1: GeneRuler Low Range DNA Ladder; Lane 2: Negative control; Lane 3: 3T3-L1 preadipocyte sample in DMEM nutrient media.

The lack of amplification in the cell lysate between the 200 bp and 300 bp markers of the ladder (Figure 3.3) demonstrates no amplification of the *Mycoplasma* spp. 16S gene, either circulating within the nutrient media, or attached to the cell surface of the cultured preadipocytes. This indicated that the cells were free of *Mycoplasma* contamination. Routine screening of cultured cells for contamination of *Mycoplasma* spp. was performed consistently throughout experimental analysis. This was to confirm that the culture of 3T3-L1 preadipocytes, and the integrity of the preadipocytes had not been affected by *Mycoplasma* spp. contamination.

3.4.2. 3T3-L1 differentiation evaluation

In order to validate that induced adipogenesis was occurring, and to evaluate the time taken for cultured 3T3-L1 to predominantly exhibit adipogenic traits following the introduction of differentiation media, differentiating cells were closely monitored by microscopy every two days for morphological changes and for the presence of lipid vacuoles. Kramer *et al.* (2014), reported that 14 days of differentiation is sufficient to demonstrate enough fatty lipid formation, indicating that mature adipocytes have formed. To confirm this, 3T3-L1 preadipocytes were allowed to differentiate for 13 days before Oil Red O fluorescent staining

(as 13 day adipocytes were used as for the negative selection for cell-SELEX). Figure 3.4 below demonstrates, the evaluation of 3T3-L1 preadipocyte adipogenesis over a 13 day period.

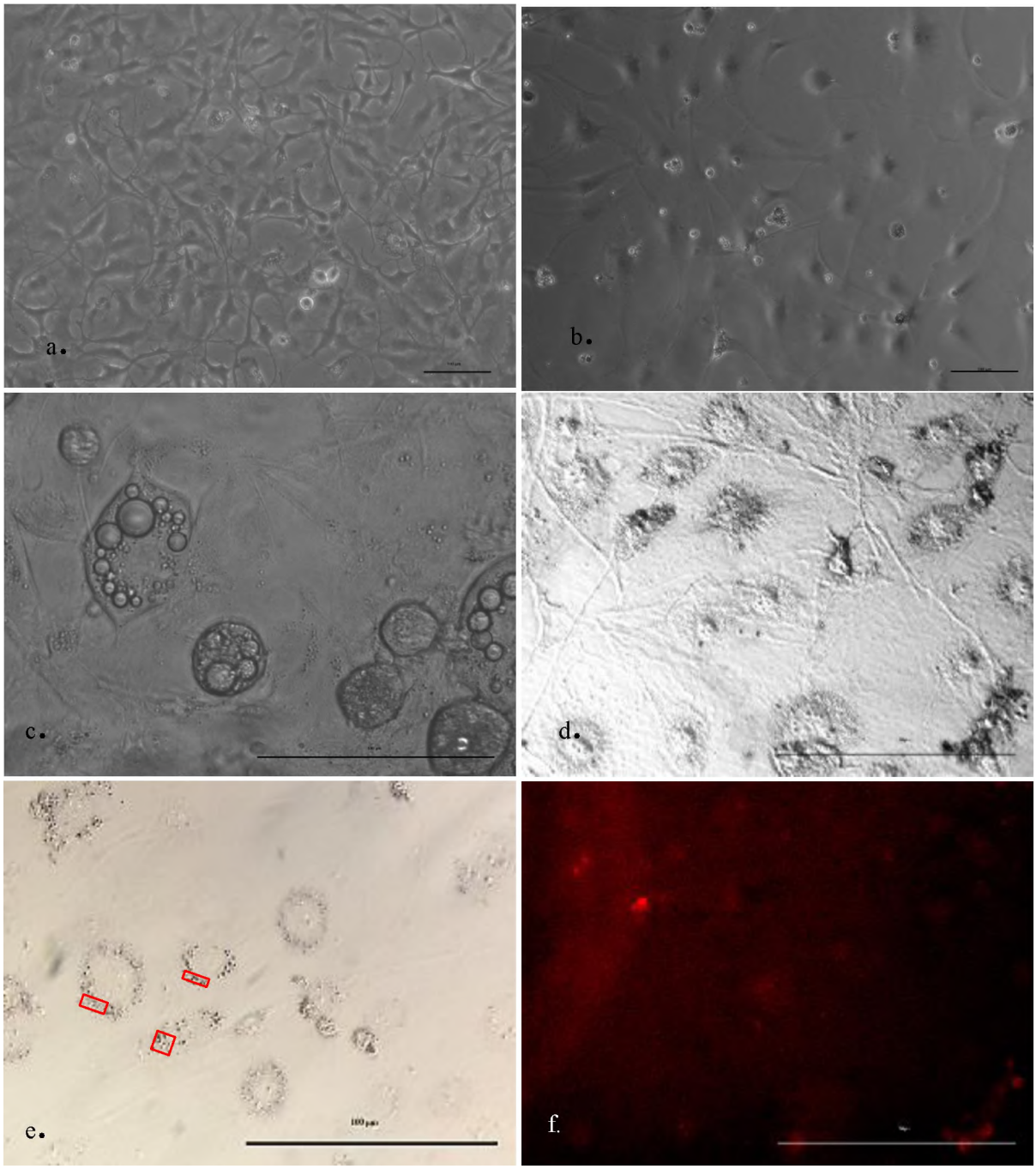

Figure 3.4: Micrograph analysis of 3T3-L1 preadipocyte differentiation with time.
Scale bar in each micrograph represents 100 µm.

a) 10 X magnification phase contrast micrograph of preadipocytes following 1 day differentiation. b) 10 X magnification phase contrast micrograph following 7 days' differentiation. c) 40 X magnification phase contrast micrograph of preadipocytes following 11 days' differentiation. d) 20 X magnification phase contrast micrograph of preadipocytes following 13 days' differentiation. e) Light micrograph showing at 20 X magnification, showing Oil Red O staining of the preadipocytes (dark circles, exemplars of the staining highlighted in red boxes) following 13 days' differentiation. f) Epifluorescent micrograph at 20 X magnification evaluation of the adipocytes stained with Oil Red O.

This study sought to evaluate the differentiative state of 3T3-L1 preadipocytes from the first day of differentiation until complete differentiation. This is readily visible in Figure 3.4.a. where the cells still demonstrate a fibrous cellular morphology one day after inducing differentiation; slowly transforming to the lipid-rich adipocytic morphologies that are readily visible 11 days' post-induction, onwards (Figure 3.4.c. and 3.4.d). Oil red O staining of the adipocytes confirmed the presence of lipid-rich vacuoles, as seen in Figure 3.4.e. (Kramer *et al.*, 2014) demonstrated similar differentiation and Oil Red O staining results after 10 days' post initiation of 3T3-L1 preadipocyte differentiation. Other research done by Ramírez-Zacarías *et al.*, in 1992 claims and confirms, using Oil Red O staining techniques, that complete adipogenesis in 3T3-L1 preadipocytes took~8 days.

Epifluorescence evaluation of the Oil Red O dye was further evaluated, using the red filter set, and can be seen in Figure 3.4.f. Lipid rich cells tend to fluoresce in the red wavelength.

Hemocytometry indicated that the density of the adipocytes within the culture media decreases from~$9x10^2$ cells/ mm^2 to approximately~$4.60x10^2$ cells/ mm^2. This drop in the cell density could be the result of cellular lysis during adipogenesis of the 3T3-L1 preadipocytes. This additionally allows for a negative selection of aptamers to the polystyrene surface of the culture dish to take place.

3.4.3. ssDNA synthesis optimisation for cell- SELEX optimisation

Initially, asymmetric PCR was performed with a variety of primer and template conditions, including reactions with both forward and reverse primers added at different ratios, and with dsDNA template with forward primer only. To investigate the effect of product yield and concatemer formation for asymmetric PCR with two different amounts of reverse primer alongside a standardised forward primer amount, using a standardised template of 2.5 ng was used for the dsDNAFR and the dsDNA2.5 asymmetric PCR reactions (described in Table 3.1) and compared using gel electrophoresis, as seen in Figure 3.5 below.

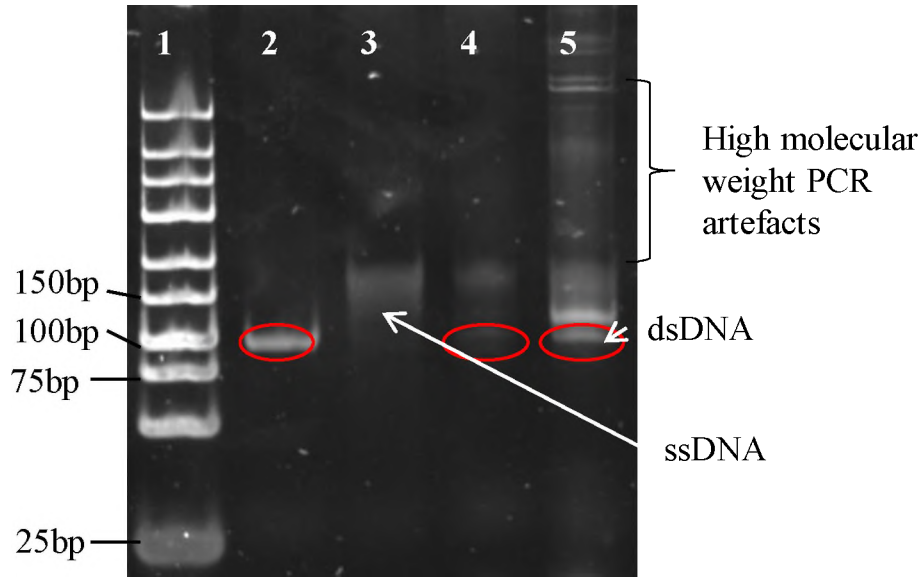

Figure 3.5: 10 % PAGE gel comparing ssDNA synthesis methods between Lambda exonuclease digestion and asymmetric PCR.

Areas corresponding to the expected presence of dsDNA are circled in red.
Lane1: GeneRuler Low Range DNA ladder. Lane2: 7.5 ng 90 bp dsDNA template. Lane3: lambda exonuclease digested ssDNA. Lane4: sample dsDNAF2.5. Lane 5: A-PCR, sample dsDNAFR2.5 (mentioned in Table 3.1).

Comparing Lanes 2 and 3 in Figure 3.5, demonstrates that ssDNA migrates at a slower rate than dsDNA. The sample of ssDNA does not migrate consistently, resulting in a smeared appearance for the visualised ssDNA, rather than the compact band visible in Figure 3.5, Lane 2. In PAGE gels, the rate of migration is based on the characteristics of the primary and tertiary ssDNA structure, giving a more variable migration pattern, whereby larger loop tertiary structures in the ssDNA do not pass though the gel's pores as easily as dsDNA molecules (Stellwagen and Stellwagen, 2008).

GelRed is twice as sensitive to dsDNA than it is to ssDNA, this results in ssDNA not being illuminated by the gel imaging software as clearly as dsDNA following gel electrophoresis, according to the product manual (FluoProbes, n.d.).

The initial testing of asymmetric PCR (Figure 3.5) indicated that while some ssDNA was being generated under these conditions, a substantial proportion of the amplicon consisted of amplification artefacts. It was suggested that to prevent concatemer formation (as presented in Figure 2.1 above) was to use a dsDNA template for the asymmetric PCR reaction, and that

the use of both forward and reverse primer with a dsDNA template creates amplicons of high molecular weight and concatemer formation in the PCR product (Figure 3.5).

An investigation into asymmetric PCR using a variety of dsDNA template concentrations was conducted as to evaluate whether it was possible maximise the production of ssDNA with the minimal synthesis of a dsDNA concatemer product, through varying of the primer proportions, concentrations and template concentrations. The composition of the resultant amplified DNA has been illustrated below in Figure 3.6.

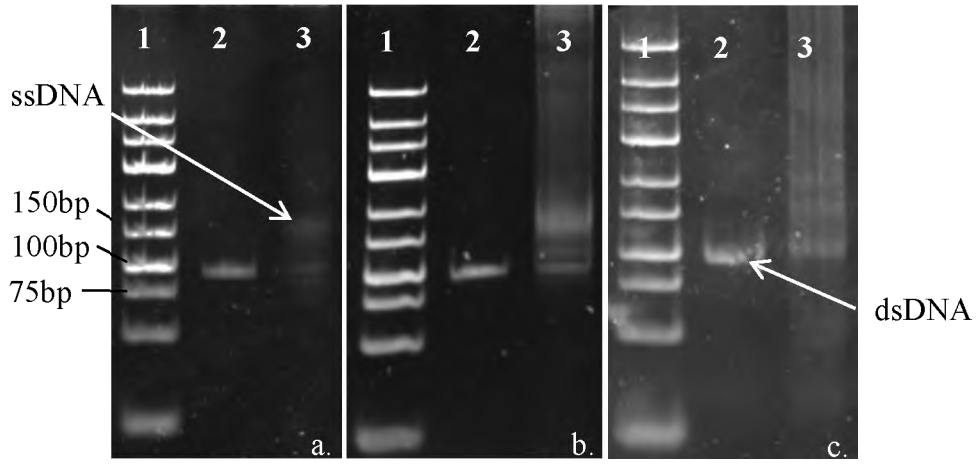

Figure 3.6: 10 % PAGE gel illustrating differences in the product between the different A-PCR reactions run with different template amounts, as set out in Table 3.1.

a) Asymmetric PCR from the dsDNA10 reaction. Lane 1; GeneRuler Low Range DNA Ladder. Lane 2; 7.5 ng 90 bp dsDNA template. Lane 3; dsDNA2.5 A-PCR reaction. b) Asymmetric PCR from the dsDNA10 reaction. Lane 1; GeneRuler Low Range DNA Ladder. Lane 2; 7.5ng 90bp dsDNA template. Lane 3; dsDNA50 A-PCR reaction. c) Asymmetric PCR from the dsDNA50 reaction. Lane 1; GeneRuler Low Range DNA Ladder. Lane 2; 7.5 ng 90 bp dsDNA template. Lane 3; dsDNAFR A-PCR reaction.

By visual analysis of the separated amplification products following asymmetric PCR (Figure 3.6), the dsDNA2.5 and dsDNA10 reactions (which vary in the amount of dsDNA template used in the reaction) showed the purest form of ssDNA product being formed: lower template levels being used in the asymmetric PCR reaction decreasing the chances of artefact formation during the PCR reaction (as was annotated in Figure 3.5). To quantify the yields of dsDNA being produced from each asymmetric PCR reaction, UV/Vis ssDNA quantification of column-purified ssDNA samples was performed (see section 2.2.1.d. for purification protocol). In addition, densitometry analysis of the bands in the PAGE gels was performed to

evaluate the relative intensity of dsDNA in each lane, using the control 7.5 ng of dsDNA template (Lanes 2; Figure 3.6) to measure the band intensity of the dsDNA. Combined, this indicated the yield and purity of ssDNA arising from the different asymmetric PCRs is illustrated in Figure 3.7 below quantifies these findings.

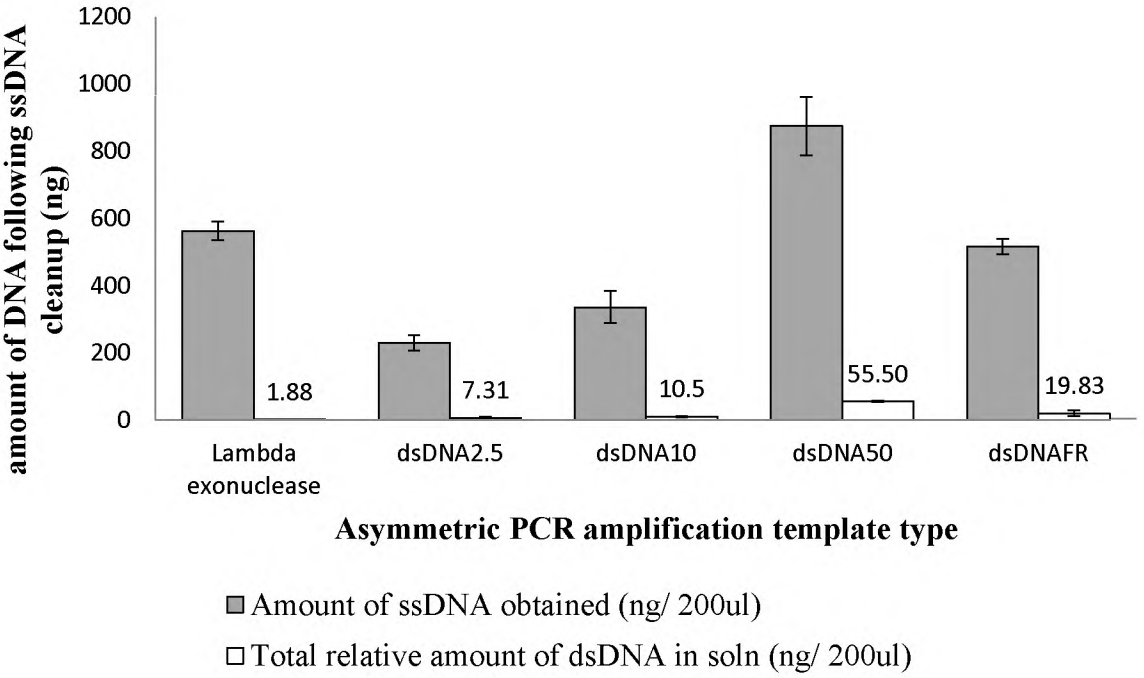

Figure 3.7: Representative bar graph illustrating the relative amounts of ssDNA product from densitometry analysis(grey) with that of the dsDNA template put into the asymmetric PCR reaction (white) / 200 µl reaction.

The proportionate percentage of the dsDNA (densitometry analysis of PAGE) compared to the total DNA present in the sample (UV/VIS spectrophotometry) is presented above the relative amount of dsDNA. Error bars represent the standard error for UV/Vis spectrophotometric measurements, n = 4.

Alteration of the template concentrations, and the concentration of reverse primer resulted in asymmetric PCR products possessing greatly different amplification yields and purity, when assessing the resultant ssDNA. Although significantly less ssDNA is produced in the dsDNA2.5 (230.2 ± 23.2 ng produced / 200 µl) and dsDNA10 (336.5 ± 48.0 ng produced / 200 µl), compared to the other two tested conditions, it appears the amounts of dsDNA contaminating product is substantially less than that of the dsDNA50 (876.2 ± 87.2 ng produced / 200 µl) reaction.

Much of the tested asymmetric PCR protocols confined the dsDNA proportion to approximately 3 – 4 % of the total DNA present in the sample. The sole exception to this is dsDNA50 (prepared using 50 ng of the dsDNA template) which had a much higher proportion of dsDNA present within the sample following amplification. This, combined with the evidence of concatemer and high molecular weight amplicons visible for dsDNA10 and dsDNA50 samples (Figure 3.6)

This suggests that smaller amounts of ssDNA are produced during asymmetric PCR with lower template concentrations. The quality of the ssDNA product, using a mixed dsDNA sequence library as a template for asymmetric PCR, generates a higher quality ssDNA product than that of asymmetric PCR with higher dsDNA template concentrations. The suggestion of the reduction of product quality with greater than 30 cycles of PCR suggested by Citartan *et al.*, (2012), does seem valid.

To evaluate the most efficient template amount, the ratio of ssDNA product: template DNA added was analysed. This demonstrated that using the dsDNA50 reaction did not promote the highest ratios of ssDNA to template, as the dsDNA contamination was higher than that of the dsDNA2.5 reaction.

Lambda exonuclease digestion proved to have a significantly higher production of ssDNA approximately 565.9 ± 27.8 ng/ 200 µl, and the relative amounts of dsDNA contamination was significantly lower, with 1.88 ± 1.22 ng/ 200 µl of dsDNA contamination, to that of all the asymmetric PCR methods evaluated. Hence, lambda excision was maintained as the means of generating ssDNA for all future SELEX amplifications.

3.4.4. Fluorescent spectra analysis of the 5'modified 6-FAM forward primer

The fluorescent spectra of the 6-FAM labelled forward primers was evaluated to confirm that excitation and emission spectra are similar to published spectral profile. Figure 3.8 illustrates the fluorescent spectrum of the 5' modified 6-FAM forward primer sequences.

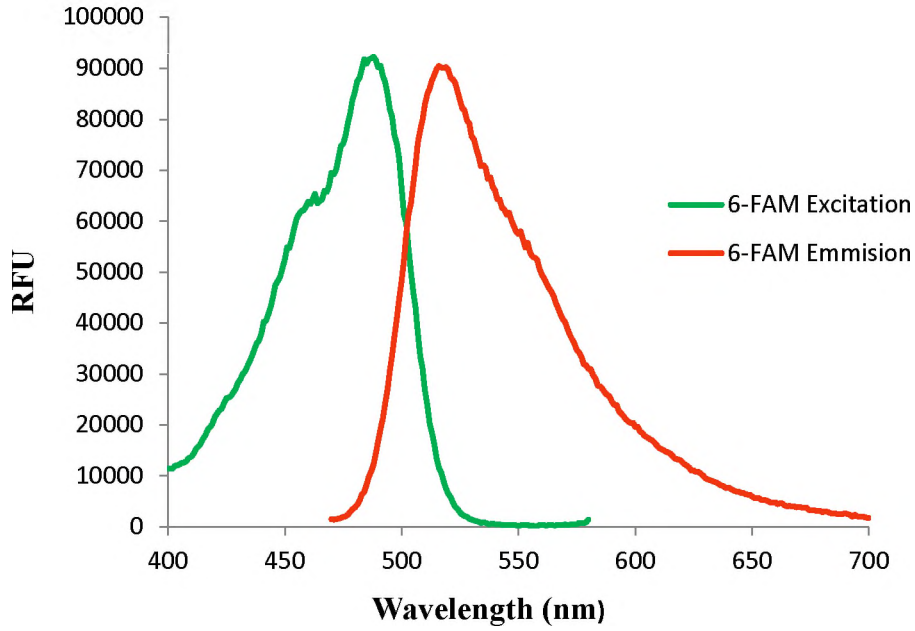

Figure 3.8: Excitation and emission spectra of the 6-FAM 5' labelled forward primer sequence between 400 nm and 700 nm.

The primers were made to a concentration of 1 µM in binding buffer (mentioned in section 2.2.1.b.).

The fluorescent spectra of the 5' 6-FAM labelled primer regions in binding buffer demonstrate similarities in both excitation and emission as cited in literature (Parish, 1999; Ishikawa-Ankerhold *et al.*, 2012). The excitation of 6-FAM demonstrated an excitation maximum at 480 nm and emission max at 518 nm.

3.4.5. Cell-SELEX selection Optimisation

Potential contaminants in solution could possibly affect the absorbance measurements of the NanoDrop2000 when evaluating the DNA concentration following a selection cycle of cell-SELEX. These contaminants include: genomic DNA, protein contaminants, and chemical contaminants used during the purification of the ssDNA for binding evaluation. To evaluate this, a mock selection cycle was set up to compare differences in the removal and purification of ssDNA candidate aptamers from cells, following a cell-SELEX cycle. Figure 3.9 below graphs the differences in yield between the various detachment protocols trialled, comparing both fluorescence spectroscopic evaluation of fluorophore-tagged oligonucleotides and UV absorption quantification of the extracted ssDNA library.

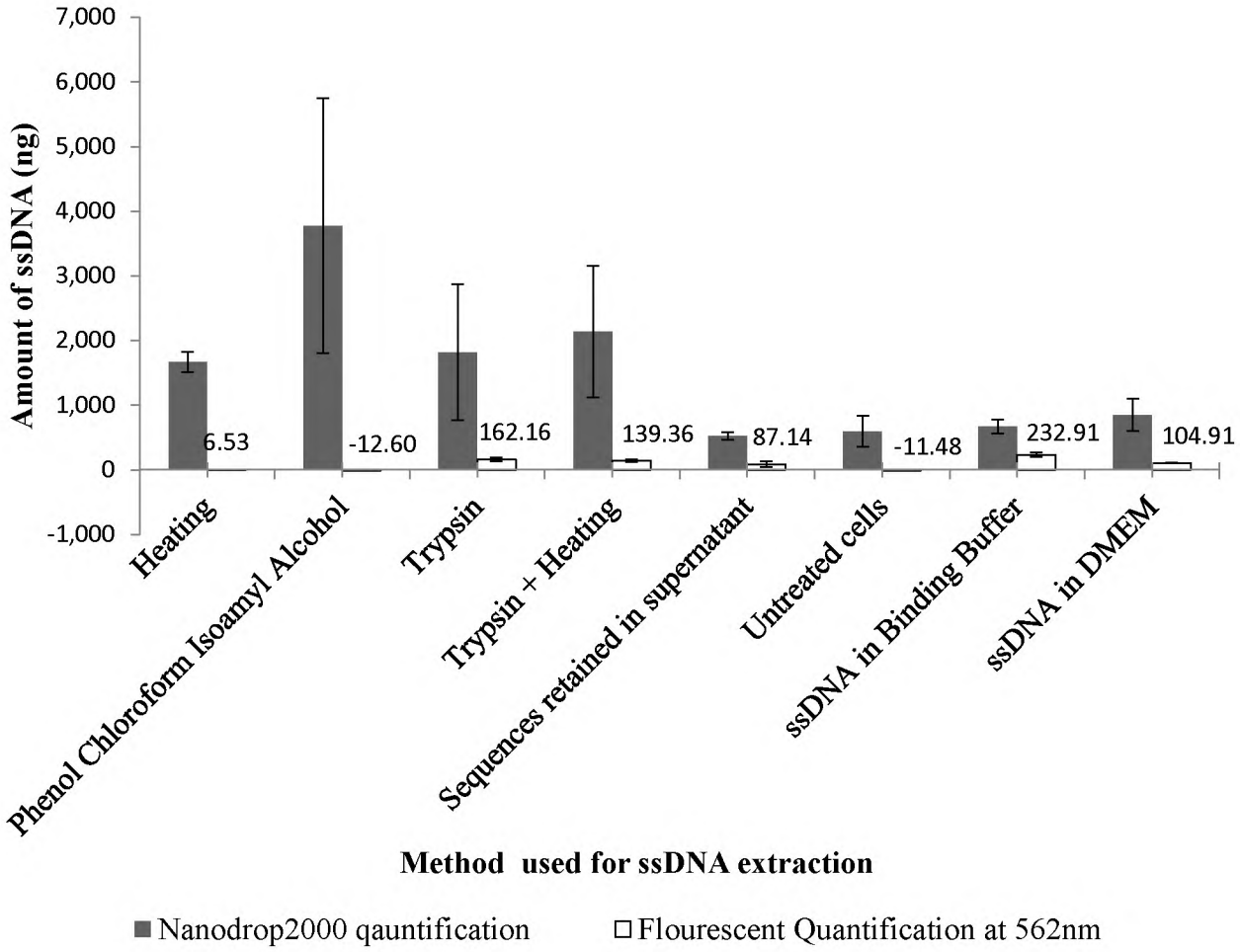

Figure 3.9: Evaluation of ssDNA separation from cellular targets between the various detachment protocols trialled, comparing UV/VIS spectrophotometry and fluorescent spectroscopic methods of DNA quantification

The ssDNA was quantified both through NanoDrop 2000 UV/VIS absorbance readings (dark grey), and 5' fluorescently labelled DNA (6-FAM) (light grey), at an excitation of 480nm and endpoint emission of 562 nm.
The following methods of extraction of the bound ssDNA library from the target sequence were tested: heating the cells to 95 °C, phenol: chloroform: isoamyl alcohol, trypsin, and trypsin with the addition of heating the cells to 95 °C.
The controls (ssDNA in binding buffer and ssDNA in DMEM), were evaluated using 200 ng of ssDNA library in the relevant solvents, and were extracted from both binding buffer and DMEM using a spin column. Error bars represent the standard error n = 3.

The graph shows that UV/ Vis spectrophotometric quantification of ssDNA from the extracted samples frequently overestimates the amounts of ssDNA extracted from the reaction. The elevated levels of ssDNA isolated and quantified by the NanoDrop2000 are attributed to the release of cellular components into the fraction, as illustrated above. ssDNA samples isolated from the binding buffer and nutrient media were similar to one-another, indicating little interference arising from the cell culture media. Furthermore, the possible

presence of phenol, in from the phenol: chloroform: isoamyl alcohol, absorption spectra ranging between 260 and 280 nm (Krauss *et al.*, 1994) extraction protocol, is attributed to the large increase in measured ssDNA via the near UV/ Vis quantification of nucleic acids between 260 and 280 nm (English *et al.*, 2006).

These elevated levels of ssDNA isolated are visible range between 2.5 – 5.6 fold greater than the value obtained from the addition of 200 ng of ssDNA placed in binding buffer only. This sample, itself, had an overestimated amount of ssDNA as quantified by UV/Vis spectrophotometry, 668.7 ± 236.9 ng / 200 µl. This demonstrates the inaccuracy of predicting the amounts of ssDNA eluted from the target cell using UV/ Vis spectroscopy.

In order to obtain a more accurate evaluation of ssDNA library extracted, an ssDNA library 5' labelled with 6-FAM fluorophores, using fluorescence spectroscopy, were compared to that of the NanoDrop2000 absorbance readings, as seen in Figure 3.9 above. In all cases, the quantities of aptamers detected by fluorescent emission was significantly lower than that of the NanoDrop2000 except within the controls: ssDNA in binding buffer, DMEM control selection and the washout control. Where Figure 3.9, illustrates an RFU intensity of 232.9 ± 36.4 ng ssDNA/ 200 µl of ssDNA extracted, with NanoDrop values of 668.7 ± 104.6 ng ssDNA/ 200 µl isolated from the binding buffer. The DMEM nutrient media ssDNA isolation control demonstrated an RFU intensity of 104.9 ± 3.1 ng ssDNA / 200 µl extracted, with NanoDrop values of 850.0 ± 250.4 ng ssDNA/ 200 µl isolated. The negative control sample of untreated cells lacking the fluorescently - tagged ssDNA library, demonstrated that 668.7 ± 236.9 ng ssDNA/ 200 µl from the NanoDrop2000 measurements with an RFU value at 562 nm having an equivalent of -11.5 ± 2.5 ng / 200 µl of added ssDNA. These results illustrated that the release of UV - absorbing compounds from the target cell lysate were detected by the NanoDrop2000 DNA quantification, while the untreated target cells do not release compounds capable of interfering with the florescence measurements.

A comparison between the fluorescent responses of the ssDNA library between the ssDNA in binding buffer control, trypsinisation extraction of ssDNA, and the two other extraction methods (heat and phenol: chloroform extraction) indicated that trypsinisation produced fluorescent responses very similar to those of the ssDNA in binding buffer. The extraction of ssDNA from the cells using the phenol: chloroform: isoamyl alcohol (25: 24: 1 v/ v/ v) creates a similar pattern to that of the untreated cells, suggesting that insignificant amounts of

ssDNA could be separated from the cells and extracted using this procedure. Despite the larger yields realised by the detachment of ssDNA aptamers from cells using trypsin (162.16 ± 27.87 ng) or heating and trypsin (139.36 ± 18.49 ng), heating of the cells to detach the bound ssDNA (6.53 ± 2.08 ng) was selected as the treatment for further SELEX processes.

The treatment and extraction of bound ssDNA from the target cell allows for the selection of the cell to any potential ligand on the cell surface (Sefah *et al.*, 2010). Treatment of the cells with trypsin might narrow the potential binding targets during aptamer generation, by targeting only extracellular and integrin proteins presented on cell surfaces.

3.5. Conclusions

Publications suggest that complete adipogenesis, in 3T3-L1 preadipocytes, takes ~8 days for the complete differentiation of the preadipocytes into mature adipocytes (Russell and Ho, 1976). The reported Oil Red O assay, illustrated in Figure 3.4 above, confirms that true adipogenesis had occurred in the preadipocytes after 13 days' post initiation of differentiation. In this case 14 days was maintained as a standard for all the experimentation completed in this research project.

Large quantities of ssDNA, with minimal concatemer production can be generated using asymmetric PCR techniques (Figure 3.7), but it is evident that the template DNA remains as a by-product of the asymmetric PCR reaction. Lambda exonuclease on the other hand requires greater amounts of dsDNA prior to the digestion of the dsDNA temple, but the results of lambda exonuclease digestion demonstrates a sample that has limited amounts of dsDNA contamination after the digestion of the antisense DNA strand.

Evaluation into the top methods of removing the bound ssDNA library from the cell surface suggests that the greater number of sequences removed from the surface of the target cell is most likely using trypsin digestion of cell surface proteins, this method limits the variety of potential target sites for the aptamer on the cell surface. To maintain the target diversity though out the cell-SELEX procedure, the heating up of the cells to 95 °C was selected as the standard method used for the removal of bund ssDNA from the target cell surface throughout SELEX.

Chapter 4 : Generation of ssDNA Aptamers for Murine 3T3-L1 preadipocytes

4.1. Introduction

4.1.1. Biosensors and bio-detection methods

As mentioned in Chapter 1, Section 1.4, the ordering of the oligonucleotide residues in the aptamer's sequences (i.e. the primary structure) is essential to both the secondary and tertiary structuring of the aptamer. This, in turn, dictates the three-dimensional shape of the folded aptamer, that is an essential aspect of the binding affinity of a given aptamer to its respective target ligand (Batey *et al.*, 1999; Tan *et al.*, 2012; Haller *et al.*, 2013).

Intra-strand base pairing in the oligonucleotide sequences creates a variety of hairpin loops and bulges within the aptamer, which provide potential active sites for the aptamer to bind to the target ligand. In addition to nitrogenous base pairing within the aptamer, additional intramolecular forces participate within the tertiary structure of the aptamer.

As further outlined in Chapter 1, Section 1.4, aptamers are generally selected for through a process commonly defined as SELEX (Sefah *et al.*, 2010). Whereby the aptamers are selected for by a series of repeating steps, discarding sequences from the library that demonstrate limited affinity toward the target ligand while amplifying sequences that have a high affinity towards the desired ligand.

4.1.2. Alternate Methods of SELEX selection

When generating aptamers using cell-SELEX (Chapter 1, Section 1.4.1), there is no specific protocol that can be applied for the selection of an aptamer to an intended target cell. Despite this, there have been several frequently-practised selective methods reported to generate aptamers. These are proposed to increase the specificity of the selection toward a desired variant of the intended target molecule (Xi *et al.*, 2014).

In order to remove binding sequences from the library capable of nonspecific binding of target ligand expressed on the surfaces of a structurally similar cell line to the intended target, a "negative selection" step is performed (Green and Murthy, 2009; Xi *et al.*, 2014). This phase involves identifying sequences within the oligonucleotide pool capable of binding to similarly expressed (in the case of cell-SELEX) analyte molecules, and eliminating them

from subsequent phases of SELEX. This type of selective steps has often been used during cell-SELEX e.g. as a method of selecting between diseased and healthy cell types for cell-SELEX (Tang *et al.*, 2007; Guo *et al.*, 2008). In addition, this method is used to select against the surface matrices that cell-SELEX is taking place on (Xi *et al.*, 2014).

4.1.3. Variations of PCR to control the replication fidelity

During SELEX, the replication fidelity of the PCR reaction often is controlled to either increase – or maintain – the diversity of the amplicon. This is possible by altering reaction conditions to promote either mutagenic (error prone) or high-fidelity replication. Mutagenesis is typically performed in the earlier stages of SELEX, to generate and screen variants of strongly binding sequences (Stoltenburg *et al.*, 2007). To retain high affinity sequences and reduce mutagenesis, high - fidelity replicating PCR protocols are often used in the later rounds of SELEX to increase variation and possibly greater affinity in aptamers that already readily selectively bind to the desired target (Stoltenburg *et al.*, 2007).

Mutagenic conditions during PCR is readily achieved by increasing the $MgCl_2$ concentrations from $1.5x10^{-3}$ M to $7x10^{-3}$ M, and including approximately $2x10^{-4}$ M $MnCl_2$ into the reaction mixture as reported by (Cadwell and Joyce, 1992). The increase in salt concentration results in the polymerase to lose fidelity, resulting in random mutagenesis. (Eckert and Kunkel, 1990; Cadwell and Joyce, 1992) reported that the fidelity of the *Taq* polymerase is reduced to $2.67x10^{-2}$ - $4.57x10^{-2}$ % per bp / cycle PCR amplification, compared to the baseline rate of $1.03x10^{-3}$ % per bp/ cycle under normal PCR conditions.

To increase the specificity of primer annealing to template molecules during PCR, two major variants of PCR are used: "hot start" and "touchdown". Hot start PCR uses an initial heating of the reaction product from room temperature to 95 °C, holding the temperature for 5 – 10 minutes. This allows any preliminary primer-primer and primer-template complexes to be denatured (Aquila *et al.*, 1991). Subsequent cooling to the appropriate annealing temperature allows for accurate binding of the primer to the template for the first PCR cycle, decreasing ssDNA - dsDNA artefacts and increasing the fidelity of PCR, overall (Aquila *et al.*, 1991; Elnifro *et al.*, 2000).

Touchdown PCR on the other hand is the result of adjusting the annealing temperature during the early cycles of PCR. The temperature is initially set a few degrees higher than the calculated primer melting temperature (T_m) of the primer sequences (Korbie and Mattick,

2008) and is lowered to the theoretical T_m over a number of cycles. This method of PCR allows for specific primer binding to occur during the first few cycles of PCR (Korbie and Mattick, 2008).

4.1.4. Sequence analysis and evaluation of aptamer sequences

Following the generation and sequencing of the final SELEX selection pool, it is often reported that there is a high diversity of sequences that are gathered from the final SELEX selection pool. The candidate aptamers need to be separately sequenced and evaluated in order to identify the best aptamers present in the pool (Blind and Blank, 2015).

This proceeds through many separate phases, starting with the identification and elimination of any potential amplification artefacts still retained by the SELEX pool (Sefah *et al.*, 2010). The remaining sequences need to be evaluated with *in silico* analysis, comparing their primary structures and the predicted secondary and tertiary structures of the candidate aptamer sequences. Subsequently, candidate aptamers need to be evaluated for their functional capability to bind to the target analyte *in vitro*.

In silico analysis of the obtained sequences allows the researcher to taxonomically group the aptamers, separating them into families based on the similarity of the aptamer sequences that were gathered. This is most easily achieved through the use of a multiple sequence alignment (MSA) algorithms (Blind and Blank, 2015). Grouping aptamers in this manner allows for the subsequent screening of aptamer sequences on a family-by-family basis, as opposed to a sequence-by-sequence basis by selecting an archetypal aptamer sequence per family for trialling purposes. MSA analysis also serves to identify conserved regions within the families (Kim *et al.*, 2010) indicating regions that might be crucial to effecting binding between the aptamer(s) and target molecule(s).

4.1.4.a. Multiple sequence alignment software

There are a variety of MSA algorithms and software available to align both amino acid and nucleotide sequences. Each MSA algorithm applies a different approach to the alignment of the sequences (Edgar and Batzoglou, 2006). The variety of MSA include the multiple sequence comparison by log expectation (MUSCLE) (Edgar and Batzoglou, 2006), ClustalW (Thompson *et al.*, 1994), Multiple alignment using fast fourier transform (MAFFT) (Katoh *et*

al., 2002; Katoh and Standley, 2013) and the tree-based consistency objective function for alignment evaluation (T-Coffee) MSA (Notredame *et al.*, 2000).

Edgar and Batzoglou (2006) and Sviatopolk-Mirsky *et al.* (2014), independently investigated the efficiency of a variety of MSA algorithms that include MAFFT, ClustalW, T-Coffee and MUSCLE. The algorithms were evaluated for the accuracy of the alignment, time taken, and the processing requirements of the alignment. (Edgar and Batzoglou, 2006) demonstrated that although the ClustalW MSA took the least time and processing requirements, it was less accurate to that of the MAFFT and MUSCLE MSA. It was noted that MAFFT took greater lengths of time and processing to align the sequences, to that of the MUSCLE and ClustalW MSA software. Furthermore both Edgar and Batzoglou (2006) and Sviatopolk-Mirsky Pais *et al.* (2014), concluded that MUSCLE was more accurate to that of ClustalW. Although it must be noted that aptamer sequences are shorter (~90 bp) than sequences used in the studies, and as such, require substantially less time to align.

4.1.4.b. Secondary and tertiary structure analysis of aptamer families

The secondary and tertiary structures of the aptamers are crucial to produce and maintain the conformation of the aptamer responsible for binding interactions between the aptamer and the target (SantaLucia and Hicks, 2004; Iliuk *et al.*, 2011).

The secondary folding patterns of oligonucleotides include a variety of motifs predictable from the sequence. These motif structures (which include hairpin-loop motifs) are established and stabilised through Watson–Crick (canonical) and non-canonical base pairing interactions between the nucleotide residues in the oligonucleotide (James, 2001; Lemieux and Major, 2002). Predictive modelling of likely ssDNA and RNA secondary structures, based on thermodynamic predictions, is obtainable using software such as UNAFold (mfold). This produces a representation of predictive models corresponding to folded structures bearing free energy minima (Zuker, 2003; Markham and Zuker, 2008), after accommodating likely base pairing and steric and torsional hindrances imposed on the molecule during base pairing. Later refinements to this suite of software include the ability to include the simulation of temperature and dissolved mono- and di-cation concentrations on the predicted structure and includes some non-canonical base interactions (SantaLucia and Hicks, 2004).

Currently, there is very little software available capable of predicting the tertiary structure of an ssDNA oligonucleotide, other than the use of computationally - expensive chemical modelling software that provide predictions *de novo* (e.g. Abalone). As an alternative, the

online prediction package RNAcomposer (http://rnacomposer.cs.put.poznan.pl) can be used for a basic tertiary prediction of the candidate aptamer sequences. This provides a predicted RNA oligonucleotide tertiary structure (Popenda *et al.*, 2006), arising from both a thermodynamic basis and from empirical structural information (Reblova *et al.*, 2003) originating from crystallography on non-transcriptional RNA. A predictive insight into the tertiary folding patterns of the aptamer was applied in this instance, to evaluate similarities of conformation across DNA aptamers and the families identified during the alignment phase of this structure. The use of RNA tertiary structure predictive software for ssDNA tertiary structure is only predictive and not definitive. RNA tertiary structure prediction software determines the structural properties of the molecule based on RNA thermodynamics, including hydrate base pairing and the sugar-base interactions across the RNA sequence.

4.2. Objectives

Cell-SELEX is an alternate method to the conventional methods used for aptamer generation, allowing for the selection of aptamers that bind to cell surface biomolecules in their native confirmation expressed on the surface of the target cell. Additionally, cell-SELEX provides a platform for the identification and use of unique cell surface markers that conventional SELEX methods are unable to selectively target.

The objective of the reported chapter is to generate a set of aptamers that selectively bind 3T3-L1 preadipocytes over adipocytes derived from the 3T3-L1 preadipocytes, using an adapted cell-SELEX protocol, proposed by Sefah *et al.*, 2010, and to bioinformatically evaluate the generated aptamer sequences for similarities and differences within the sequence.

4.3. Methods and Materials

4.3.1. Tissue culture

The 3T3-L1 cells were cultivated in 35 mm culture dishes and differentiated as detailed in the Chapter 2, section 2.2.2.a. – section 2.2.2.d.

4.3.2. Protocol followed for the Generation of Aptamers using cell-SELEX

Figure 4.1 below illustrates the process by which cell-SELEX was used on the 3T3-L1 preadipocyte cell line. The amplification and generation of ssDNA was performed in an analogous manner to that cited in Chapter 2, section 2.2.3.a. for the amplification of dsDNA and section 2.2.3.b. for the generation of ssDNA.

The library initially was amplified up to dsDNA (before any aptamer selection had happened), as mentioned in Section 2.2.3.a., with a 5' Cy5 fluorescently labelled ssDNA library. The Cy5 fluorophore was later used for aptamer quantification purposes (see Chapter 2, section 2.2.1.e).

For the first cycle of cell-SELEX the cells were resuspended in 600 µl autoclaved distilled water.

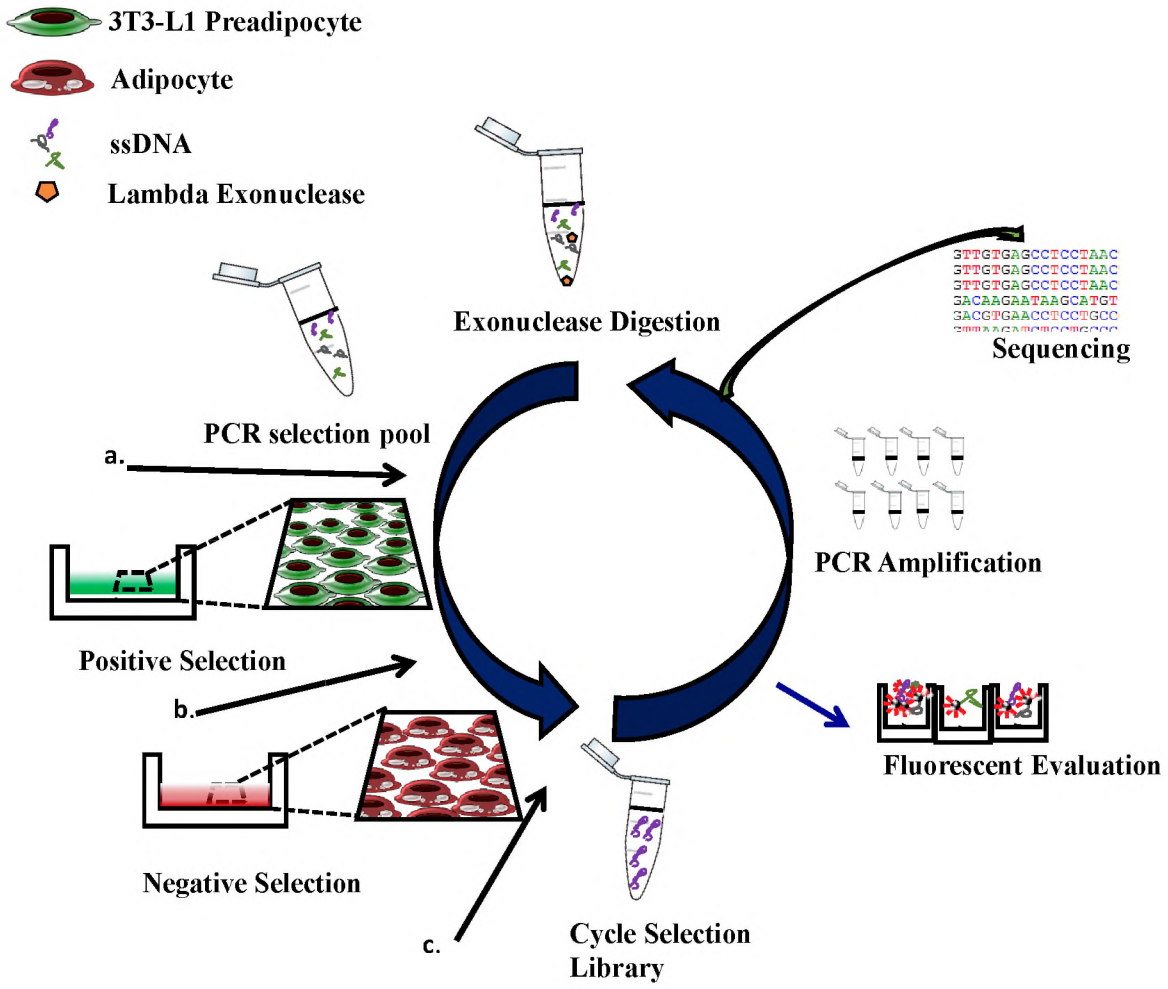

Figure 4.1: Schematic representation of the cell-SELEX protocol followed, for the generation of aptamers targeting 3T3-L1 preadipocytes.

Where samples were evaluated for cycle quantification at: a) initial library, before selection took place. b) Following positive selection. c) Following negative selection (sequences were retained as the selection library for following SELEX-cycles).

Using the ssDNA synthesised above, a 1000 µl sample of ssDNA (~3.39×10^{-4} M) in binding buffer solution was formulated. The sample in binding buffer was heated to 95˚C for 10 minutes, followed by snap-cooling at 4 ˚C for 5 minutes.

Positive SELEX proceeded using a 35 mm culture dish containing preadipocytes grown to confluency. Cells were washed three times with the wash buffer described in Chapter 2, section 2.2.1.b. Following the cell washes, the dissolved ssDNA in binding buffer was added to the culture flask, and incubated at 37 ˚C for 1 hour on a slowly rotating horizontal shaker (50 rpm).

Following incubation with the aptamer, the supernatant containing nonbinding sequences, was removed from the cells in the culture dish and set aside into a 1.5 ml microcentrifuge tube. Followed by three washes of the cell culture dishes in wash buffer, 500 µl of sterile water was added into the culture dish. The cells were then detached from the dish surface using a cell scraper.

The detached cell suspension was heated to 95 °C for 10 minutes. The binding ssDNA was recovered from solution by centrifugation at 13 100 x *g* for 5 minutes.

Negative SELEX proceeded in the same manner as described above, using a 35 mm culture dish containing mature adipocytes. Cells were washed three times with the wash buffer described in Chapter 2, section 2.2.1.b. Following the cell washes, the dissolved ssDNA in binding buffer was added to the culture flask, and incubated at 37 °C for 1 hour on a slowly rotating horizontal shaker (50 rpm). The sequences remaining in the supernatant (non-binding aptamer sequences to mature adipocytes) were retained as the selection library of sequences for following cell-SELEX cycles.

The supernatant containing the ssDNA from the selection library was purified and concentrated, using the NucleoSpin® Gel and PCR protocol according to manufacturer's instructions, see Chapter 2, section 2.2.1.d. and fluorescently quantified as seen in Chapter 2, section 2.2.1.e.

To quantify the amount of aptamer binding fluorescently quantification of aptamer binding to both the preadipocytes and adipocytes, a 50 µl sample from each of the following phases of the SELEX selection were abstracted: initial binding buffer/ selection pool (Figure 4.1.a.), preadipocyte binding aptamers (Figure 4.1.b.), and the sequences binding to adipocytes (Figure 4.1.c.) were maintained for quantification.

Each 50 µl sample was purified using the NucleoSpin® Gel and PCR Clean-up system, as per manufacturer's instructions, see Chapter 2, section 2.2.1.d.

Minor alterations to the protocol was made between each cycle of cell-SELEX, to enhance the selection of a strong, favourable binding sequences while minimising the amount of selection steps required for aptamer generation. These alterations include the use of either mutagenic (error prone), or conventional PCR methods, additionally the primary selection method used. Table 4.1 below illustrates these alterations between the different cell-SELEX made to the protocol followed for each cell-SELEX cycle.

Table 4.1: **Alterations made to the relevant cycles of the standard mentioned cell-SELEX protocol followed from the above mentioned.**

Cycle number	PCR type	Purpose
0	Normal	Cloning of 5'-Cy5 tag to library
1	Mutagenic	Positive selection only
2	Mutagenic	Positive and negative selection
3	Mutagenic	Positive and Negative selection
4	Normal	Positive and Negative selection
5	Normal	Positive selection only
6	Normal	Positive selection only
7	Normal	Negative Selection only
8	Normal	Positive and Negative selection
9	Normal	Negative Selection only
10	Normal	Positive and Negative selection
11	Normal	Positive and Negative selection

4.3.2.a. Quantification of binding sequences following selection each cycle

Quantification of binding was conducted using detection of a Cy5 fluorophore from different fractions of the selection library arising from the SELEX process. Fluorimetry was conducted as mentioned in Chapter 2, section 2.2.1.e.

The samples of ssDNA library, labelled at the 5' site with Cyanine 5, were exposed to an excitation wavelength of 640 $\pm$ 9 nm, and the subsequent emission spectra between 500 and 800 nm were measured. For quantification purposes, a peak wavelength present around ~660 nm was selected for evaluation of fluorescent intensity, as mentioned in Chapter 2, section 2.2.1.e.

4.3.2.b. PCR amplification of sequences

The protocol for the amplification of the selection pool through PCR was followed as discussed in Chapter 2, section 2.2.3.a. above. Initially a mutagenic PCR reaction was used for the first three selection cycles to allow for minor variation in the selected sequences to occur. The changes in the PCR reaction mix to promote mutagenic PCR involved an increase

in the concentration of $MgCl_2$ for each reaction up to 8.52 x 10^{-3} M. The standard proportions of PCR components are tabulated below

Table 4.2: **Standard PCR conditions and concentrations maintained for SELEX rounds**

Reagent	Concentration
10x reaction buffer with 1.5 mM $MgCl_2$	1 X
10 mM dNTP	1.00 x 10^{-4} M
Forward Primer	9.09 x 10^{-12} M
Reverse Primer	9.09 x 10^{-12} M
Sterile Water	Up to total volume
Template	2 ng/ 100 µl
Taq Polymerase	2.5 U/100 µl

*The PCR reagents were purchased through Lasec (South Africa), product code: DKAPBK1000

4.3.2.c. Synthesis of ssDNA through lambda exonuclease

The generation of ssDNA using lambda exonuclease digestion, was done as mentioned in Chapter 2, section 2.2.3.b.

4.3.2.d. Cloning and sequencing of developed aptamers

Nutrient agar (Lasec, South Africa), was formulated according to manufacturer's instructions and autoclaved. While the autoclaved agar was cooling, ampicillin (AMP), sourced from Sigma-Aldrich, was added to make a final concentration of 100 $mg.ml^{-1}$ ($2.86x10^{-1}$ M), and $1x10^{-6}$ M of Isopropyl β-D-1-thiogalactopyranoside (IPTG). The media was poured into Petri dishes and cooled before subsequent use.

Before the competent cells were transformed 40 µl of a 20 $mg.ml^{-1}$ (2.45E-01 M) 5-bromo-4-chloro-3-indolyl-β-D-galactopyranoside (X-GAL) solution was spread evenly on the surface of the nutrient agar plates and allowed to bake on the nutrient plate surface at 37 °C for 30 minutes.

PCR fractions were then drawn - in different transformation reactions - from the Cycle 11 and Cycle 8 sequence pools. These were ligated into the pGEM®-T easy vector system

(Promega), by mixing the reagents mentioned in Table 4.3 below, the ligation of the insert into the vector was allowed to take place at 4 °C overnight.

Table 4.3: Reagents used for ligation of the selected aptamer sequences into the pGEM®-T easy vector system

Reagent	Insert Ligation	Positive Control	Background Control
2 X rapid ligation buffer (µl)	5	5	5
pGEM®-T easy Vector (unligated) (50ng) (µl)	1	1	1
PCR Product (ng)	R/ A	0	0
Control Insert (µl)	0	2	0
T4 Ligase (3 Weiss units/ µl) (µl)	1	2	1
Deionised Water (µl)	X	0	3
TOTAL (µl)	**10**	**10**	**10**

X = The required volume water (µl) to make up to final reaction volume.
R/ A = The required volume (µl) of insert DNA to make up correct insert: vector ratios.

Adaptations were made to the protocol to increase the ligation and transformation likelihood: doubling the amount of T4 ligase added from 2 µl to 4 µl for the final transformation reaction mixture, and trialling PCR insert: vector ratios of 1: 1 (~15 ng insert dsDNA) and 3: 1 (~45 ng insert dsDNA).

The ligated vectors (~0.19 ng/ µl) were used to transform 100 µl (~4.8 $x10^7$ CFU/ ml) ampicillin susceptible *Escherichia coli* DH5α competent cells. Whereby the cells were transformed by adding 4 µl of the ligated insert in vector to the competent cells (~4.8 $x10^7$ CFU/ ml) in a 1.5 ml microcentrifuge tube, and incubated on ice for 20 minutes. The competent cells were heat shocked at 42 °C for 45 seconds, followed by cooling on ice for an additional 2 minutes. 950 µl of nutrient media (purchased from Lasec, South Africa) was added to the transformed cells and incubated at 37 °C for 1.5 hours, with shaking on a horizontal shaker at~ 150 rpm, 100 µl of the transformed cells were then spread-plated on prepared NA/ AMP/ IPTG/ X-GAL nutrient agar plates and incubated overnight at 37 °C.

Following blue/ white screening, 20 white colonies containing the ligated vector with insert, were randomly selected with a sterile toothpick and smeared on the inner surface of a PCR tube. The vectors within the selected colonies were then suspended in 50 µl of colony PCR mix (comprising of 5 µl reaction buffer, 2 U KAPA Taq polymerase, $1.00x10^{-11}$ mol M13 forward (5' – GTAAAACGACGGCCAGT - 3') and reverse primer (5' – AGCGGATAACAATTTCACACA - 3') sequences. 4.00 $x10^{-9}$ mol dNTP's, and made up to 50 µl reaction with sterile Milliq water was added to each PCR tube and amplified.

Thermocycle conditions for colony PCR were set to: 95 °C for 3 minutes, followed by 95 °C for 30 seconds, 54 °C for 30 seconds, 72 °C for 30 seconds for 35 cycles, followed by a 72 °C annealing for 8 minutes, and 4 °C hold. Similarly, a ligated vector in a growing bacterial colony (blue colony) was used as a control for the amplification of the vector.

The PCR amplification product was analysed on a 2.5 % $^{w}/_{v}$ agarose gel to confirm vector amplification, as described in Chapter 2, section 2.2.1.c. The remainder of the product from colony PCR was purified using the NucleoSpin® Gel and PCR Clean-up system according to manufacturer's instructions, see Chapter 2, section 2.2.1d.

To confirm the ligation of insert into the vector,~4 ng/ µl dilution of the reaction volume from the colony PCR, was made as a template for insert verification PCR. The PCR reaction was performed with the conditions, as seen above in Chapter 2, section 2.2.3.a. With minor alterations to the reaction mix concentrations, these alterations included a 50 µl total reaction volume with 5 µl 10 X reaction buffer, $5x10^{-9}$ mol dNTP's, $4.55x10^{-12}$ mol forward and reverse primer sets, 1 µl template, 2.5 U *Taq* polymerase, made up to 50 µl per reaction.

Thermocycle conditions remained the same as that for the normal SELEX PCR product amplification, as seen above in the commonly used methods and materials section, for 10 PCR amplification cycles. The products of the PCR amplification were evaluated on a 2.5 % agarose gel to confirm insert into the vector, as described in Chapter 2, section 2.2.1.c.

The sequences vector regions within the M13 primer sets, gathered from the colony PCR, were sent for sequencing at Inquba biotech (South Africa), using only forward Sanger sequencing, using the M13 primer regions for sequencing initiation.

4.3.3. Primary, Secondary and Tertiary Structure analysis of the sequences

The sequences gathered from cell-SELEX (Table 4.5 and Table 4.6 below) were evaluated at the primary, secondary and tertiary structural levels.

4.3.3.a. Primary Sequence analysis

The sequences were aligned using the MUSCLE MSA algorithm (http://www.ebi.ac.uk/Tools/msa/muscle/). Based on the MUSCLE sequence alignment, a phylogram was generated to investigate sequence similarity to group individual sequences within families. Alignments and sequence phylograms were visualised using BioEdit (version 3.6a2.1).

4.3.3.b. Secondary and Tertiary Sequence analysis

Secondary structure prediction and analysis was performed by individually processing single sequences using the UNAfold analysis web server (http://unafold.rna.albany.edu/) (Zuker, 2003), to analyse secondary structure motifs within the sequence family groups. The temperature and ion conditions of ssDNA folding were kept to conditions used for the cell-SELEX (i.e. 37 °C, with monocations set at 0.163 M) and dications set at 250 mM. These correspond to salt concentrations in the binding buffer conditions (Cell-SELEX buffers and protocol in Chapter 2): Na^+ (0.157 M) and K^+ (5.62 mM) and Mg^{2+} (250 mM).

To provide a preliminary tertiary structure of the aptamers, RNAcomposer (http://rnacomposer.ibch.poznan.pl/) was used to determine a predictive tertiary structure of the best representative sequences for each family group of aptamers. To limit the single stranded RNA tertiary folding predictions made by the software of the aptamer sequences the predicted ssDNA dot-bracket format of the aptamers secondary structures were used as a

template for the folding characteristics of the developed aptamers – generated from UNAfold – were used as a template for the tertiary folding predictions of the aptamers. The tertiary structures of the generated aptamers were visualised using the Chimera candidate version 1.11.1 (build 41280).

4.4. Results and Discussion

4.4.1. Development of aptamer sequences through cell-SELEX

Shao *et al.*, (2011) investigated the result of multiple sequences being used as a template, when amplifying a selection library (large variety between multiple sequences used as template for DNA amplification) in the SELEX protocol.

The over-amplification of the PCR product, is the result of sequence hybridisation in both the template and primer sequences. Figure 4.2, illustrates the result of over amplification of the amplicon in lanes 6-10. The generation of high molecular weight amplicon sequences is the result of sequence hybridisation and concatemer formation (Sun and Åkerman, 2014). To reduce the level of concatemer from formation in the PCR product during SELEX, an optimisation into the number of PCR amplification cycles needs to be investigated before amplifying the selected aptamer pool of a given SELEX cycle.

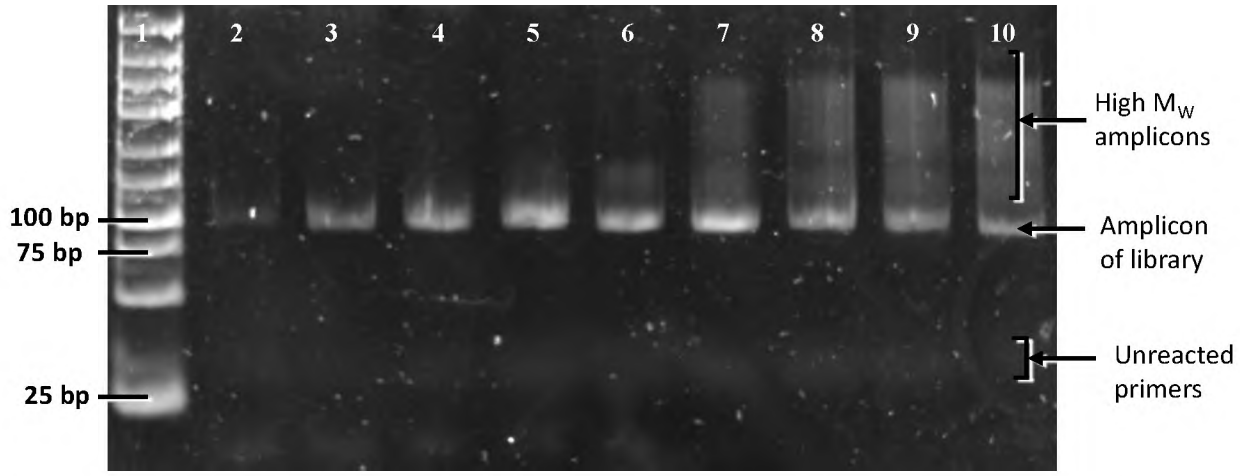

Figure 4.2: 10 % PAGE Gel illustrating the influence of PCR cycle number with the quality of dsDNA obtained from ssDNA SELEX pools.

This demonstrates ssDNA pools obtained for SELEX cycle 4. Lane 1; GeneRuler Low Range DNA ladder; Lane 2-10: 4-12 PCR amplification cycles respectively. The gel illustrates over amplification of the product forming a high molecular weight product starting around 8 cycles of PCR.

Figure 4.2 illustrates that the over-amplification of the library retained for SELEX cycle 4 becomes visible around 6 cycles of amplification. The schematic illustration of concatemer formation described in Figure 2.1 in Chapter 2 above. The above figure illustrates that the maximum number of PCR amplification cycles that could be performed this particular cycle of SELEX before amplification artefacts begin to dominate the amplified pool would be seven PCR amplification cycles. However, five cycles of PCR appear to provide substantial amplification of the pool while minimising artefact formation. Similar assessments were performed for each amplification before finalising the cycle numbers.

Before exonuclease digestion can be performed, 5 µg (8.56×10^{-11} mol) of dsDNA needed to be amplified, after the PCR cycle evaluation. Figure 4.3 below illustrates the generated ssDNA present in solution following exonuclease digestion.

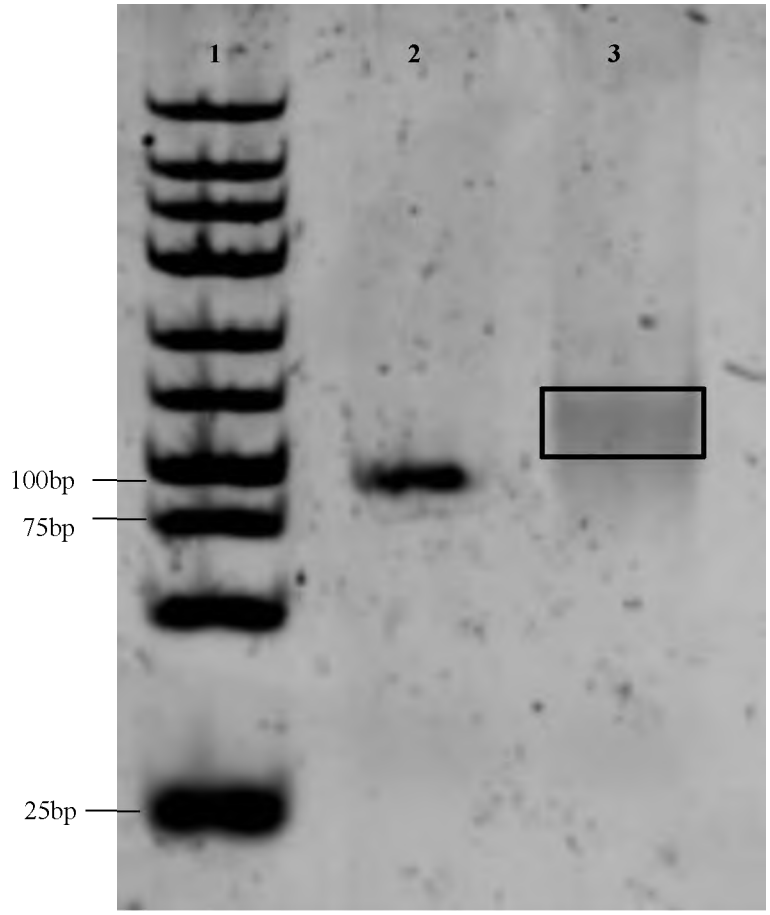

Figure 4.3: 10 % PAGE gel illustrating lambda exonuclease digestion of dsDNA for generation of ssDNA library.

Lane 1; GeneRuler Low Range DNA ladder. Lane 2; dsDNA control sequence. Lane 3; ssDNA generated from exonuclease digestion. Although very faint, the ssDNA has been highlighted in the black box.

Figure 4.3 illustrates the product of exonuclease digestion does not contain visible dsDNA sequences in the selection pool before proceeding cycles of cell-SELEX. dsDNA, as seen in lane 2 of Figure 4.3, migrates faster than that of the ssDNA exonuclease product in lane 3. The rapid migration rate of the dsDNA in relation to that of the ssDNA was also previously discussed in Chapter 3, section 3.4.3.

The relative amounts of DNA exposed to exonuclease digestion and the amount of ssDNA yielded was monitored using NanoDrop 2000. UV/ vis absorbance spectroscopy revealed that after completing 10 cycles of cell-SELEX, where the mean input of dsDNA for lambda exonuclease digestion was 5.07 ± 0.16 µg dsDNA. The mean output of ssDNA gathered from exonuclease digestion was 1.65 ± 0.31 µg ssDNA following 2 hours of exonuclease digestion. The drop below the predicted 50 % of DNA attained following exonuclease digestion, suggests that there is exonuclease digestion occurring in the aptamer sequence strand (sense) of the DNA template.

4.4.1.a. Fluorimetric quantification of cell-SELEX progress

Following each selection cycle, the presence of candidate aptamer sequences was assessed in the different selection fractions of the cycle: samples of the initial ssDNA in binding buffer, and a sample of the ssDNA pool sequences that bound to both the preadipocytes and adipocytes in the cycle selection pool were fluorescently quantified. Quantification of the candidate sequences was proceeded using fluorescence spectroscopy as outlined in Chapter 2, section 2.2.1.e.

Over the first three SELEX selection cycles, the amount of sequences positively binding to the 3T3-L1 cells was not quantifiable using fluorescent spectroscopy. Figure 4.4.a, to Figure 4.4.d, illustrate differences between the positive and negative binding at various phases within four cycle selected from the 11 cycles of cell-SELEX performed. The percentage binding efficiency between the positive (3T3-L1 preadipocyte binding) and negative (mature adipocyte binding) RFU from that of the initial RFU from the selection buffer with the selection pool added before the SELEX selection of that cycle was initiated, this was done for all the cycles of SELEX. The graphical representation of four of these cycles is illustrated in Figure 4.4 below, with Table 4.4 illustrating numerical values for all the cell-SELEX cycles 3-11.

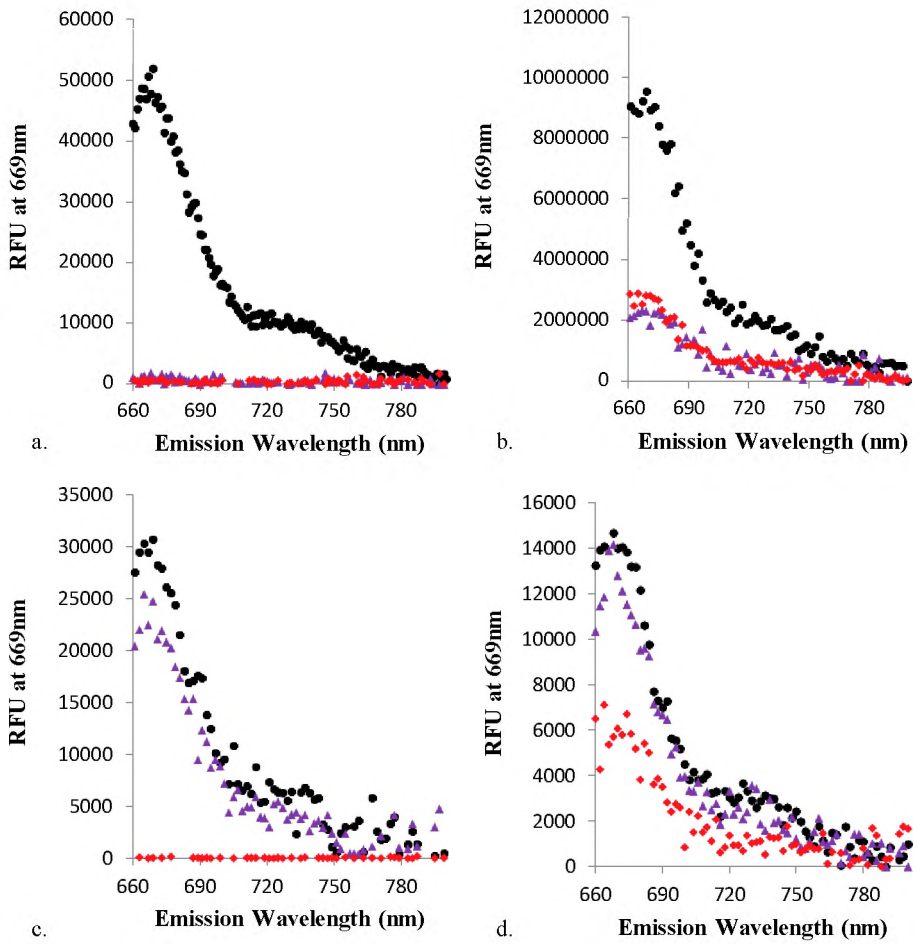

Figure 4.4: Relative fluorescent responses of aptamer sequences that bound to 3T3-L1 preadipocytes

Reference standard sample of 9.1 pmol fluorescent primer (black dots), sample pool binding to positive-SELEX samples of 3T3-L1 preadipocytes (Purple diamonds), and aptamer sequences that bound to mature adipocytes (red diamonds).

a) Cycle 3. b) Cycles 6 (positive SELEX) and 7 (negative SELEX). c) Cycle 8. d) Cycle 11. (see Appendix A for raw RFU data)

The RFU value is a relative fluorescent unit of measurement, based on the relative fluorescence of a sample established on a reference fluorescence sample at the time of measurement. The arbitrary nature of this unit alters the RFU fluorescent readings between different fluorescent spectrophotometer measurements. The fluorescent assays were evaluated with a standard reference of 9.09×10^{-12} mol of the forward primer in 50 µl of binding buffer. As the fluorescent signal for the binding evaluation of each SELEX cycle was characterized with the same reference fluorescent signal for each reading. An understanding into the binding properties within a specific cycle may be compared to each other.

The RFU intensity max value at 669 nm, relatively compared with the initial fluorescents of the selection pool before each SELEX selection cycle. The sample were evaluated to compare percentage binding between the positive and negative sequences for each round as tabulated in Table 4.4, below.

Table 4.4: Important metrics arising from the different cycles of SELEX

Cycle Number	PCR, optimum number of cycles	Negative (%) Binding	Positive (%) Binding	Negative /Positive
3	5	1.25	1.81	0.69
4	7	-2.41	3.31	0.73
5	10	N/A	2.23	N/A
6	8	N/A	49.06	N/A
7	7	66.40	N/A	N/A
8	9	0.69	74.11	0.01
9	11	9.07	N/A	N/A
10	10	3.21	48.14	0.07
11	11	43.30	91.43	0.47

*RFU intensities evaluated at 669nm emission. *N/A= No data available as selection cycle not performed

The results in Table 4.4 demonstrate that there was a general increase in the specificity of the binding of the aptamer library to the 3T3-L1 preadipocytes from 1.81 % to 74.11 % between the third and eighth round cell-SELEX. Table 4.4. also shows that, although there was an increase in the positively bound sequences binding to the preadipocytes from 74.11 % to 91.43 % between the eighth and eleventh SELEX cycle, there was a substantial increase in the negative binding of the library to the adipocytes from 0.69 % to 43.3 % of the sequences binding (see Appendix A for the raw data demonstrating the RFU values for binding calculations).

This increased the ratio of negatively binding sequences/ positive bound sequences from 0.01 in SELEX cycle 8 to 0.47 in SELEX cycle 11. This suggests that there was a decrease in the selectivity of the aptamer selection pool in the last three cycles of SELEX.

This was evaluated by cloning and sequencing the aptamers from both the cycle 8 and cycle 11 selection pools, the sequences from both the cycle 8 and cycle 11 selection pools are illustrated in Table 4.5 and Table 4.6.

Table 4.4, further illustrates a general increase in the number of PCR amplification cycles with each cell-SELEX cycle. The diversity of sequences present within the selection pool is expected to decrease with progressing cycles of SELEX, as potential aptamer sequences are excluded from the selection pool with subsequent SELEX cycles. This suggests that there was a positive selective pressure toward aptamer sequences binding to the surface of the 3T3-L1 preadipocytes.

4.4.2. Cloning vector/insert uptake

To amplify and evaluate ligation and transformation of sequences within the final cell-SELEX selection pool into the cell, colony PCR initiated using the M13 forward and reverse primer set. The results from the colony PCR reaction are illustrated Figure 4.5 below.

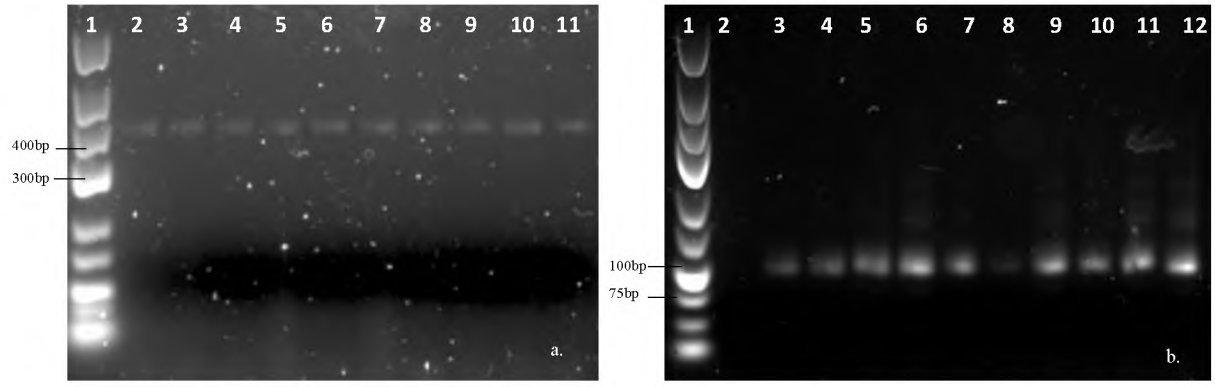

Figure 4.5: 2.5% Agarose gel evaluation of successful vector transformation in DH5α competent *E. coli* and insert ligation into the pGEM®-T easy vector.

a.) Colony PCR evaluation of vector in competent cells. Lane1; GeneRuler Low Range DNA ladder. Lane 2-11; Representative of different colony PCR reactions with insert in them. b.) Insert confirmation from the colony PCR product. Lane1; GeneRuler Low Range DNA ladder. Lane 2; Negative, vector with no insert control. Lane3-11; Representative insert amplification evaluation of MR801-MR810 sequences respectively.

From both Figure 4.5.a and Figure 4.5.b, illustrates that the inserts were amplifying from the vector using the aptamer-specific primers. The minor presence of amplification artefacts present in the DNA product exhibited in Figure 4.5.b, could arise from binding of the template sequences together, causing a variation in the length of the PCR product. However, these are minor relative to the band under examination and occur after 30 cycles; in contrast

to the amplification artefacts rapid rise in the amplification pool when multiple template sequences co-exist (e.g. Figure 4.2)

Twenty sequences from both the cycle 11 and cycle 8 selection pools were evaluated for the progression of sequence selection between the SELEX selection pools with high binding affinity to the preadipocytes.

Visual inspection of the sequences, tabulated in Table 4.5 for the pool of sequenced sequences after 11 cell-SELEX cycles, demonstrate high levels of sequence conservation within the selected aptamer pool that was sequenced.

Table 4.5: Twenty sequences gathered at the end of 11 cell-SELEX cycles.

Sequence Title	Sequence
MR01	**GCCAAGAATAAGCATG**ATTGTGTTCATGGCGCGATATCTTGAATATTGAGCTGCTACTACCGAGCAT**GATGATTCTTGACTCCC**
MR02	**GCCAGACGAGAGCCTC**ATGCCGCTGTGTTCATTGCGCGATATCTTGTCTATTCAGGTGCTACTACCGAGCAT**GATGATTCTTGACTCCC**
MR03	**GCCAGACGAGAATAAG**CATGCCGCTGTGTTCATGGCGCGATATCTTGTCTATTCAGGTGCTACTACCGAGCAT**GATGATTCTTGACTCCC**
MR04	**GCCAGACGTGAATAAG**CTGCCGCTGTGTTCATTGCGCGATATCTTGTCTATTCAGGTGCTACTACCGACCAT**GATGATTCTTGACTCCC**
MR05	**GCCAGACGAGAGCCTC**ATGCCGCTGTGTTCATTGCGCGATATCTTGTCTATTCAGGTGCTACTACCGACCAT**GATGATTCTTGACTCCC**
MR06	**GCCAGACGAGAACCTC**CTGCCGCTGTGTTCATTGCGCGATATCTTGTCTATTCAGGTGCTACTACCGACCAT**GATGATTCTTGACTCCC**
MR07	**GCCAGACGAGAGCCTC**ATGCCGCTGTGTTCATTGCGCGATATCTTGTCTATTCAGGTGCTACTACCGACCAT**GATGATTCTTGACTCCC**
MR08	**GCCAACGAGAATAAGC**TGCCCTTGTGTTCATTGCGCGATATCTTGTCTATTGAGGTGCTACTACCGAGCAT**GATGATTCTTGACTCCC**
MR09	**GCCAGACGAGAATAAG**CTGAACTTGTGTTCATGGCGCGATATCTTGTCTATTGAGGTGCTACTACCGACCAT**GATGATTCTTGACTCCC**
MR10	**GCCAGACGTGAGCCTC**ATGCCGCTGTGTTCATTGCGCGATATCTTGTCTATTCAGGTGCTACTACCGACCAT**GATGATTCTTGACTCCC**
MR11	**GCCAGACGAGAGCCTC**ATGAGCTTGTGTTCATTGCGCGATATCTTGTCTATTGAGGTGCTACTACCGACCAT**GATGATTCTTGACTCCC**
MR12	**GCCAGACGAGAATAAG**CATGCCGCTGTGTTCATTGCGCGATATCTTGCCTATTCAGGTGCTACTACCGACCAT**GATGATTCTTGACTCCC**
MR13	**GCCAGACGTGAGCCTC**ATGTGCTTGTGTTCATTGCGCGATATCTTGTCTATTCAGGTGCTACTACCGACCAT**GATGATTCTTGACTCCC**
MR14	**GCCAGACGTGAGCCTC**ATGCCGCTGTGTTCATTGCGCGATATCTTGACTATTCAGGTGCTACTACCGACCAT**GATGATTCTTGTCTCCC**
MR15	**GCCAGACGAGAGTACT**GCATGACCCCTGTGTTCATTGCGCGATATCTTGTCTATTCAGGTGCTACTACCGAGCAT**GATGATTCTTGACTCCC**
MR16	**GCCAGACGTGAATAAG**CTGCCGCTGTGTTCATGGCGCGATATCTTGTCTATTGAGGTGCTACTACCGACCAT**GATGATTCTTGACTCCC**
MR17	**GCCAGACGTGAATAAG**CATGCCGCTGTGTTCATTGCGCGATATCTTGTCTATTCAGGTGCTACTACCGACCAT**GATGATTCTTGACTCCC**
MR18	**GCCAGACGAGAATAAG**CATGAGCTTGTGTTCATTGCGCGATATATTGTATATTGAAGTGCTACTACCGAGCAT**GATGATTCTTGTCTCCC**
MR19	**GCCAGACGAGAGCCTC**ATGCCTTGTGTTCATTGCGCGATATCTTGTCTATTCAGGTGCTACTACCGACCAT**GATGATTCTTGACTCCC**
MR20	**GCCAGACGTGAATAAG**CATGCCGCTGTGTTCATTGCGCGATATCTTGACTATTCAGGAGCTACTACCGACCAT**GATGATTCTTGACTCCC**

*Primer regions highlighted in bold text

Sequence diversity and phylogeny of sequences from cycle 11 was evaluated through a MUSCLE MSA. Figure 4.6 below illustrates sequence conservation between the cycle 11 pool that was selected, (see Appendix B below for the MUSCLE multiple sequence alignment of the cycle 11 generated aptamer sequence).

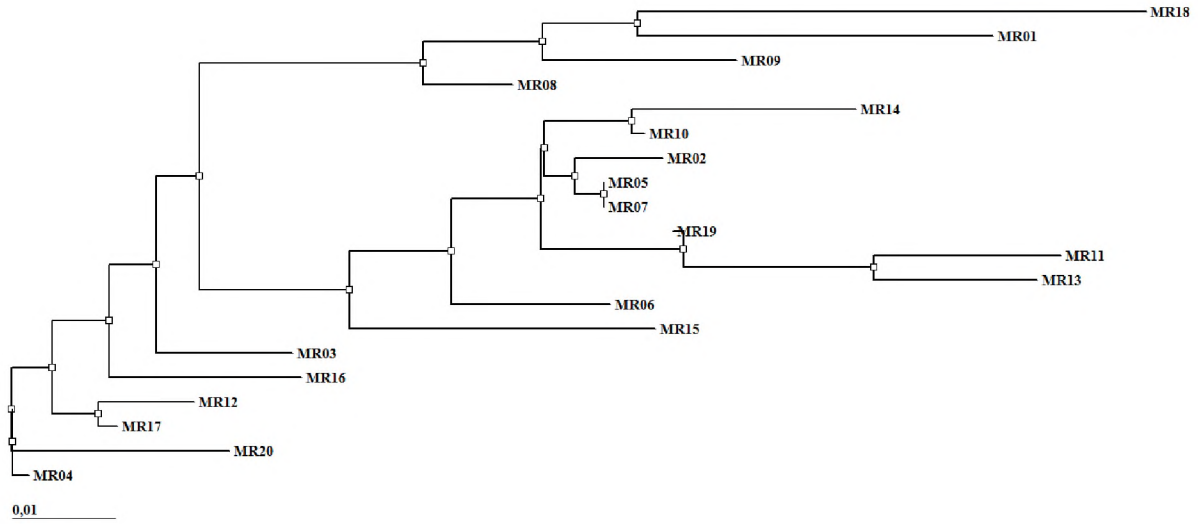

Figure 4.6: Phylogram of aptamer sequences gathered from the SELEX cycle 11 selection pool.

Using a MUSCLE multiple sequence alignment algorithm for the evaluation of the generated aptamer sequences. The 0.01 scale bar, presented in the bottom-left of the figure, refers to~1 nt. mutation.

The phylogram presented in Figure 4.6 illustrates high levels of similarity within the sample of selected sequences. This results from the formation of several sequence subfamilies within the cell-SELEX cycle 11 sequences sampled. The high degree of conservation observed in the obtained sequences (Figure 4.6, Table 4.5) and the lack of primer regions (high mutation levels from the original primer sequences) on the flanking regions of the sequences, suggest that the sequences gathered from the 11 cycles of cell-SELEX were the product of concatemer formation this has been demonstrated below in Figure 4.7.

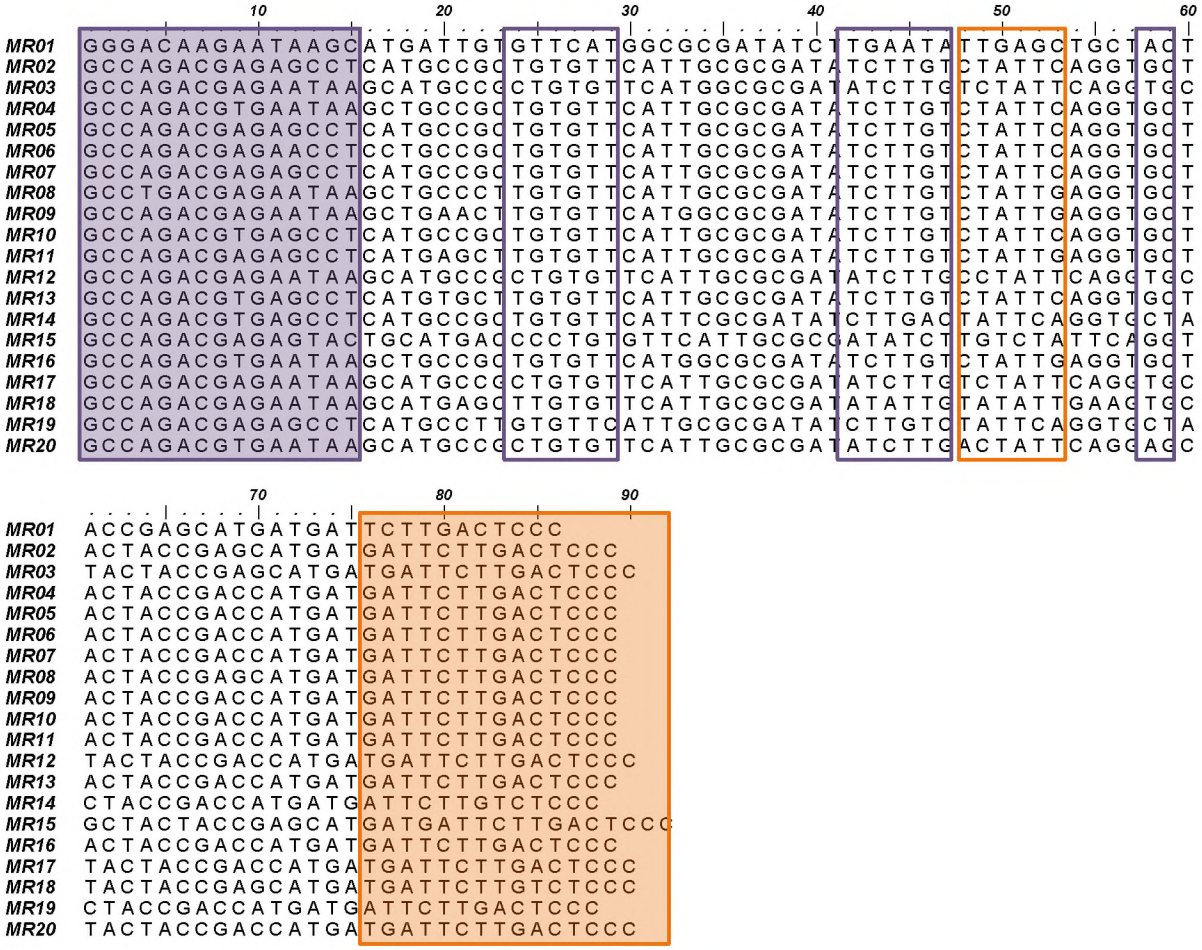

Figure 4.7: illustrative description of concatemer formation in the aptamer pool after 11 cell-SELEX cycles.

Demonstration of repeating sections of the forward primer (purple boxes) and reverse primer (orange boxes), the original primer binding regions of the sequences are highlighted in the shaded purple (forward primer) and orange (reverse primer) binding sites.

Figure 4.7 illustrates repeated sequences from both the original forward (purple blocks) and reverse (orange blocks) primer regions being prominently repeated throughout the twenty representative samples of the cell-SELEX selection pool. Additionally, both the flanking primer regions for the forward and reverse primer sets, highlighted in purple and orange shaded boxed in Figure 4.7 respectively, suggest high mutagenesis or sequence hybridisation from the original primers used.

The high levels of sequence similarity, and high levels of mutation in the primer binding regions of the aptamer sequences (highlighted in Figure 4.7) suggest that there were high levels of hybridisation in the aptamer sequences during the amplification of the SELEX selection pool for cycles 9-11.

To confirm that the sequences gathered were the product of hybridised sequences rather than that of mutagenesis from the cycle 11 selection pool, an additional twenty sequences from the cycle 8 selection pool were then sequenced, and tabulated in Table 4.6 below.

The cell-SELEX cycle 8 selection pool specifically was chosen for sequencing, as both the affinity of the positive aptamer illustrated a decrease in the binding efficiency toward the positive cell line, as shown in Figure 4.4 above. Additionally, Table 4.4 above illustrates that the general increase in the number of optimal PCR amplification cycle started to stabilise at 11 PCR amplification cycles, after the eighth cell-SELEX cycle.

Table 4.6: Twenty sequences gathered from the cycle 8 representation of the selection pool of cell-SELEX

Sequence Title	Sequence
MR801	**GCCTGTTGTGAGCCTC**CTAACTATATATTATCACGTGGACATACATTTACGGACACTTAGTCTCGGATAGCAT**GCTTATTCTTGTCTCCC**
MR802	**GCCTGTTGTGAGCCTC**CTAACTTGCTCGTATATGGCGACAGAGCGAACATTGGTCGTTTATTGACTATCCAT**GCTTATTCTTGTCTCCC**
MR803	**GCCTGTTGTGAGCCTC**CTAACTATATATTATCACGTGGACATACATTTACGGACACTTAGTCTCGGATAGCAT**GCTTATTCTTGTCTCCC**
MR804	**GCCTGACAAGAATAAG**CATGTGCTAAGTGTTCTTGCGCCATATCAGGTCTATTCAGGTGGAACTACCGAGCAT**GATGATTTATGACTCCC**
MR805	**GCCTGACGTGAGCCTC**ATGCCGCTGTGTTCATGGCGCGATATCTTGACTATTCAGGTGCTACTACCGACCAT**GATGATTCTTGACTCCC**
MR806	**GCCTGTTGTGAGCCTC**CTAACTATGTATACAACGTCCTGCGGAATCCGGTCAGTAATTTTGCACTTGGTTCAT**GCTTATTCTTGTCTCCC**
MR807	**GCCTGTTGTGAGCCTC**CTAACAAGGAGCAGCGCACGTATTAATTTGTGGTAGGTTCGGGGTTCGTACGTACAT**GCTTATTCTTGTCTCCC**
MR808	**GCCCGCGAATTCACTA**TTGATTGGGACTCAAGAATAATCATGGTCGGTAGTAGCTATGGAATAAGCAATATCTCGCGCAATTATTCAGCG TCA**GCTTATTCTTGTCTCCC**
MR809	**GCCTGTTGTGAGCCTC**CTAACTATATATTATCACGTGGACATACATTTACGGACACTTAGTCTCGGATAGCAT**GCTTATTCTTGTCTCCC**
MR810	**GCCTGTTGTGAGCCTC**CTAACCCTAGTTGAAAATTACGATTACCATTATCCTTTTTCCTCGAGATCGGGTCAT**GCTTATTCTTGTCTCCC**
MR811	**GCCTGACAAGAGCCTC**ATGCCGCTGTGTTCATTGCGCGATATCTTGTCTATTCAGGTGCTACTACCGACCAT**GATGATTCTTGACTCCC**
MR812	**GCCTGACGTGAACCTC**CTGCCGTCGTAATCATTGCGCGATATCTTGTCTATTCCGCTGCTACTACCGACCAT**GATGATTCTTGACTCCC**
MR813	**GCCTGACAAGAATAAG**CTGACGATGTGTTCATGGAGCGACATCTTGTCTATTCAGGTGCTACTACCGAGCAT**GATGATTCTTGACTCTC**
MR814	**GCCCGCGGGATTCGAT**TGCCTGACGCATAAGCTGCCTTGTGTTCTTGCGCGATATCTTGTCTATTCAGGTGCTACTACCGACCAT**GATGA TTCTTGTCTCCC**
MR815	**GCCTGACGTGAGCCTC**CTGCCCTTGTGTTCATTGCGCGATATCTTGTCTATTCAGGTGCTACTACCGACCAT**GATGATTCTTGACTCCC**
MR816	**GCCAGACAAAAGCCTC**ATGCCGTTGTGTTCATTGCGCGACATCTTGTCTATTCAGGAGCTACTACCGACCAT**GATGATTCTTGACTCCC**
MR817	**GCCTGACGTAATAAGC**TGCCCTTGTGTTCATTGCGCGATATCTTGACTATTGAGCTGCTACTACCGACCAT**GATGATTCTTGACTCCC**
MR818	**GCCTGACGTGAGCCTC**CTGCCGCTGTGTTCATTGCGCGATATCTTGTCTATTCAGGTGCTACTACCGACCAT**GATGATTCTTGACTCCC**
MR819	**GCCTGACAAGAATAAG**CATGTCGCTGTGTTCATTGCGCGATATATTGTCTATTGAGGTGCTACTACCGAGCAT**GATGATTCTTGACTCCC**
MR820	**GCCAGTTAAGATCTCC**TGCCCCTGCGCTCACCACGCCACATCTTGTCTATTCCCCCTCACTCCCCAGCAC**GATTATTCTTGACTCCC**

*Primer regions highlighted in bold text, sequences in grey blocks were evaluated sequences

Evaluation of the cycle 8 selection pool, shows that there are sequences in the selection pool containing the original primer sequences and show levels of variability higher than that of the cycle 11 selection pool.

After 11 cycles of cell-SELEX selection, there were several sequences that demonstrate large regions of high sequence conservation within the sample of sequences that were sequenced. These sequences demonstrated potential concatemer formation within the sample of the selection pool following eleven cell-SELEX cycles. To confirm the formation of concatemer sequences the cycle 8 selection pool was transformed, sequenced, and compared to that of the cycle 11 selection pool. This demonstrated that although there were several of the aptamer sequences that resembled that of the cycle 11 selection pool, there were a few sequences that had maintained the original primer binding regions within the aptamers, with a less sequence repetitive nature to that of the sequences gathered following eleven SELEX selection cycles.

These sequences sampled from the selection pool after 8 cycles of SELEX were subsequently compared for possible similarity to each other at the primary, secondary and tertiary structural level.

4.4.3. Sequence evaluation of the Cycle 8 selection pool representative aptamer sequences

Following sequencing of the cycle 8 selection pool, a MUSCLE sequence alignment and phylogenetic analysis was performed on the selection pool. As the relative fluorescence of the cycle 8 selection pool, seen in Chapter 4 above in Figure 4.4, demonstrated the highest binding difference before the binding affinity of the aptamer started to decrease in subsequent SELEX cycles. Of the cycle 8 selection pool, 35 % of the sequences (MR801, MR802, MR803, MR806, MR807, MR809, and MR810) demonstrated unmutated forward and reverse primer sequences, with the remainder showing similar sequence mutations noted for cycle 11 pool sequences (seen in Table 4.5).

A MUSCLE multiple sequence alignment (see Appendix B) and phylogram (Figure 4.8) was produced was performed on the Cycle 8 selection pool sample, to determine sequence similarities in the selection pool.

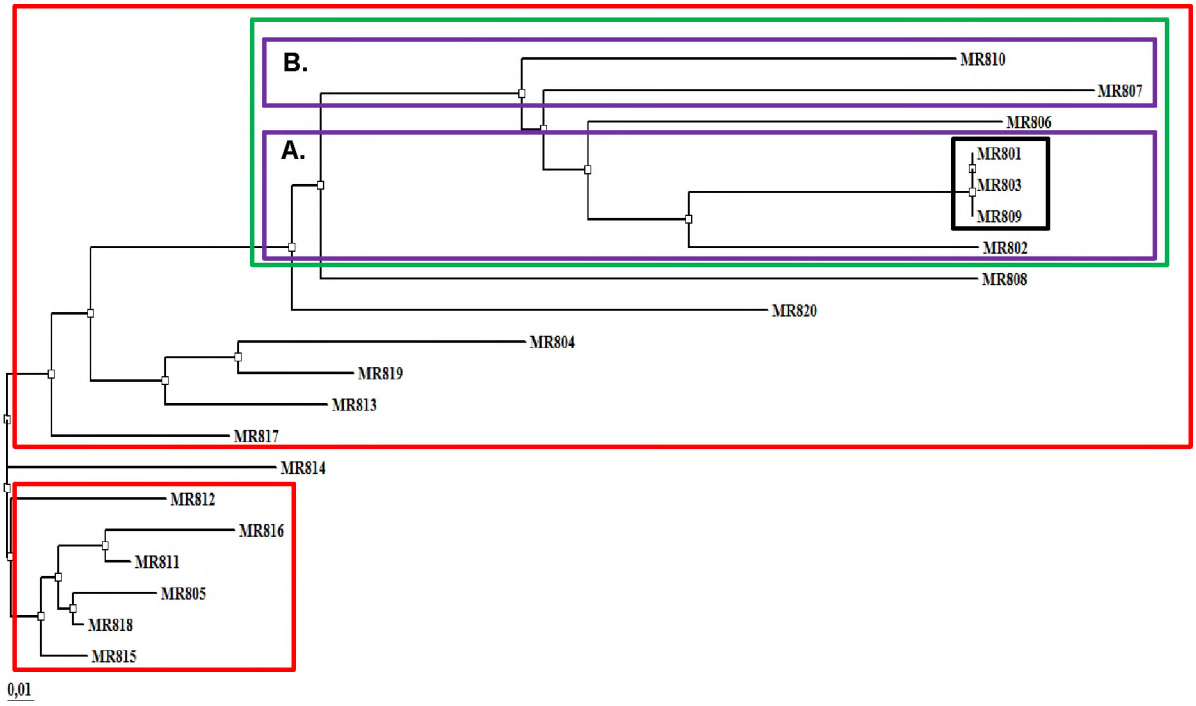

Figure 4.8: Phylogram of aptamer sequences gathered from the SELEX cycle 8 selection pool.

The 0.01 scale bar, presented in the bottom-left of the figure, refers to ~1 nt. mutation.
The red blocks differentiate the two distinct sequence families found in the pool.
The green block represents the seven sequences that maintain the original non-mutated primer regions.
The purple blocks within the aptamer family highlight the subfamilies "A" and "B" of aptamer sequences with the complete primer set for further discussion.

As presented in Figure 4.8, phylogenetic analysis of the sequences drawn from Cycle 8 of the SELEX process grouped the sequences into two distinct sequence family regions (red boxes, differentiate between the two distinct sequence families).

One subfamily "A" (MR801/3/9, MR802, and MR806), demonstrate a 70 % base pair consensus within the family. Additionally, there were sequences that demonstrated a similar sequence identity although they do not really belong to any specific subfamily "B" (MR807 and MR810), which demonstrated a 42 % consensus across the different subfamilies. The subfamily and the closely related sequences highlighted in purple boxes (Figure 4.8). These subfamilies included sequences that contain the unaltered and unchanged primer binding sequences, highlighted within the green blocks.

As concluded above, the sequences from the other sequence family have altered primer binding regions and sequences that demonstrate similarities to the representative sequences gathered from the cycle 11 selection pool i.e. demonstrate possible concatemeric and hybridised sequence identities.

To evaluate the variability of the internal (i.e. non-primer) sequences within the individual sequences, from the aptamer family that did not demonstrated hybridisation within the sequences. A MUSCLE MSA was generated using only this section (variable regions) of the aptamer sequences with the primer regions excluded from the sequences. Figure 4.9 demonstrates the differences in the sequence family groups within the generated aptamers with the non-hybridised sequences. As a control, this included one of the concatemeric sequences (MR808) from the cycle 8 selection pool.

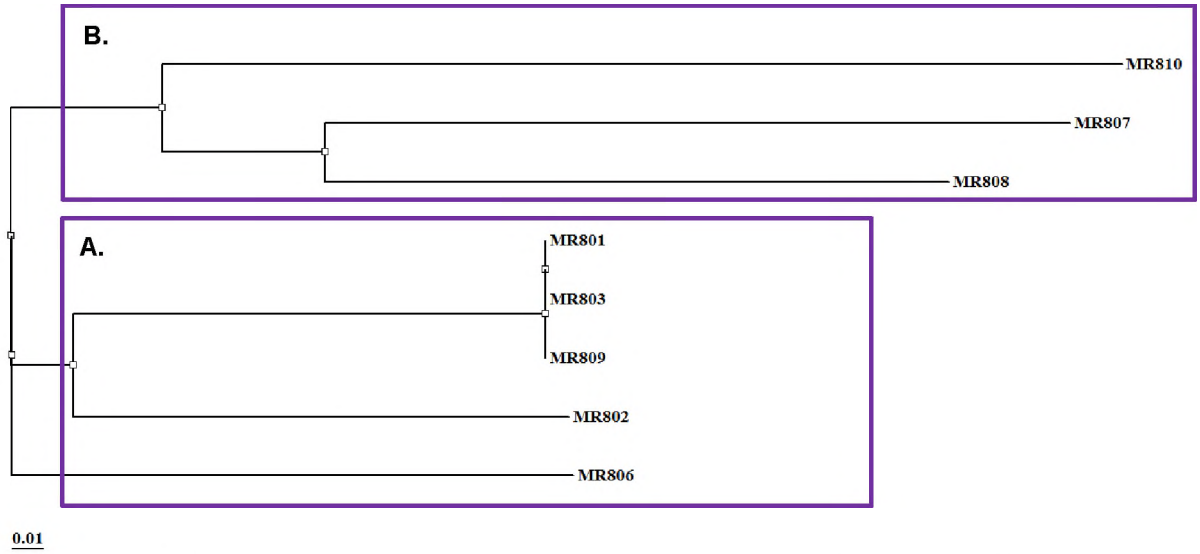

Figure 4.9: Phylogram generated from a MUSCLE MSA of the cycle 8 aptamer sequences following the removal of the conserved primer regions on the flaking regions of the sequence, with a removed primer MR808 sequence.

Where the scale bar of the phylogram represents~5.4 % of an approximate difference of 2 base pairs.

Figure 4.9 illustrates that although there is greater variability noted between the aptamer sequences when removing their primer binding regions from consideration (alignment between the full sequences being presented in Figure 4.9), the proposed sequences within both subfamilies "A" and "B" remain the same and the sequences retain their relative positions. The MR808 sequence demonstrated that the MR807 and MR8010, subfamily "B",

sequences appear to be more similar to the concatemer sequences that of the sequences in sub-family A.

4.4.4.a. Comparison of primary and secondary structures between aptamer subfamilies A and B

During sequence analysis, the aptamer sequences of the aptamer families were compared within their family groups at a higher order structural level (Blind and Blank, 2015).

Primary sequence analysis of the aptamer sequences showed the presence of at least one predicted secondary structure within all the generated aptamers, typically indicative of stem-and-loop motifs within the secondary structures. The GC content of these families ranged between 43 % and 47 %.

Within subfamily "A", both the GC content (and hence, the melting temperatures) were very consistent. Analysis of the sequences MR802, MR801 and MR806 provided an average GC content of 45.7 $\pm$ 2.1 %; calculated melting temperatures of the double-stranded form of the sequences were calculated to be 77.7 $\pm$ 0.1 °°C.

A visual comparison of the alignment of primary sequences and the secondary structure within subfamily "A" is presented in Figure 4.10 below.

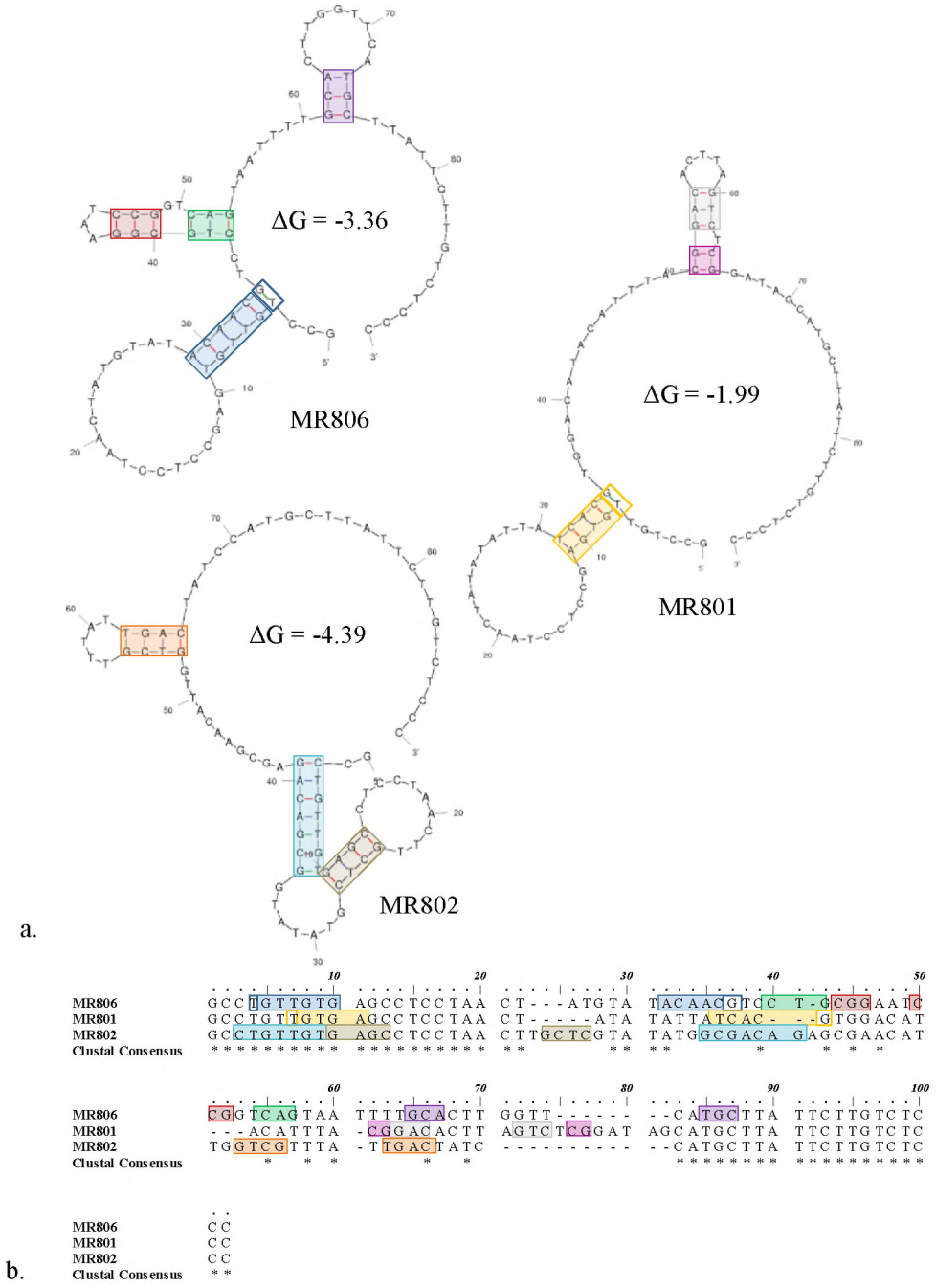

Figure 4.10: Consensus sequences stabilising intra-aptamer secondary structures conserved within sub-family A. MUSCLE MSA alignment was performed using the EMBLE-EBI online software (http://www.ebi.ac.uk/Tools/msa/muscle/).

Software used for secondary structure prediction was UNAFold (http://unafold.rna.albany.edu/).
a) Predictive secondary structure of the evaluated aptamer sequences MR806, MR801 and MR802. Secondary structures possessing the lowest free energy are presented, with the calculated free energy change (kcal/mol) in the centre of the sequences.)
b) MUSCLE multiple sequence alignment of the aptamer family.
The stem regions highlighted in a) of this Figure are presented in b) with the colour scheme unchanged.

Alignment of the aptamers in subfamily "A" (Figure 4.10) illustrates some evidence of sequence conservation within this taxonomic group. Apart from the primer-binding regions of the sequences, 15 of the 49 variable nucleotide residues are conserved within this sub-family following alignment. Noteworthy conserved regions within the family of aptamer sequences is the "TATAT" at position 27 - 31 in MR802 and MR806 that continues with an "ATTAT" region from position 22 - 30 in MR801.

In addition, secondary structure analysis reveals that there are numerous structural similarities between the sequences. Sequence regions of individual aptamers that bind canonically within the secondary structure contributing to stem arrangements are highlighted in Figure 4.10. (colour coded). A combination of canonical and non-canonical base pairings was predicted to occur to stabilise the predicted secondary structure at the lowest free energy of the sequence, with two separate G-T non-canonical base pairs predicted for MR801 and MR806 sequences, respectively.

A conserved secondary motif present throughout the sequences within the family of aptamer sequences is observable (Figure 4.10.a.): a hairpin loop strongly associated with the 5' primer-binding site of the sequence. Highlighted in blue in Figure 4.10.b, the hairpin loop on MR802 is larger than that of MR801 and MR806. Additionally, all three sequences have a small (~ 5 nt.) T-rich region further upstream.

At the primary structural level, MR801 shared more sequence similarity to both MR806 and MR802, than either of the other two exemplars within this subfamily. In addition, the frequency of this aptamer, sequenced in no fewer than three samples from the final selection pool (Figure 5.5), may indicate favourable binding properties. MR801 was selected as the exemplar of this sub-Family for subsequent evaluations

A comparison of the GC and melting temperature of subfamily "B" revealed a much greater variability in this taxonomic group than occurred in subfamily "A". Evaluation of sequences MR807, MR810 and MR808 revealed an average GC content of 47.2 ± 4.0 %; calculated melting temperatures of the double-stranded form of the sequences were calculated to be 76.9 ± 0.4 °C, compared to the more consistent grouping of these values determined for subfamily "A". A visual comparison of the alignment of primary sequences and the secondary structure within sub-Family B is presented in Figure 4.11.

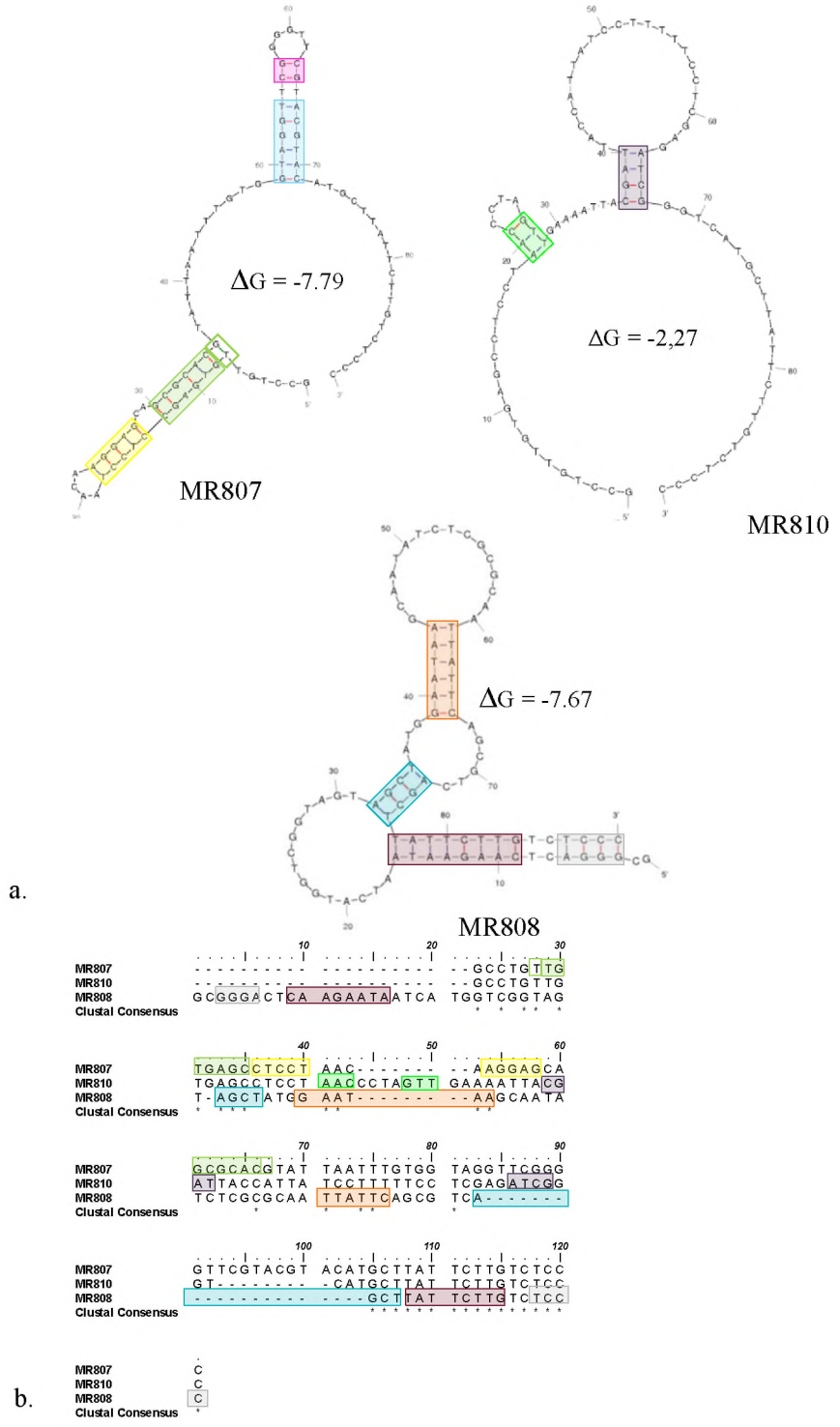

Figure 4.11: Consensus sequences stabilising intra-aptamer secondary structures conserved within sub-family B.

MR807, MR810, and MR808 secondary structure. b) MUSCLE multiple sequence alignment of the aptamer family. The secondary structures with the lowest free energy (given in the centre of the sequences) for each of the aptamer sequences were taken, at the selection conditions of the aptamers. The stem regions highlighted within the secondary structure are unchanged in the primary sequence. Predictive software used for secondary structure folding was, UNAFold DNA folding forum (http://unafold.rna.albany.edu/?q=mfold/dna-folding-form). MUSCLE MSA was evaluated using the EMBLE-EBI online software (http://www.ebi.ac.uk/Tools/msa/muscle/).

As with the aptamer family, the internal sequence binding regions within the MR810 sequence showed little conservation of the secondary structure of the aptamer sequence to other members of its subfamily, as seen in Figure 4.11.b above. The sequence self-binding region identified in the MR807 influences the secondary structure, where the first stem loop (highlighted in both blue and green) in Figure 4.11.a is the result of the internal sequence binding regions within the aptamer sequence.

A MUSCLE MSA comparing the MA-33 aptamer sequence developed by (Kim *et al.*, 2014), with that of the MR801 and MR807 sequences, evidence (data not shown) suggests that there is a 29.7 % alignment of the MA-33 aptamer. In particular, the "GTGG" region~50 base pairs into the MA-33 sequence demonstrated consensus between all three aptamers although closer evaluation into the sequence secondary structures illustrates no secondary structures associated with this consensus point in the MR807 and MR801 sequences (Figure 4.10 and Figure 4.11).

4.4.4.b. Tertiary structure analysis of MR801, MR807 and MR810

Tertiary structure prediction of the generated aptamer sequences was achieved using RNAcomposer (http://rnacomposer.ibch.poznan.pl/) to identify any potential actively binding regions of the aptamers. By comparing the conserved motifs in the aptamers using RNA tertiary structural prediction software. RNAcomposer folds nucleotide sequences according to the folding properties of an RNA sequence, the structure analysis in Figure 4.12 below gives a representative idea to the tertiary structure of the MR801, MR807 and MR810 aptamer sequences. Although it needs to be noted that thymine nucleotides have been substituted by uracil and nucleotide rotation is based on that on the rotational properties of an RNA molecule. In addition, the electrostatic properties of this molecule are calculated on the basis of ribonucleic acid, rather than deoxyribonucleic acid tertiary folding properties.

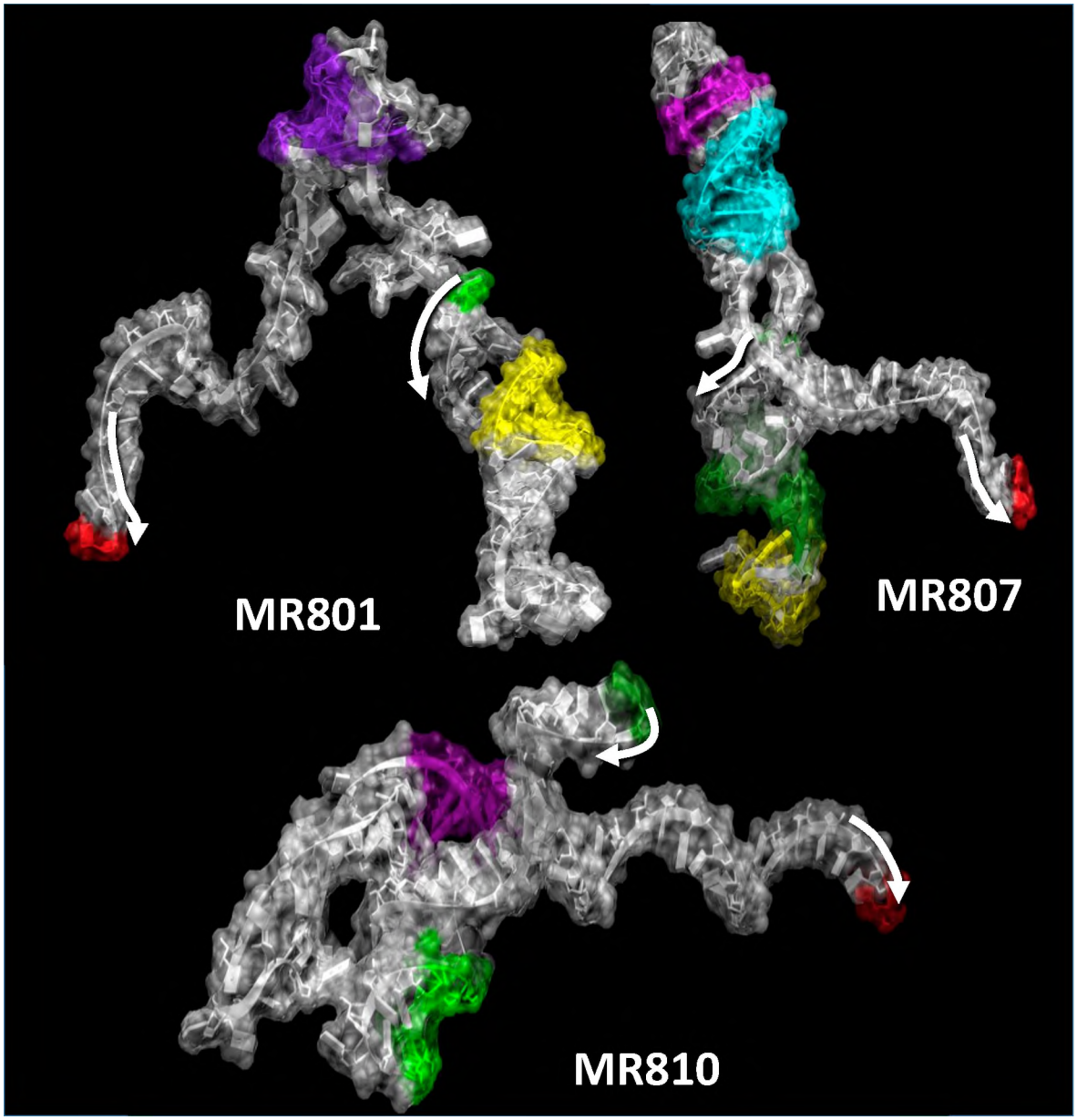

Figure 4.12:. Predicted tertiary structures of the selected sequences MR801, b) MR807, and c) MR810.

Secondary structures are shaded as presented in Figures 5.6 and 5.7 for the relevant structures. Arrows indicate the sequence direction of the oligonucleotide, from 5' end (green nucleotide residue) to 3' (red nucleotide residue).
The structures were predicted using the RNAcomposer online predictive software (http://rnacomposer.ibch.poznan.pl/), with the Vienna secondary structure of the sequences gathered from UNAFold (http://unafold.rna.albany.edu/?q=mfold/dna-folding-form) DNA folding forum.

At the primary structural level, MR807 and MR801, share a 56 % sequence similarity within the nonprime regions of the aptamer. This, however, does not appear to strongly influence either the predicted secondary structure (Figure 4.10 and Figure 4.11) or the predicted tertiary structure (Figure 4.12) of the oligonucleotide sequences.

While the secondary structure indicates that only a select number of residues readily form predictable secondary structures, the tertiary structures (Figure 4.13) demonstrates a sizable portion of the aptamer is capable of self-association. This is evident from a comparison of the regions of the aptamer highlighted in colour with those areas that are coloured light-grey in Figure 4.13. The 3' regions of both MR801 and MR807 do not appear to take part in the tertiary folding of the aptamer sequence. Unlike MR801 and MR807, neither the 5' nor 3' regions of the aptamer of MR810 play a role in the tertiary folding of the aptamer.

4.5. Conclusions

After completing 11 cycles of cell-SELEX, it was evident that high levels of sequence hybridisation and consumerisation between both the selection library and the primer sequences had occurred. Although the representative sequences from the cycle 8 selection pool demonstrated a degree of concatemer formation within the selection pool sample, several aptamer sequences that were not hybridised with other sequences were gathered after 8 cycles of cell-SELEX.

These sequences demonstrated similarity, as determined from a muscle MSA, although there was variability in both the secondary and tertiary structures of the developed aptamer sequences. To evaluate potential best binding sequences, the aptamers making up subfamily "B" (MR807 and MR810) were further analysed, through an epifluorescent assay, to compare the best binding sequence within the sub-family. Furthermore, from sub-family A of aptamer sequences, MR801 demonstrated identity to two other sequences in subfamily "A" and illustrated comparatively the highest similarity toward the other sequences within the secondary structures of the sub-family (Figure 4.10). For these reasons MR801 was used as the representative of subfamily "A" to compare the binding efficiency of the subfamily "B" sequences. Furthermore, the high differences in primary sequence consensus and lack of structural similarity between the two different aptamer subfamilies could possibly the result of multiple targets on the cell surface being targeted.

On comparison to the MA-33 aptamer sequences, developed by (Kim *et al.*, 2014) targeting differentiated 3T3-L1 preadipocytes. The MR807 and MR801 sequences showed a 29.7% MSA alignment consensus with the MA-33 aptamer suggesting that there is little similarity between the adipocyte targeting aptamer (MA-33), and the aptamer sequences developed in this project targeting the undifferentiated 3T3-L1 preadipocytes. This suggests evidence that the developed aptamers could possibly demonstrate a preferable binding to the intended 3T3-L1 preadipocytes rather than that of the differentiated adipocytes.

Chapter 5 : Evaluation of cell-binding and cell-capture abilities of selected sequences

5.1. Introduction

Following *in silico* analysis of the generated aptamers and selection of archetypal sequences, the binding ability of selected aptamers needs to be evaluated and compared through *in vitro* binding assays. There have been a number of reported techniques in aptamer-binding assays, including: electrical impedance spectroscopy or fluorescence-activated cell sorting (FACS) (Avci-Adali, Metzger, *et al.*, 2010), epifluorescence microscopy, and quartz crystal microbalance with dissipation monitoring (QCM-D) (Luzi *et al.*, 2003), flow cytometry and confocal microscopy (Lyu *et al.*, 2016).

Regardless of the technique employed, these assays fall into two separate categories – either the dissolved aptamer is applied to an immobilised target and the binding measured, or the aptamer is itself immobilised onto a solid support and the binding of the target to this immobilised aptamer is measured.

From the dictates of this research project, the aptamer's binding ability was evaluated using techniques derived from both of the mentioned categories. For the purposes of biosensing, the ability of fluorescently-tagged aptamers to bind to target and non-target cells was evaluated. To evaluate the aptamers ability to recruit specific cells and to direct subsequent differentiation, thiol-tagged aptamers were attached onto gold surfaces.

5.1.2. Epifluorescence and Confocal Microscopy

The use of a small fluorophore as a reporting agent allows the aptamer to adopt a folded conformation with minimum steric hindrance from the reporting agent. Monitoring the strength and binding location of the aptamers to the selected target cells could be performed using a fluorescent-based microscopy technique.

Both epifluorescence and confocal microscopy are optical fluorescent microscopic imaging systems capable of the excitation, and detection of the resultant emission, of a desired fluorophore. This fluorophore is typically bound to a probe; thus, this technique serves to evaluate the binding of an external probe to highlight desired regions within the biological system. Using a dichroic beam splitter, the light emitted from the fluorophore may be

imaged, this allows for a qualitative evaluation into fluorophore isolation within the cell (Lichtman and Conchello, 2005) to isolate single molecule fluorescence (in confocal microscopy), and reduce background fluorescence by reducing the area of the illuminated sample. This is achieved using a detector pinhole (approximately 1 μm^2) removing out of focus background fluorescence (Stephens and Allan, 2003).

Epifluorescence and confocal microscopic analysis is often used as a conformational assay system to evaluate the aptamer binding to the cell surface. The increased resolution from the pinhole in confocal microscopy, allows for a high-resolution analysis into the regions of the cell that the aptamer binds.

5.1.3. Controlled seeding of tissue monolayer with aptamer sequences

Self-assembled monolayer (SAM) layers represent a synthetic manner of controlling the surface chemistry at a variety of interfaces. As such, SAM layers provides a means of functionalising surfaces with specific chemical and biochemical moieties. (Lucarelli *et al.*, 2004). SAM layers are constructed on the principle of the spontaneous and highly-ordered aggregation of specific organic materials, occurring either at solid or liquid surfaces (Newton *et al.*, 2013).

Thiol-modified aptamer sequences have often been reported for their use in the formation of SAM surfaces possessing defined binding properties (Lucarelli *et al.*, 2004). Evaluation of the binding abilities of these surfaces is often conducted by gravimetric (e.g. QCM-D) and impedimetric quantification methods. Of the impedimetric methods, a technique that lends itself well to both cell-aptamer interactions - and multiplexed analyses in general - is the use of the xCELLigence Real-Time Cell Analyser (RTCA).

The xCELLigence system is a Roche-developed cell analysis technology, which permits for the real time cellular tracking of phenotypic shifts of cellular migration, proliferation and invasion readouts in a label-less manner (Kustermann *et al.*, 2013). Through the use of interdigitated gold microelectrodes within the wells of a 96-well microtiter plate, this system impedimetrically monitors cell growth across the surface of the electrodes (Zhang, 2014). The differences in the impedance with time are converted into an arbitrary unit termed as the cell index (CI). Figure 5.1 below provides a schematic overview of the 94-well layout and CI software conversion formulae used by the xCELLigence system Real-Time Cell Analyser.

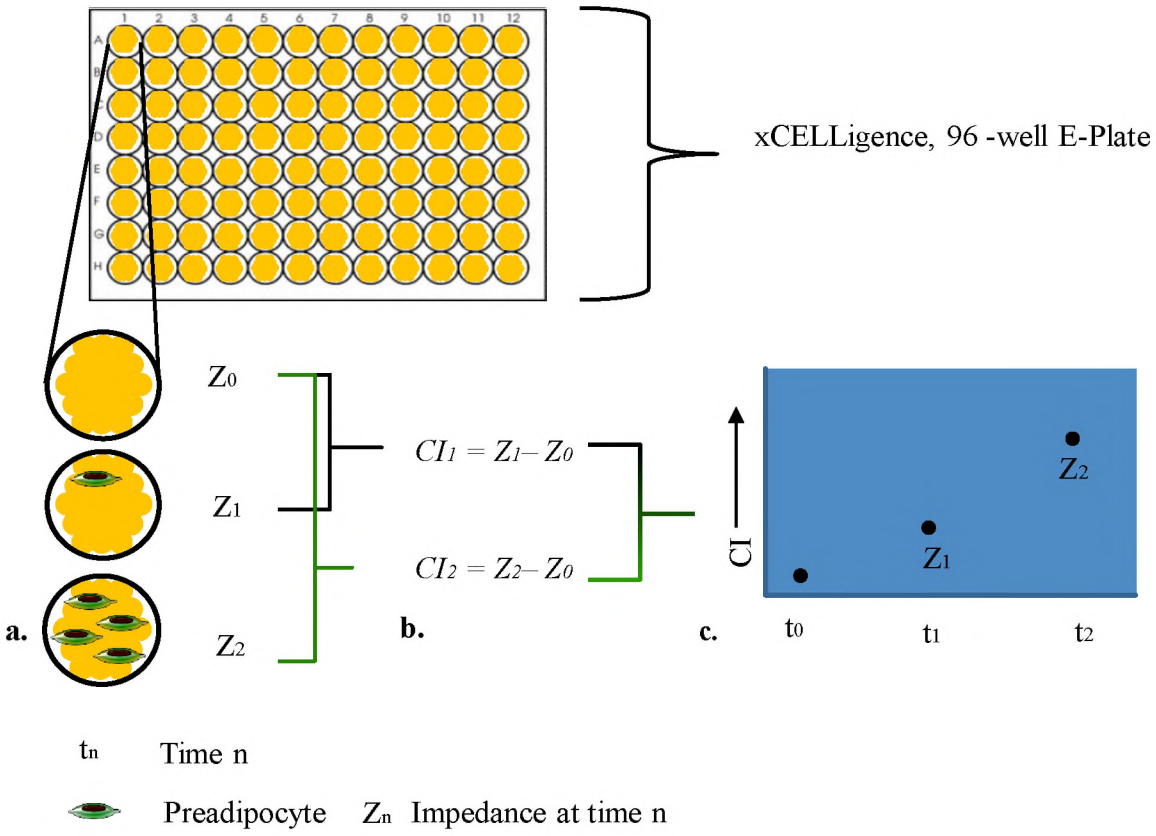

Figure 5.1: Schematic representation of the CI Impedimetric measurement with time.

a) Cell growth on the surface of the gold electrode. b) Formulae used in the calculation for the change in cell index with time, and c) plotting of change in cell index with time. Z_n and CI_n represent the measured impedance and Cell Index at time = n (t_n).

An arbitrary property derived from the electrochemical impedance signal response, the CI provides a comparative measure describing the cellular state of the seeded cells adhered on the E-plate surface at the given time point (Martinez-Serra *et al.*, 2014) and monitoring it relative to the signal responses from other wells present within the plate. In general, the more cells adhering to the sensor surfaces, the greater the resultant CI value would be (Zhang, 2014), as schematically represented in Figure 5.1. Additionally the xCELLigence cell monitoring system has been able to determine changes with regard to real time cellular interaction of small molecules in solution (Zhang, 2014).

5.2. Objectives

Exemplars from the families of the developed aptamer sequences (Chapter 4) were sourced and compared by various binding assays to compare and evaluate the best sequences for the staining of preadipocytes 3T3-L1 cells and to selectively capture the said cells. The affinity of the aptamer binding to the targets was evaluated using a combination of epifluorescent microscopy, confocal microscopy and SAM binding analysis using the Roche xCELLigence real time cell analyser.

5.3. Methods and Materials

5.3.2. Epifluorescence analysis of aptamer binding

5.3.2.a. Amplification of selected sequences for preliminary epifluorescent

The amplification of specific aptamer sequences (MR807 and MR810) and Lambda exonuclease digestion of the dsDNA PCR template was achieved as mentioned in the dsDNA amplification of selection library for cell-SELEX section above, using the 5' labelled 6-FAM forward primers in Chapter 2 section 2.2.3.a and 2.2.3.b.

A 400 µl binding buffer solution containing 7.11 $x10^{-3}$ pmol (~ 0.4 µg) of ssDNA aptamer was formulated for each of the selected aptamer sequences. The binding buffer solution, preparation of the 3T3-L1 preadipocytes and the binding conditions of the assay was followed as mentioned in the protocol followed for cell-SELEX selection in Chapter 4 section 4.3.2.

5.3.2.b. Binding assay condition

The binding conditions of the assay were performed at a reduced volume to that of the aptamer selection conditions using, 200 µl/ well of a 24-well plate (approximately 2×10^5 cells/ well). A blank solution containing 200 µl of only binding buffer was added to samples of adhered cells to quantify and account for any cellular autofluorescence arising from the attached cells.

The aptamers were then incubated at 37 °C for 1 hour, with gentle shaking at~50 rpm on a horizontal orbital shaker. The binding buffer was removed and the wells rinsed 3 times with the wash buffer, as described in section 2.2.1.b.

5.3.2.c. Epifluorescent visualisation of cells exposed to different aptamer sequences

Epifluorescent binding analysis of the aptamers to the preadipocytes and adipocytes were evaluated as mentioned in Chapter 2, Section 2.2.1.f.

Fluorescent microscopy was performed using the Zeiss filter set 44, with an excitation waveband between 450-500 nm and the emission between 500 – 550 nm. To maintain comparable data, the exposure and capture settings for each image were maintained.

5.3.3. Confocal Microscopic visualisation of cells exposed to different aptamer sequences

Sequence MR801, MR807 (as developed in Chapter 4) and C27, (an in-house aptamer developed and patented in South Africa by Cromhout *et al.*, (2015), (5' - GCCTGTTGTGAGCCTCCTAACTAGCTCGTAGAAAAAAAATATAGCGTGTGCTGG GACTGCTCGGGATTGCGGACACATGCTTATTCTTGTCTCCC - 3') were sourced from IDT DNA (South Africa). All the sequences were labelled on the 5' end with a Cy5 fluorophore in binding buffer (as described above in Chapter 2, section 2.2.1.b.). These were used at 1 μM concentrations (formulated from a stock concentration of $1x10^{-4}$ M dissolved in TE buffer), using binding buffer.

A binding assay of the aptamers to both the 3T3-L1 preadipocytes and the adipocytes was conducted, as mentioned in a similar method as that done in Chapter 5, section 5.3.2.b. Where 200 μl of each of the aptamer solution was formulated in the described binding buffer ($3.55\ x10^{-3}$ pmol, ~ 0.2 μg aptamer/ well), and added into a 24-well tissue culture plate with the 3T3-L1 preadipocytes and adipocytes (previously grown to confluency and cultivated as mentioned in Chapter 2, section 2.2.2. above) over the surface of a sterilized glass slide coverslip.

Following the binding assay the cells were washed three times with the wash buffer, formulated as described above in Chapter 2, section 2.2.1.b and fixed to the surface of the glass coverslip using 4 % $^{w}/_{v}$ formaldehyde solution (purchased from SaarChem, (35 % $^{w}/_{v}$ initial concentration) for 30 minutes. The coverslips were mounted onto the surface of a microscope slide using Dako Fluorescence Mounting Media (Sigma-Aldrich), and left to dry in the dark at room temperature for 48 hours.

Prepared slides were then visualised using confocal microscopy as stated in Chapter 2, section 2.2.1.g. As mentioned in section 2.2.1.g the exposure and imaging settings for the microscope were maintained throughout the imaging of the cells.

5.3.4. RTCA xCELLigence real time cell analysis

The proposed method of aptamer/ SAM cell capture and binding to the surface of the xCELLigence E-plate has been illustrated in Figure 5.2 below. The formation of the SAM and aptamer binding to the surface of the SAM was assessed using the Roche xCELLigence real time cell analyser SP system operated inside a 37 ˚C humidified incubator, with 5% CO_2 levels. The sensor surface of the xCELLigence E-plate is comprised of a gold surface on the bottom layer of the 96 well plate configuration illustrated in Figure 5.1 above. The surface electrode allows for cellular growth and changes in the electrode impedimetric readings.

This study was divided into three distinct phases: the formation of the aptamer SAM on the electrode surfaces (Figure 5.2.a), the binding of cells to these aptamers (Figure 5.2.b), and the growth and differentiation kinetics of the cells thereafter. The 3T3-L1 preadipocytes were cultured and placed in suspension as mentioned in Chapter 2, section 2.2.2.b above, using trypsin to separate the adhered preadipocytes from the surface of the culture flask, although the cells were suspended in the mentioned binding buffer (see Chapter 2, section 2.2.1.b.) instead of the mentioned preadipocyte nutrient growth media.

The binding capabilities of the preadipocytes to the aptamer sequences was also evaluated in the complex nutrient growth media of the preadipocytes (mentioned in Chapter 2, section 2.1.1 above)

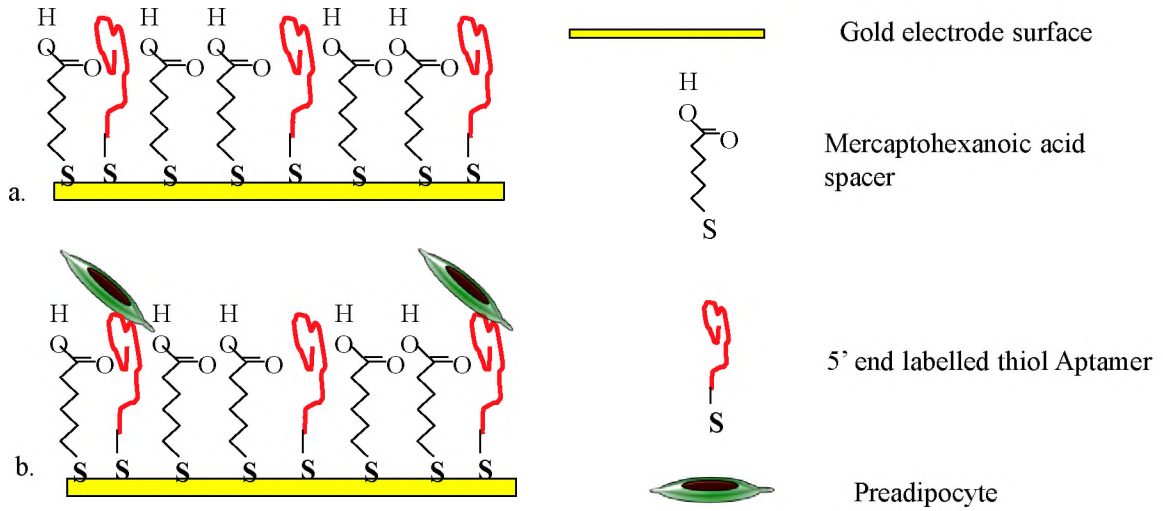

Figure 5.2: Schematic representation of the proposed aptamer/ Mercaptohexanoic acid SAM on the electrode surface of the E-plate.

a.) Aptamer / mercaptohexanoic acid SAM before preadipocytes bind. b.) proposed binding regions of the preadipocytes on the SAM surface

5.3.4.a. Buffers and reagents used for RTCA xCELLigence real time cell analysis

Surfacing of the electrodes was achieved using the formation of a 5' thiolated MR807 sourced from WhiteSci IDT DNA (South Africa), with a final concentration of 0.5 µM and 1 µM aptamer solution mixed with a 73 µM β-Mercaptohexanoic acid (Sigma-Aldrich). Several controls were employed for this analysis: a 1 µM 5'-thiolated C27 aptamer, sourced from WhiteSci IDT DNA (South Africa): 73 µM β-Mercaptohexanoic acid spacer in 10 X HMCKN; and 73 µM β-Mercaptohexanoic acid spacer only. Additionally a 1 µM of a previously developed aptamer (MA-33) developed by (Kim *et al.*, 2014) was 5'-thiolated and used alongside 7.30 $x10^{-5}$ M β-Mercaptohexanoic acid was used as an additional control aptamer sequence.

All thiols were dissolved in a 10 X HMCKN buffer ($2x10^{-3}$ M 4-(2-hydroxyethyl)-1-piperazineethanesulfonic acid, $1.50x10^{-2}$ M NaCl, $2x10^{-4}$ M KCl, and $2x10^{-4}$ M $MgCl_2$, $2x10^{-4}$ M $CaCl_2$ pH 7.4. Before exposing the surface to the thiol mixture, the thiol solutions were heated to 95 °C for 10 minutes and immediately cooled at 4 °C for 5 minutes.

5.3.4.b. RTCA xCELLigence real time cell analysis system conditions

An initial blanking sweep of the electrodes was performed using 100 µl of the 3T3-L1 preadipocyte nutrient medium (formulated as discussed, as per Chapter 2) for 1 sweep for 1 minute. The nutrient media was removed and the wells washed once with a 10 X HMCKN buffer, followed by the addition of a 10 X HMCKN buffer with the added aptamer/ β - Mercaptohexanoic acid spacer. The E-plate was loaded into the RCTA system and SAM formation was measured every 10 minutes for 60 minutes, following which the E-Plate was removed and the remainder of the SAM solution was removed and the wells washed with 10 X HMCKN, followed by a wash using the binding buffer.

A suspension of 5 000 cells/ ml in binding buffer was formulated from harvested 3T3-L1 as seen in Chapter 2, Section 2.2.2.b, and wells were seeded using 500 cells. As a further control, 500 preadipocytes suspended in 3T3-L1 growth media were seeded into a set of surfaces modified with 1 µM MR807: 75 µM mercaptahexanoic acid SAM layer.

The binding of the cells to the SAM layer was measured every 10 minutes for 2 hours, using the RTCA system. Subsequently, the solutions were replaced with 3T3-L1 preadipocyte nutrient media, whereby the cells were incubated for a 20 hour period.

Following the 20 hour cell growth stage, the E-plate was removed and the wells were washed with PBS, followed by the addition of differentiation media and maintenance media, which proceeded as outlined in Chapter 2, section 2.2.2.d. The cells were then allowed to initiate differentiation for 68 hours in RTCA system with 10 minute data intervals.

5.3.4.c. RTCA xCELLigence Data Analysis and Interpretation

All samples presented in this section were performed in triplicate and the data is presented in text as the average of the samples $\pm$ the standard error of the means.

As well as the direct comparison of sample using CI values, other data transformations of the xCELLigence software can yield interesting and pertinent analysis into the growth properties of the cells. This includes the Delta Cell Index (DCI) (Biosciences, 2013), presented in Equation 5.1 below. The DCI normalises the CI at a designated time point in the reaction, and further calculates the difference between the CI of the sample to a desired reference sample at a desired CI time point. This allows for changes in CI to be controlled across a variety of treatment samples, when treated at different stages over the experimental analysis. this minimises the effects of chemical changes during the analysis of cellular growth on the CI

value. Allowing for a more accurate analysis of cellular binding and growth across a variety of chemically-variable samples.

$$DCI = CI\,[original] + (DCI\,[reference] - CI\,[delta\ time])$$

Equation 5.1: Alternate equation used to calculate the Delta Cell Index.

To account for differences in CI between surfaces bearing varying aptamer/ β-Mercaptohexanoic acid ratios SAMs, the DCI of each sample was evaluated at each time point: i, ii, iii, and iv (Figure 5.9) at the start of each nutrient media or buffer change durnig the xCELLigence assay. Each sample containing cells was referenced to the CI of samples containing a control SAM layer with the same aptamer/ β-Mercaptohexanoic acid ratios without any cells added.

5.4. Results and Discussion

5.4.1. Epifluorescent microscopy analysis of binding selectivity of MR807 and MR810

An epifluorescence binding assay between MR807 and MR810 was used to evaluate the potential binding efficiencies between the MR807 and MR810 sequences. Initially, sequences were amplified using PCR, because of the repetitive nature of the sequences as seen in Section 2.2.3.b. and ssDNA was synthesised as proposed in Section 2.2.3.c.

Figure 5.3.a - f. below demonstrates the comparison of the two selected aptamers, MR807 and MR810, ability to bind to adipocytes and preadipocytes, as investigated using epifluorescent microscopic imaging.

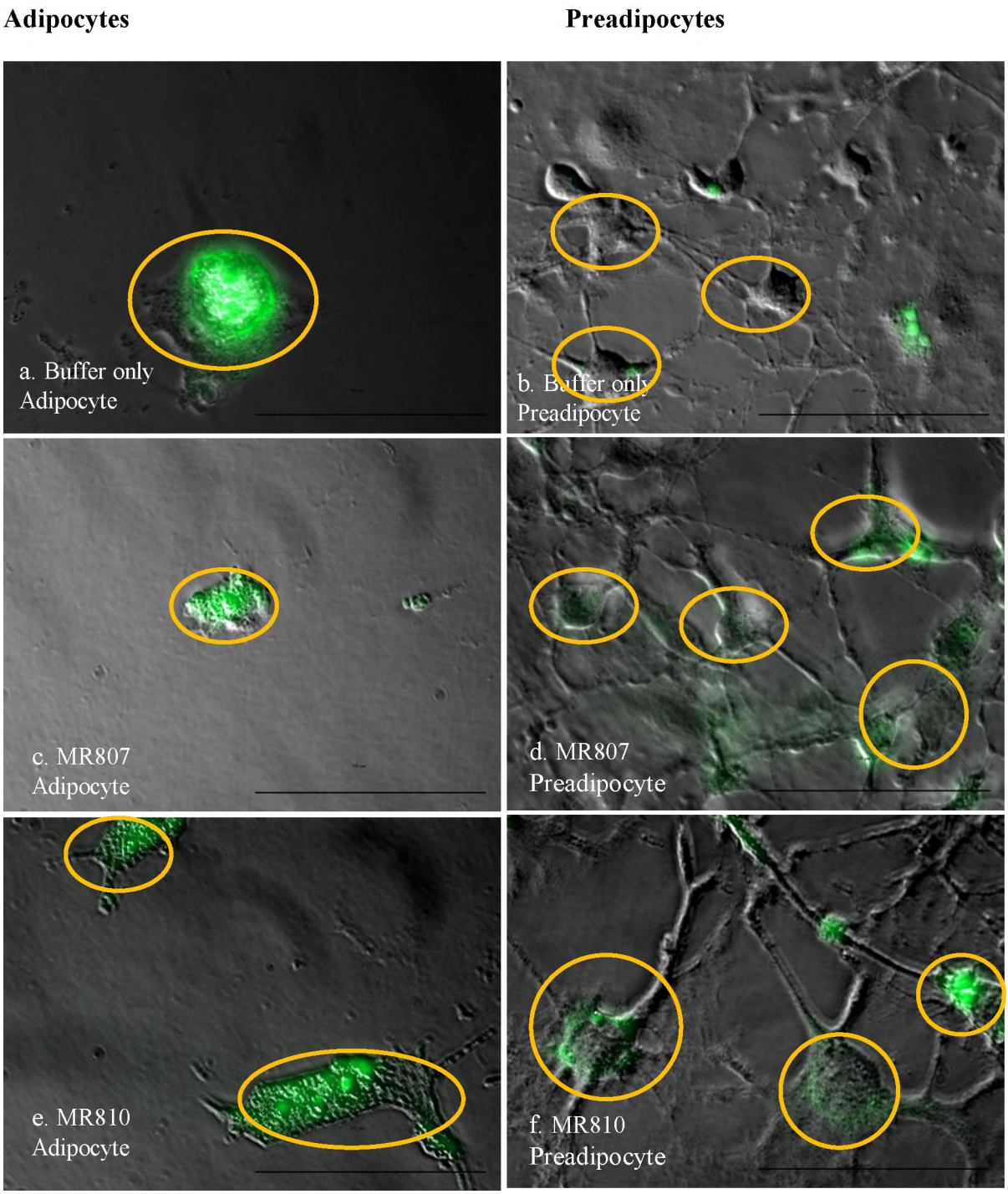

Figure 5.3: Epifluorescent micrographs comparing sequence binding specificity with both the 3T3-L1 preadipocytes and adipocytes, using 5' 6-FAM labelled MR807 and MR810.

The micrographs were obtained at 40 X magnification. Presented scale bars are 100 μm in length. Images a) Binding buffer only, c) MR807 and, e) MR810 aptamer sequences. Negative binding assay with differentiated 3T3-L1 preadipocytes having undergone differentiation for 14 days. While micrographs b) binding buffer only, d) MR807, and f) MR810 aptamer sequences are positively

selected sequences using 3T3-L1 preadipocytes not having undergone differentiation. Cells highlighted in yellow circles.

Autofluorescence, i.e. the tendency of the cells themselves to generate fluorescent signal, was notable in both the adipocytes (Figure 5.3.a) and to a lesser extent, the 3T3-L1 preadipocytes (Figure 5.3.b) during epifluorescent imaging of the cells. As expected, the adipocytes possess stronger autofluorescence compared to the preadipocytes (Salomatina *et al.*, 2011), which is attributed to the high levels of light refraction occurring within the circular lipid vacuoles within the cells. These are clear in both adipocytes and preadipocytes, but are more frequent and larger within samples of adipocytes (comparing Figure 5.3.a. with Figure 5.4.b.). The cell vacuoles were excluded from consideration when evaluating binding of the 6-FAM - conjugated aptamer to the two different cell lines.

Comparison of both the MR807 and MR810 aptamer sequences in Figure 5.3 suggests that there is preferential binding to 3T3-L1 preadipocytes (Figure 5.3.d. and f) as opposed to mature adipocytes (Figure 5.3.c and e.): little fluorescence was notable in the outer regions of the adipocytes where vacuoles are not located upon aptamer staining. This was anticipated, since the yield from the aptamer pool in cycle 8 of SELEX still showed limited binding to adipocytes and preferential binding to preadipocytes, with 74.11 % of the selection library - binding to the 3T3-L1 preadipocytes and 0.69 % of the selection library binding to the adipocytes (Chapter 4, section 4.4.1).

Fluorescent evaluation into the binding properties of both the MR807 and MR810 aptamers, indicate that different regions of 3T3-L1 cells are preferentially bound by the respective aptamers. The MR807 sequence seems to bind to the outer regions of the preadipocytes, especially located around cell-cell interaction regions (Figure 5.3.d.). This suggests that the aptamer could possibly bind a protein or protein complex involved in either cellular communication or a protein involved with cellular adhesion. Unlike the MR807 fluorescence profile, the binding fluorescence of MR810 tends to focus around the upper central regions of the preadipocyte, although autofluorescence given off from the cells are still predominant in the inner regions of the adipocytes (Figure 5.3.e.).

Due to the high degree of interference from cellular components from the 6-FAM fluorophore The MR801 and MR807 sequences were later purchased with a 5' labelled cy5 fluorophore to use for high resolution confocal microscopy, due to instrument limitations in visualising the 6-FAM tag on the aptamer sequences.

5.4.2. Confocal microscopic imaging of aptamer sequences

Confocal microscopic analysis of aptamer binding allowed for high resolution fluorescence analysis and confirmation of fluorescently labelled aptamer binding to the 3T3-L1 preadipocytes. Figure 5.4, and Figure 5.5 below demonstrates the binding of the aptamer to both the 3T3-L1 preadipocytes and adipocytes with no aptamer, additionally with an independent evaluation of the MR801, and MR807 sequences. While Figure 5.6 illustrates the binding of the preadipocytes from a combination of both a 0.5 μM MR801 and 0.5 μM MR807 aptamer sequences. An additional control used in the binding assay was the inclusion of C27 aptamer, an in house aptamer bearing the same primer-binding regions, developed to bind to the human CD4 transmembrane protein (Figure 5.6), (Cromhout *et al.*, 2015) laser intensities remained the same between samples, allowing for comparable image analysis. A 405 nm excitation laser with an emission filter set between 410–505 nm was added as an additional baseline control for regions of high cellular autofluorescence on the micrographs.

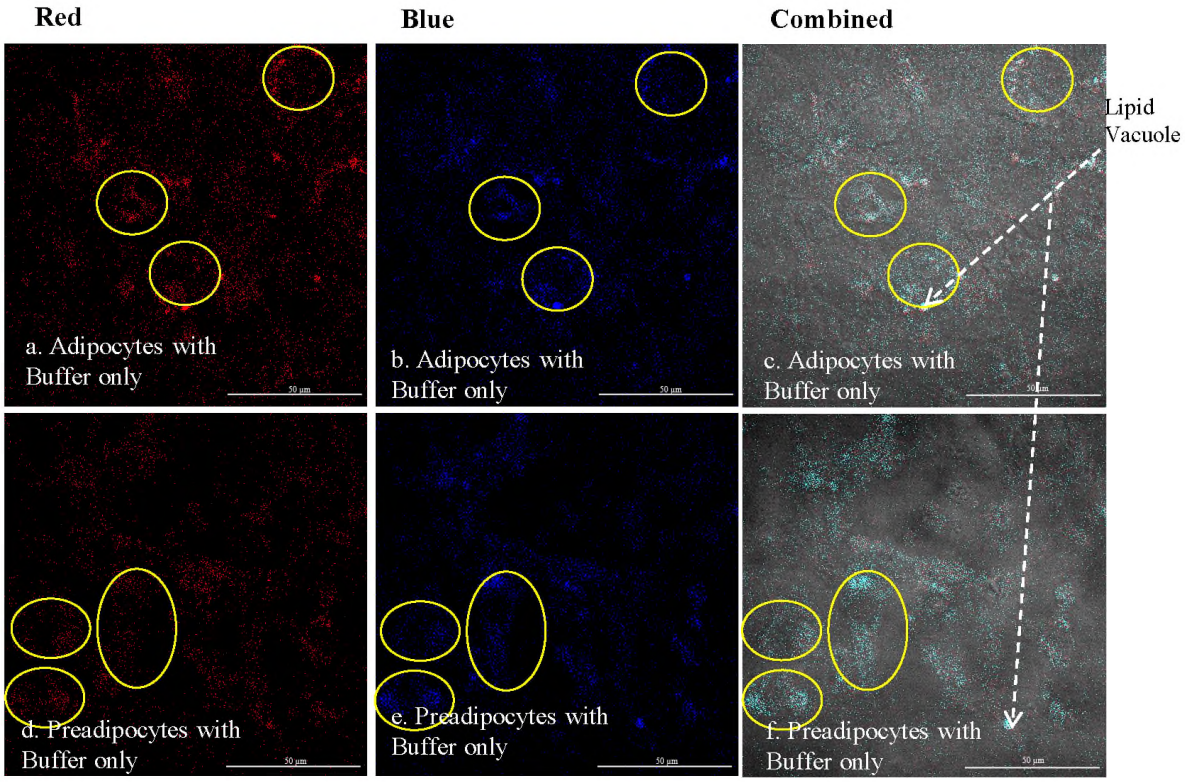

Figure 5.4: Confocal micrograph demonstrating autofluorescence present in both 3T3-L1 preadipocytes, and the derived mature adipocytes.

Demonstration of autofluorescence in the mature adipocytes using a.) red, b.) blue filter sets. c.) Phase contrast image overlaid with both the red and blue filters.
Autofluorescence of 3T3-L1 preadipocytes is presented using d.) red, e.) blue filter sets f.) Phase contrast image overlaid with both the red and blue (depicted as turquoise) filters in binding buffer only.
The yellow circles highlight cells that are difficult to visualise. Filter settings are outlined in Chapter 2, Table 2.1. Scale bars in all the micrographs represent 50 μm.

Baseline confocal analysis demonstrates that cellular autofluorescence is present in both the 3T3-L1 preadipocytes and mature adipocytes. This autofluorescence tends to occur in the spectral region of interest of the cells, overlapping those portions of the spectra occupied by Cy-5 (red filters, Figure 5.5 a. and d.). However, it is stronger in other portions of the spectrum (e.g. blue filter Figure 5.4 above) and is more prominent when comparing mature adipocytes (Figure 5.4.a-c.) to preadipocytes (Figure 5.4.d-f.). This reinforces the selection of Cy-5 as a fluorophore to decrease interference from the sample when monitoring potential fluorescent binding of the aptamer to the cell targets.

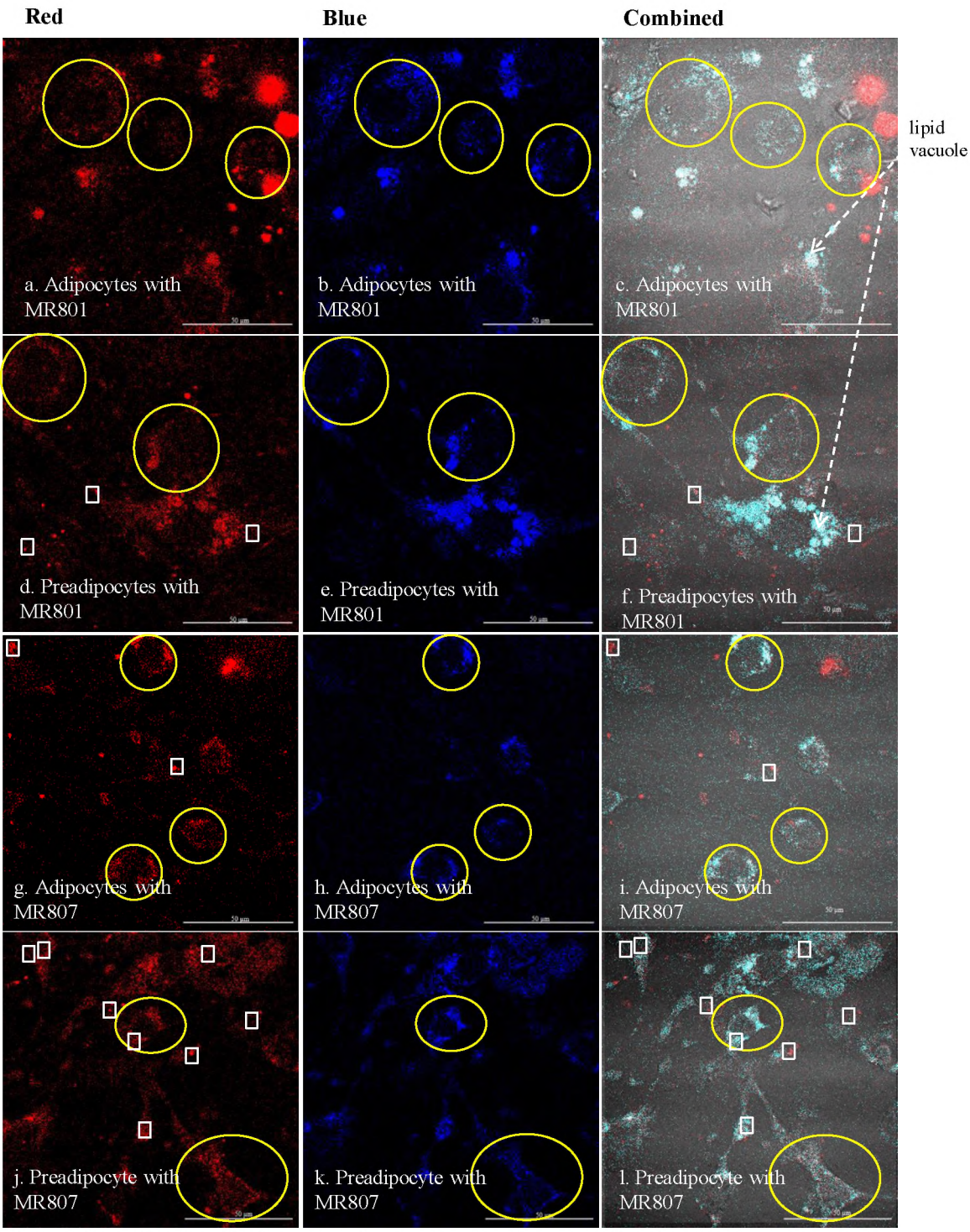

Figure 5.5: Confocal micrograph demonstrating the binding of the aptamer sequences MR801 and MR807 to the surface membranes of both 3T3-L1 preadipocytes and mature adipocytes.

Demonstration of MR801 binding to the surface of adipocytes using a) red, b) blue filter sets with c) Phase contrast image overlaid with both the red and blue (depicted as turquoise) filters. Demonstration of MR801 to the preadipocytes d) red, e) blue filter sets with f) Phase contrast image overlaid with both the red and blue (depicted as turquoise) filters. A demonstration of MR807 binding to the surfaces of mature adipocytes g) red, h) blue filter sets with i) Phase contrast image overlaid with both the red and blue (depicted as turquoise) filters. Demonstration of 3T3-L1 preadipocytes

binding to the surfaces of 3T3-L1 preadipocytes j) red, k) blue filter sets with l) Phase contrast image overlaid with both the red and blue (depicted as turquoise) filters. White blocks represent regions of high red fluorescence excited with the 630 nm laser highlighting possible aptamer binding regions to the cells. yellow circles highlight individual cells. Scale bars in all the micrographs representing 50 μm.

Figure 5.5 above presents confocal micrographs illustrating the binding of the MR801 and MR807 aptamers under standard aptamer binding conditions, to both 3T3-L1 preadipocytes and mature adipocytes. Aside from vacuole-generated auto-fluorescence, there do not appear to be regions of high red-channel fluorescence on the surface of the MR801-treated adipocytes (Figure 5.5.a-c); in contrast, preadipocyte samples treated with MR801 demonstrated regions of high red fluorescence, some of which are highlighted in white squares in Figure 5.5.d-f, as well as an overall greater extent of cellular fluorescence.

Similarly, there appeared to be decreased red fluorescence in the mature adipocyte samples presented with the MR807 aptamer (Figure 5.5.g-i.), although there did appear to be discrete regions of the mature adipocyte cell surface that the aptamer binds to. In contrast to MR801, fluorescence of preadipocytes treated with MR807 aptamers appear to outline the cell margins more evenly, resulting in a greater contrast between the cells and the extracellular spaces (comparing Figure 5.6.j. to Figure 5.6.d). Areas exhibiting large, discrete, red fluorescence appeared to be much lower in extent than that of the MR807 aptamer sequence binding to the surface of the 3T3-L1 preadipocytes, but still exhibit greater overall red fluorescence than the mature adipocytes (Figure 5.6.j. vs. Figure 5.6.g).

The MR801 and MR807 sequences were then combined and used to simultaneously stain the target cell lines. A mixture containing $5x10^{-7}$ M of each aptamer sequence was employed to evaluate the efficiency of aptamer binding to the surface of both the preadipocytes and mature adipocytes (Figure 5.6.a-f), and a control C27 aptamer (targeted to human CD4) with mature adipocytes and 3T3-L1 preadipocytes (Figure 5.6.g-l).

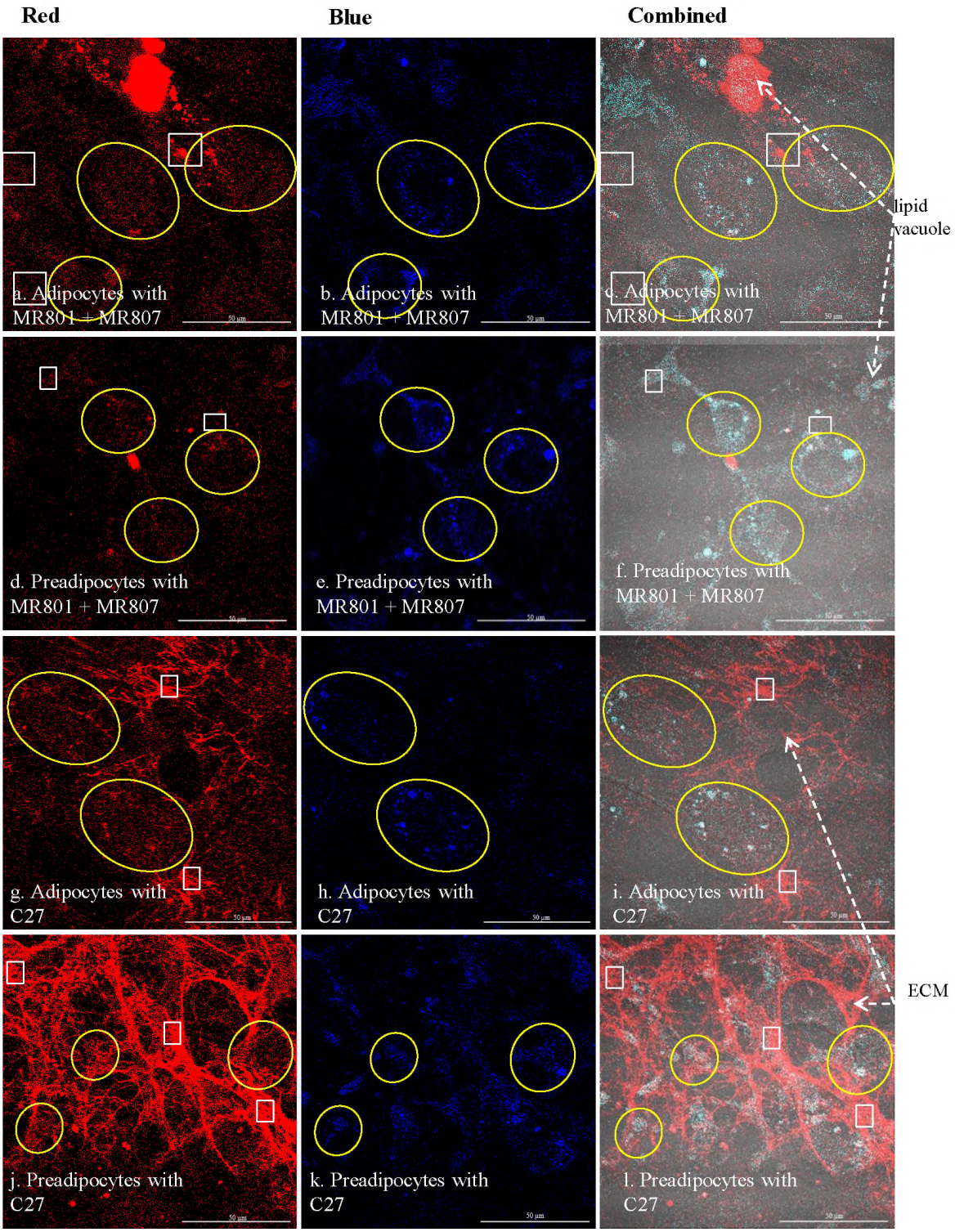

Figure 5.6: Confocal micrograph the binding of C27 and a combination of MR801 and MR807 to the surface membrane of both 3T3-L1 preadipocytes and mature adipocytes.

Demonstration of a 1: 1 combination of the MR807 and MR801 sequences binding to the surfaces of mature adipocytes a) red, b) blue filter sets with c) Phase contrast image overlaid with both the red and blue (depicted as turquoise) filters. Demonstration of a 1: 1 combination of the MR807 and MR801 sequences binding to the surfaces of 3T3-L1 preadipocytes d) red, e) blue filter sets with f) Phase contrast image overlaid with both the red and blue (depicted as turquoise) filters.

Demonstration of C27 (Cromhout *et al.*, 2015) binding to the surface membrane of mature adipocytes g) red, h) blue filter sets with i) Phase contrast image overlaid with both the red and blue (depicted as turquoise) Demonstration of C27 (Cromhout *et al.*, 2015) binding to the surfaces of 3T3-L1 preadipocytes j) red, k) blue filter sets with l) Phase contrast image overlaid with both the red and blue (depicted as turquoise) filters. White blocks represent regions of high red fluorescence excited with the 630 nm laser highlighting possible aptamer binding regions to the cells. The yellow circles highlight cells that are difficult to visualise. Scale bars in all the micrographs represent 50 μm.

Confocal analysis from Figure 5.6 of the combined application of MR807 and MR810 sequences suggest that there was a decrease in the binding of the combined aptamers to the preadipocytes, in contrast to the fluorescent response of individual sequences. This could possibly arise from hybridisation of the MR807 and MR801 sequences disrupting the secondary and tertiary active sites in both of the aptamers, evaluated in Figure 5.8.a. in standard aptamer binding conditions, and Figure 5.8.b. at room temperature. This reduction in the binding of the MR801 and MR807 mix was later confirmed and demonstrated in Figure 5.6.

The binding of C27 to what appears to be a component of the extracellular matrix (ECM) secreted by both the preadipocytes and adipocytes (albeit, to a lower extent in the mature adipocytes) was an unanticipated result. C27 is an aptamer sequence targeting human CD4, specifically the extracellular domain presented on the surface of cells (Cromhout *et al*, 2015). The decrease in emission intensity between the ECM of the preadipocytes (Figure 5.7.j) and adipocytic ECM (Figure 5.7.g) stained with C27 suggest that the aptamer is binding to a target that is downregulated in the ECM of the adipocyte culture.

The ECM (basal lamina) in mature adipocytes has been shown to demonstrate similar characteristics on a number of cell lines including osteoblasts, chondrocytes (Mariman and Wang, 2010). Not only does the ECM provide a scaffold for cellular support, evidence suggests that a strong basal lamina is essential to reduce extracellular mechanical stress within the lipid filled adipocyte (Mariman and Wang, 2010). It has been well documented that changes in the expression levels of different protein matrices during cellular differentiation occur (Mariman and Wang, 2010). The basal lamina of adipocytes is made up of at least 215 proteins (Ojima *et al.*, 2016), of these Collagen (I, II, III, IV, and VI) has been cited as a major part of the adipocyte ECM (Mariman and Wang, 2010; Ojima *et al.*, 2016).

From the confocal images presented in Figure 5.6.g-l, the C27 aptamer sequence appears to bind strongly to a fibrous extracellular matrix component of the cells that appears to be downregulated during adipogenesis. There is a variety of potential target molecules in the

ECM of the preadipocytes that could be implicated, including: collagen (Frith *et al.*, 2012) (human MSCs), fibronectin (Fu *et al.*, 2011) (human ESC), laminin (Fu *et al.*, 2011) (human ESC), and actin (Liu *et al.*, 2005) amongst others.

To quantitatively analyse the binding of the MR801, MR807 and C27 sequences to both the mature adipocytes and preadipocytes to that of cellular autofluorescence given off by the cells. The fluorescent responses given off by the aptamers were evaluated the and the difference in the relative florescent intensity of the cells to that of the background fluorescence given off by the microscope. The red fluorescent emission between 638 – 739 nm, cellular regions were highlighted and fluorescent intensity were interpreted as the difference in the fluorescent intensity between the cell and the extracellular space. These results have been illustrated in Figure 5.7 below.

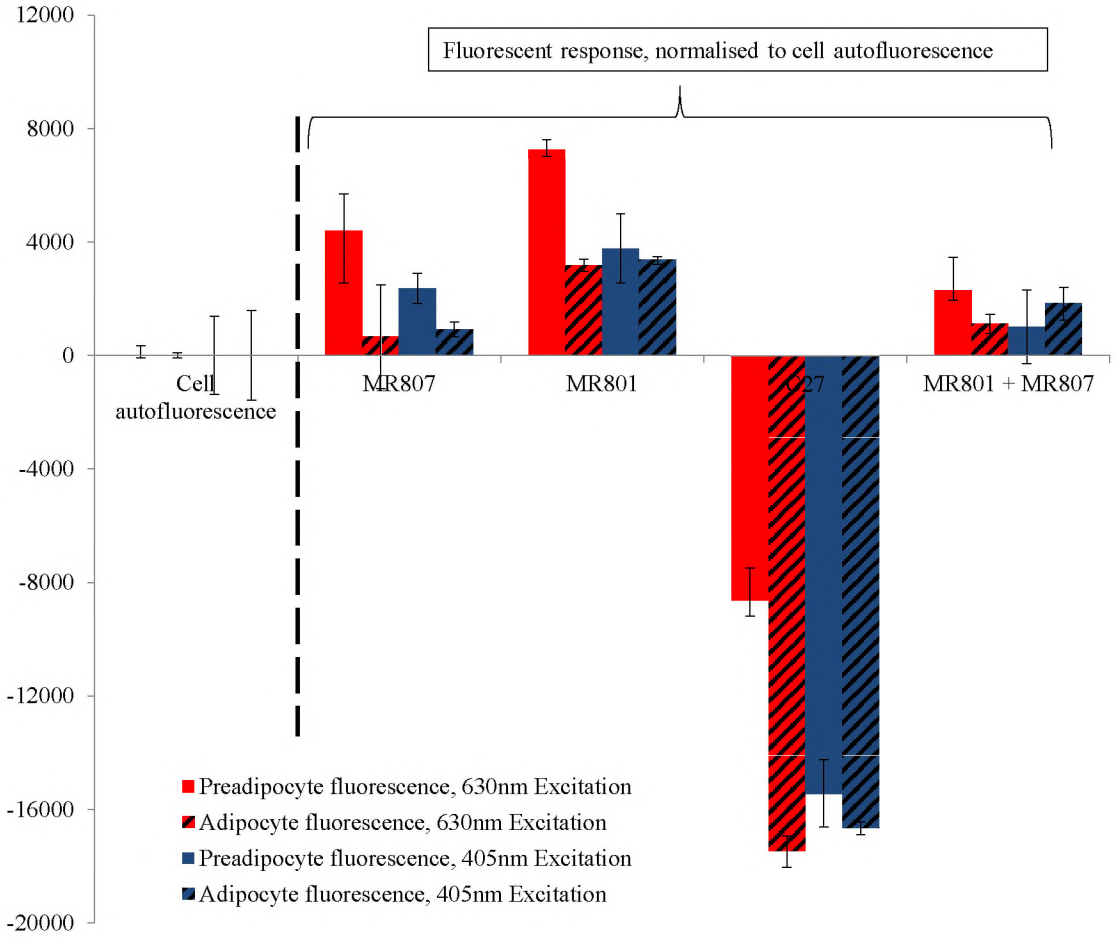

Figure 5.7: Quantitative analysis of fluorescent emission intensities of cells visualised by confocal microscopy exposed to different aptamer sequences.

Relative fluorescence is determined as the difference between cells and the extracellular spaces surrounding cells. Cells (n = 4) sampled from confocal microscopy images; excitation wavelengths of 630 nm and 405 nm selected.
Error bars represent the standard error from the mean of the fluorescent intensity given off by n = 4 cells.

Figure 5.7 provides quantitative information illustrating that broadly affirms that preferable binding of the aptamer sequences toward preadipocytes when compared to that of the mature adipocytes. The negative values for C27 confirm that there is higher extracellular fluorescence rather than cellular fluorescence suggesting that the C27 aptamer sequence is binding in the extracellular regions of the cells that is observable in Figure 5.6.

After accounting for the differences in autofluorescence between the two cell types (3T3-L1 preadipocytes and adipocytes), MR801 appears to bind to a greater extent, when compared to the MR807, with a fluorescent intensity of 7277 ± 1578 vs. 4395 ± 1118 for MR801 vs. MR807 respectively. However, MR807 appears to bind more specifically to preadipocytes:

adipocytes possess 20.6 % of the fluorescence of preadipocytes for cells treated with MR807, compared to the 59.2 % exhibited for MR801 (Figure 5.8).

The scaling of fluorescent responses between the 630 nm (red channel) and 405 nm (blue channel) excitation wavelengths upon treatment with the aptamers was not an anticipated result. Subsequent spectroscopic investigations (data not shown) confirmed that no cross-talk arising from the fluorophore conjugated to the aptamer resulted in the aptamer generating signal in the blue channel for either the microscopy (Figure 5.4 to Figure 5.6) or the quantitation of the confocal microscopy (Figure 5.7).

The decreased levels of fluorescence in the sample containing the combination of MR801 and MR807, do not demonstrate any preferable binding of the aptamers toward the preadipocytes or the mature adipocytes, demonstrated in Figure 5.7. This is clear from the overlapping and large error bars. This could be the result of sequence hybridisation between the MR801 and MR807 sequences.

An investigation into the possible hybridisation of the MR801 and MR807 sequences, as seen in Figure 5.8 below, demonstrates that the hybridisation of the aptamers is possible and may disrupt the binding conformation of either of these sequences, either at 37 °C or room temperature.

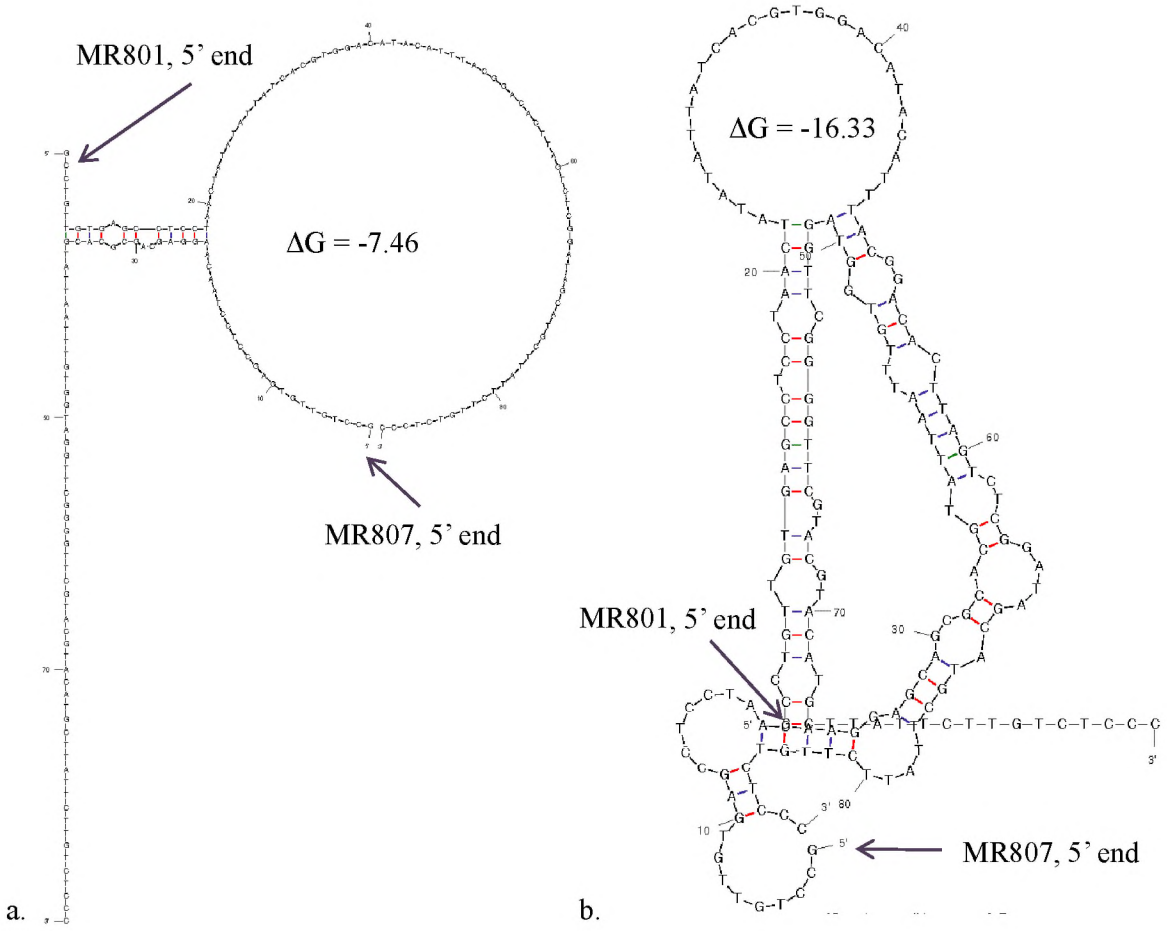

Figure 5.8: Secondary structural analysis of hybridisation between aptamer sequences MR807 and MR810, at a) 37 ˚C and b) room temperature.

The secondary structures with the lowest free energy (kJ/ mol), is provided in the centre of the sequence.

Hybridisation between the MR801 and MR807 sequences, at both 37 ˚C and room temperature is possible, resulting in extended and structurally - complicated complexes to form between the sequences (Figure 5.8). The hybridisation of the MR801 and MR810 sequences may be the causative factor in the decrease of both the aptamers' binding efficiency to the respective targets exhibited in Figure 5.6 and Figure 5.7.

5.4.5. RTCA xCELLigence real time cell analysis

The ability of the aptamers to facilitate cell binding and affect the differentiation capabilities of the 3T3-L1 preadipocytes were monitored in real time using the Roche RTCA xCELLigence real time cell SP reader.

The cells were analysed at several various stages of cellular attachment to the SAM layer and subsequent stages, this including the attachment of the cells to a mixed SAM layer made from either thiolated MR807, C27, or MA-33 aptamer sequences and the β-Mercaptohexanoic acid spacer. This permitted the analysis on the binding capabilities of the cell to the SAM layer over a short time period, the ability of the cells to grow on the surface of the SAM layer and the differentiative capabilities of the cells after a shortened 24 hour period of growth of the cells on the surface of the SAM layer. The growth of the cells was inhibited following the 24 cellular growth stage through the induction of cellular differentiation in the seeded 3T3-L1 preadipocytes.

The xCELLigence system was evaluated for a continuous 97 hours, a span of time that encompassed SAM formation (1 hour), seeding and attachment of cells into the various wells (4 hours), growth of the cells (20 hours), until the end of the first three days of differentiation (72 hours). To compare each sample, the delta cell index (DCI) was reset at the starting time for each step in the experiment, Figure 5.9 illustrates the DCI with time over the entire xCELLigence assay, the distinct stages of the assay have been labelled i, ii, iii, and iv.

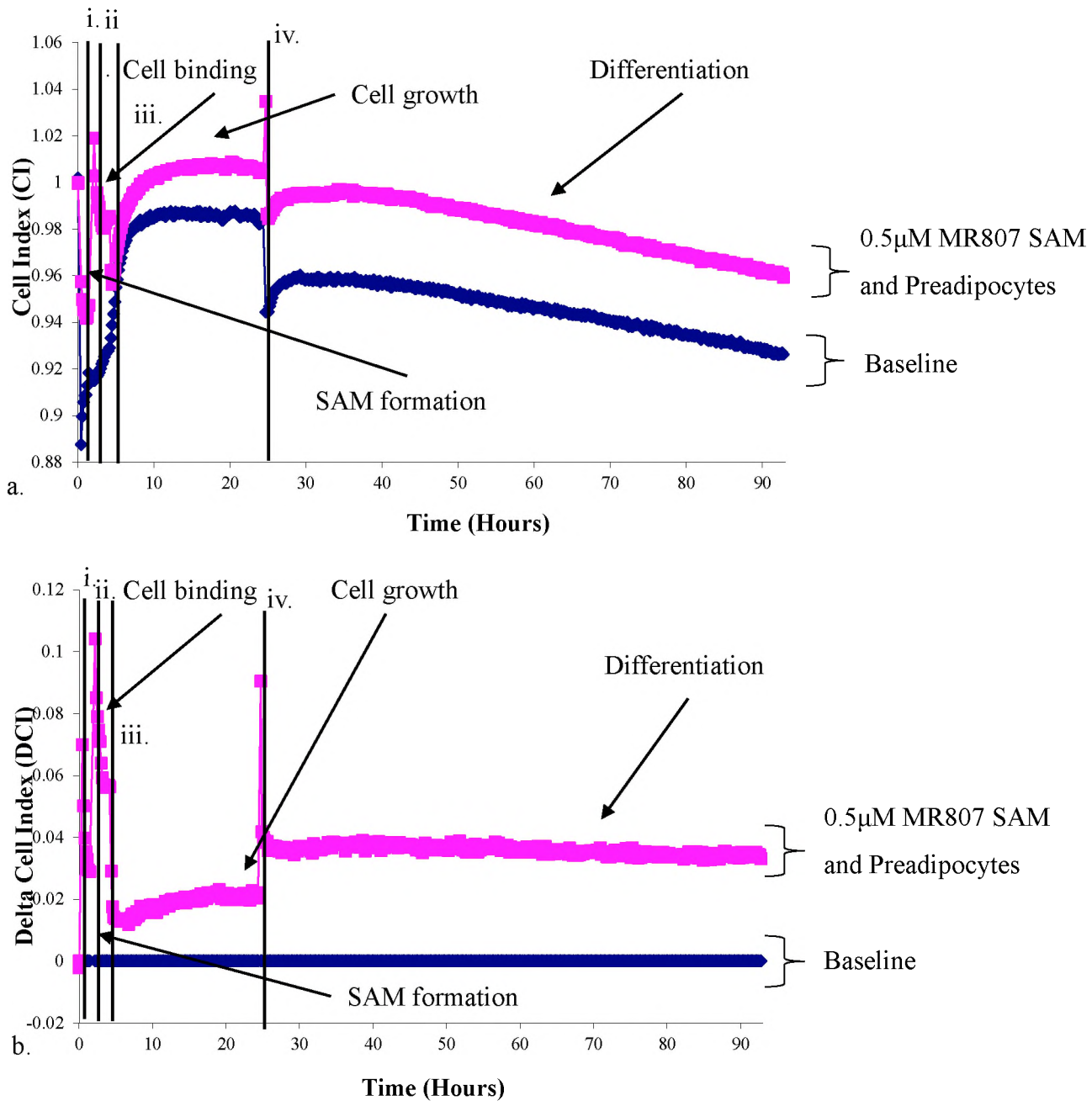

Figure 5.9: Typical data obtained from assessing aptamers' ability to capture cells, evaluated using the xCELLigence RTCA. Delta Cell Index vs time complete xCELLigence assay evaluated for 92hours, the delta time taken at Time 0.

a) Unprocessed data, measured as Cell Index. This compares the 0.5 µM MR807 SAM with the complex media only. The various phases of analysis used are labelled using vertical lines: i) formation of the SAM, ii) preadipocyte binding, iii) preadipocyte growth, iv) preadipocyte differentiation.
b) The Delta Cell Index, used henceforth in this study. b) With the complex media set as the reference sample. Representative 0.5 µM MR807/ Mercaptohexanoic acid SAM layer and cells (Pink squares) and) at various stages of the xCELLigence assay. The various phases of analysis used are labelled using vertical lines: i) formation of the SAM, ii. preadipocyte binding, iii) preadipocyte growth, iv) preadipocyte differentiation.

Figure 5.9 above demonstrates the effect of adding a baseline to the DCI of the xCELLigence assy. In order to evaluate and record the formation of the SAM (Figure 5.10), the DCI was recorded with reference to the buffer starting, at 25 minutes after the starting baseline recording of the E-plate, Figure 5.10 illustrates below the change in DCI with time with a baseline sample set to the complex media. The preparative time to wash and load the wells with the aptamer/ spacer took 25 minutes to complete, although it was recorded by the RTCA system during SAM formation.

To reduce complexity in Figure 5.10 - Figure 5.13 below, the baseline for each of the sample wells were altered to the reference SAM in media only for each of the respective aptamer concentrations in the SAM.

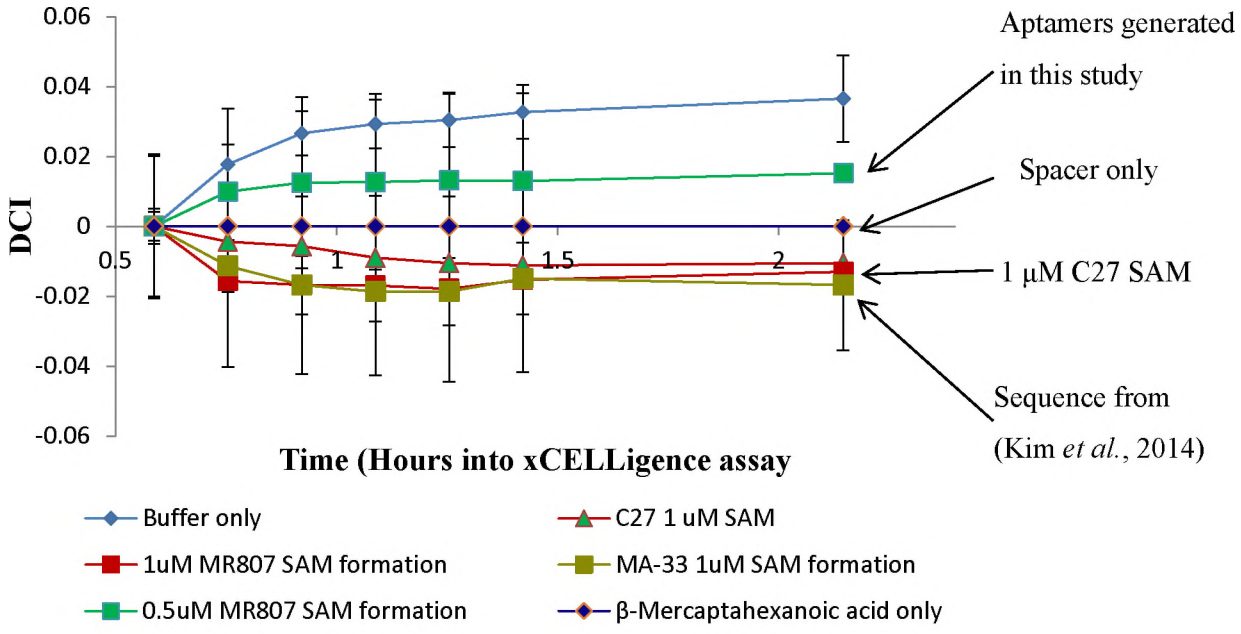

Figure 5.10: Baselined DCI vs time (hours) analysis of the formation of the SAM on the surface of the gold electrode of the Roche RTCA xCELLigence real time E-plate surface.

The baseline was set to the same surfaces exposed to the Mercaptohexanoic acid spacer only, to evaluate the effect of 3T3-L1 cells binding to the various modified surfaces presented here. Error bars represent standard error of n = 6 sample replicates for blank and MR807 SAM and n = 3 for β-Mercaptohexanoic acid spacer and MA-33 SAM.

Figure 5.10 illustrates that a general decrease in the DCI is noted when surfacing the electrodes with SAM components. This is evident when comparing the control lacking thiols (buffer only, Figure 5.11) with the other samples. DCI in this Figure is baselined relative to the responses produced when creating a SAM comprised solely of β-mercaptohexanoic acid, negating the effect that this spacer has on the comparative DCI value. The further decrease in the DCI to approximately -0.016 ± 0.025 for the 1 μM aptamer sequences suggests that the presence of the aptamer is decreasing the DCI when attaching onto the electrode surface. The increase in the DCI, relative to the β-mercaptohexanoic acid spacer surface, for the 0.5 μM aptamer sequence suggests that although there is aptamer binding to the electrode surface, the 0.5 μM aptamer is behaving differently on the surface of the E-plate surface to the 1 μM aptamer sequences.

The binding efficiency of the MR807, C27 and the adipocyte developed MA-33 control aptamer (Kim *et al.*, 2014) towards the developed 3T3-L1 preadipocytes to the surface of the SAM layer was then evaluated over a four hour period, in the aptamer binding buffer and evaluated as seen in Figure 5.11. An additional control of a cell binding evaluation was used with the cells added to bind directly in the cell culture nutrient media on the surface of a 1 μM MR807/ β-Mercaptohexanoic acid SAM layer.

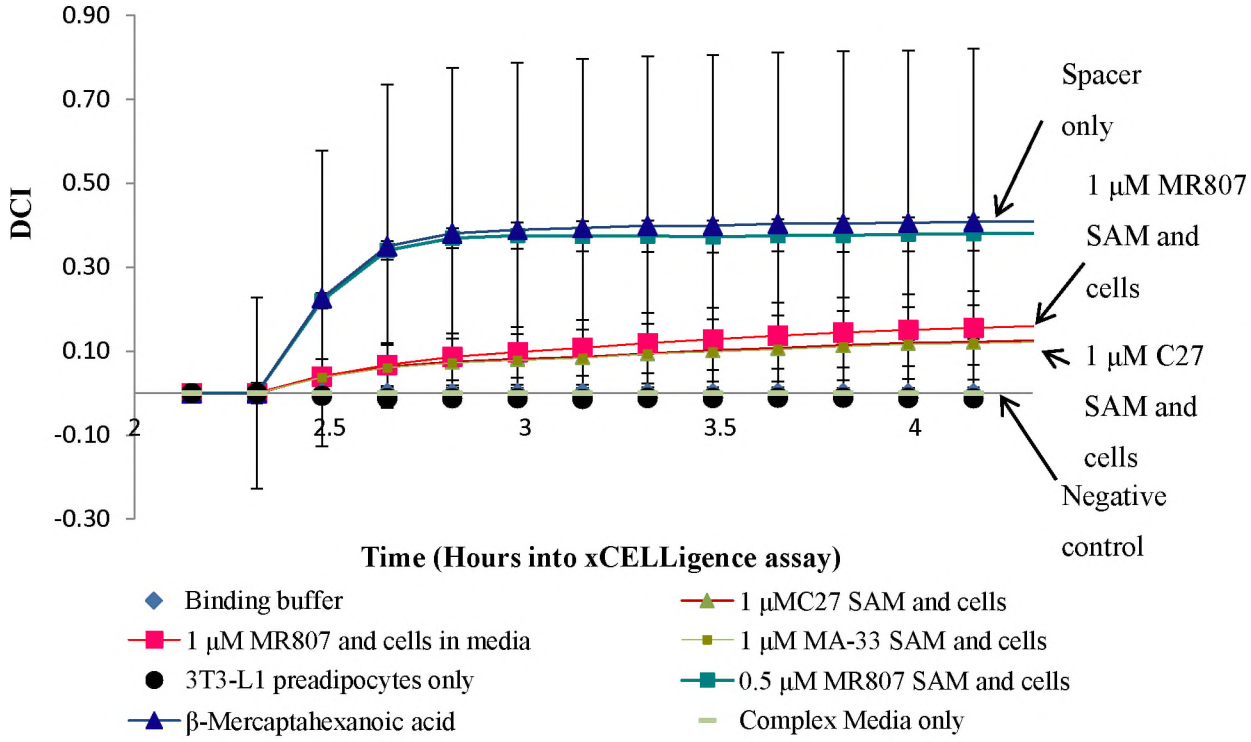

Figure 5.11: Baselined DCI vs time (hours) analysis of the binding of the 3T3-L1 preadipocytes to the SAM surface.

The baseline was set to the binding buffer for cells binding directly to the surface electrode. To compensate for the effect of the SAM on the surface the electrode, the other samples were baselined to the respective SAM layer exposed to the relevant buffers.
Error bars represent standard error of n = 3 sample replicates.

The baselined cell index illustrates a sudden decrease in the delta cell index following half an hour of the addition of the preadipocytes to the wells of the electrode. To compensate for any shifts in the chemical nature of the SAM, with the change in media, the cells binding to the aptamer were baselined to the respective concentration of the electrode bound SAM only in additional control wells, for further cell/ SAM interactions.

Relative to the baseline lacking cells, increases in the DCI for all the modified electrode surfaces occurring after one hour of exposure to 3T3-L1 cells suggests that there is a preference of preadipocyte binding to the modified surface. The similarity of response between surfaces exposed to buffer and unmodified gold electrode surfaces exposed to 3T3-L1 cells suggest that preadipocytes attach poorly to unmodified surfaces. In particular, the sample with the 0.5 µM MR807 SAM and the β-Mercaptohexanoic acid only samples that had indistinguishable preadipocyte binding levels but the standard error for the β-

Mercaptohexanoic acid spacer had a greater standard error to that of the 0.5 μM MR807 SAM, this suggesting less consistency of the cells binding to the surfaces of the preadipocytes. The difference between the binding of the preadipocytes to the surface of the 1 μM MR807 SAM and the 0.5 μM MR807 SAM, could possibly have been the result of steric hindrance between the aptamers on the electrode surface – where the aptamers are too closely packed together – to adopt their preadipocyte binding conformation on the surface of the electrode (this explains the decrease in cell binding to the SAM surface from a DCI of 0.4 in the 0.5 μM MR807 SAM to a DCI of 0.1 in the 1 μM MR807 SAM). However, the deviation between replicates in this study make statistical comparison between these surfaces difficult.

Interestingly enough, the binding of the preadipocytes was marginally faster and greater when the preadipocytes are seeded using the nutrient media, rather than binding buffer, on the surface of the SAMs formed using 1 μM of MR807. A more detailed graph illustrating this is presented in Figure 5.11 above.

The following step was to evaluate the cellular growth capabilities of the cells after the four hours of the binding of the aptamers to the SAM layer, the data points have been illustrated below in Figure 5.12.

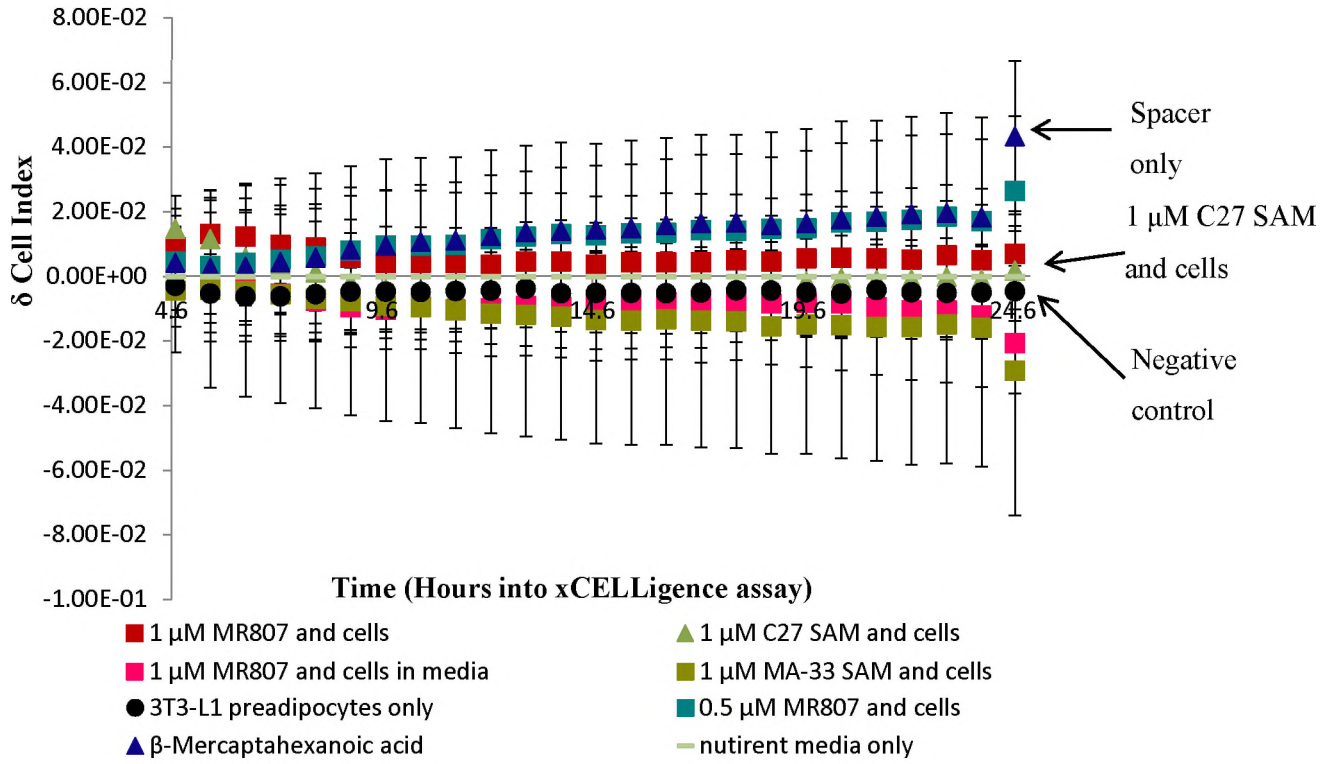

Figure 5.12: DCI vs Time evaluation into the growth of the cells on the surface of the Aptamer/ β-Mercaptohexanoic acid SAM, an average between every fifth cell index reading.

The samples were baselined with the growth media of the 3T3-L1 preadipocytes only, compensation for the electrode bound SAM layer, and were baselined to their representative SAM layer in media only.

Error bars represent standard error of n = 3 sample replicates.

There was no significant growth of the cells on the SAM surface for the entire 20 hour period that the cells were allowed to grow in, although there was a maintained constant positive cell index for the preadipocytes bound to both the MR807/ β-Mercaptohexanoic acid SAM layer. While the SAM layer containing the C27 and MA-33 aptamer sequences demonstrated a gradual descent in the cell index, suggesting that cells were lifting off the surface of the SAM layer. The consistent maintenance of the cell index over the 20 hour period was most likely not the result of the requirements for the cells to re-establish themselves to a nutrient rich media, as the cells that were bound in culture media demonstrated comparable results to that of the other cells in the nutrient media. The final stage of analysis into the cells growth was intended to inhibit cellular growth on the surface monolayer, and evaluate the differentiation

capabilities of the preadipocytes that were able to bind to the surface of the SAM layer. Figure 5.13, illustrates the result of cellular differentiation. The preadipocytes were induced to differentiate for 60 hours with the standard differentiation media used.

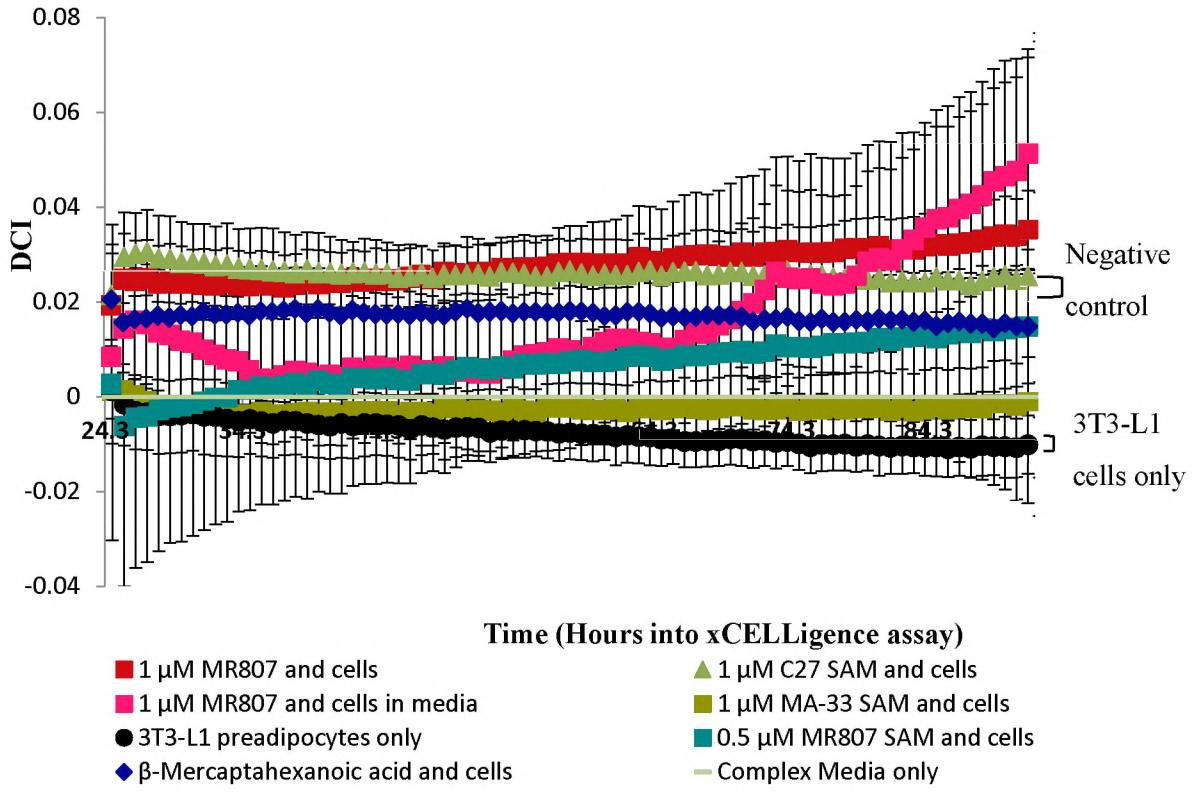

Figure 5.13: Baselined DCI vs time (hours) analysis of the differentiation of the 3T-L1 preadipocytes on the aptamer SAM surface, an average between every fifth cell indexes reading.

The baseline readings were set to the differentiation media only of the cells, and compensation for the electrode bound SAM layer, and were baselined to their representative SAM layer in media only. Error bars represent standard error of n = 3 sample replicates.

Following approximately 24 hours of cellular differentiation, there was a general reduction in the DCI from both the C27 SAM, the β-Mercaptohexanoic acid, and the preadipocytes only. This suggests that the cells are lifting off the surface of the surface reducing the cell index, as suggested by (Kramer *et al.*, 2014). The SAM layers containing the MR807 sequence appear to be having the opposite effect on the cell index, where by there appears to be an increase in the DCI. The increase appears to begin with an exponential growth phase at around the same time the other samples are exhibiting a decrease in the DCI. The exponential growth phase

does not correlate similarly to the late increase in DCI that the MA-33 aptamer sequence exhibits.

Following xCELLigence analysis, micrographs of the cells were imaged directly after the assay had been completed. Figure 5.14 compares the differences between the micrographs of the different control and experimental wells of the 96-well E-plate after the xCELLigence protocol had been terminated.

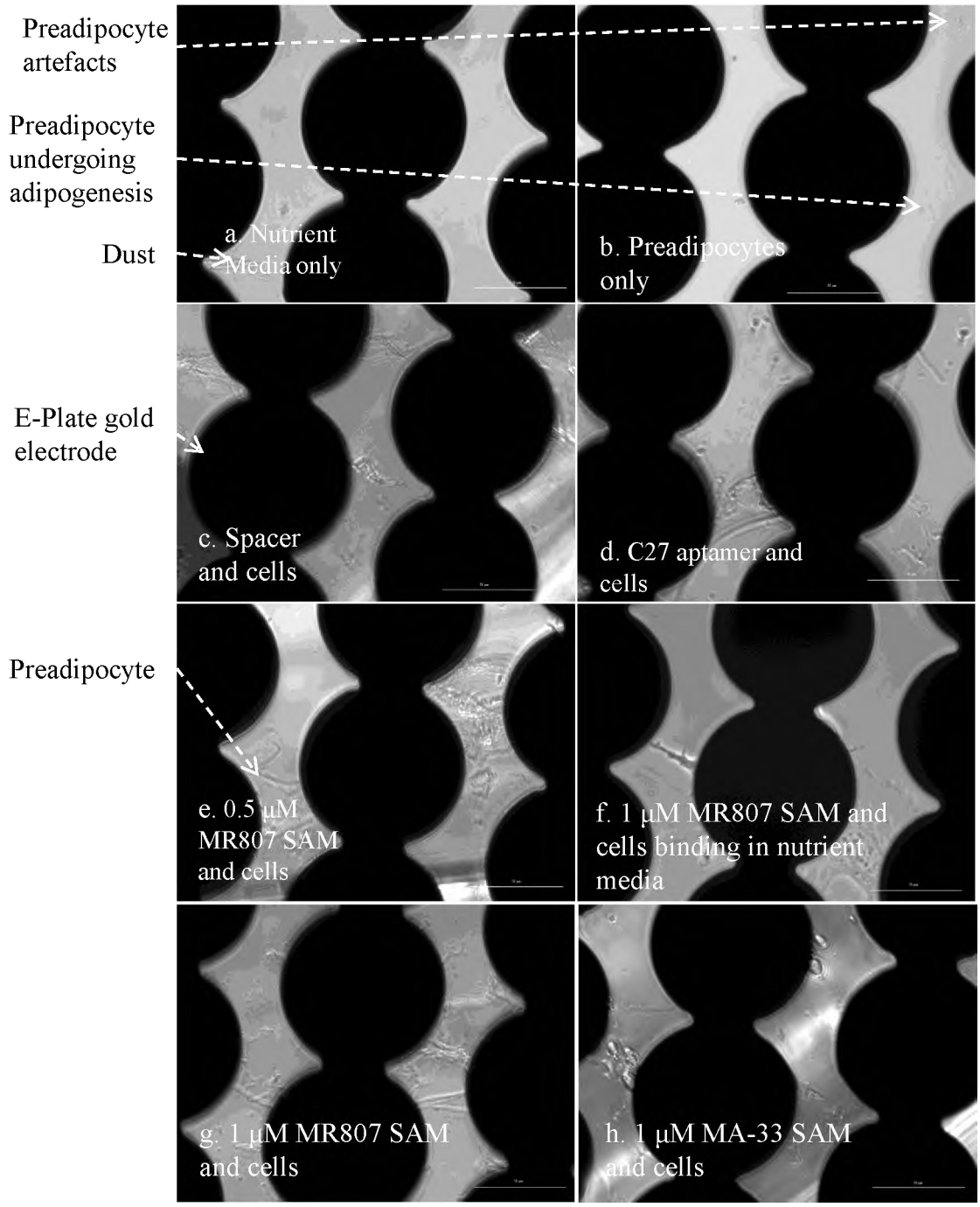

Figure 5.14: Micrograph images of the E-plate surface following the xCELLigence binding and cell growth assay on several surfaces.

Scale bars represent 50 µm on the micrograph. a.) 40 X magnification of the well containing Nutrient Media only. b.) 40 X magnification of the well containing preadipocyte cell seeding without any SAM layer. c.) 40 X magnification of the well containing preadipocytes on a β-Mercaptohexanoic acid SAM surface. d.) 40 X magnification of the well containing preadipocytes on a C27 SAM surface. e.) 40 X magnification of the well containing preadipocytes using 0.5 µM MR807 SAM surface. f.) 40 X magnification of the well containing preadipocytes using 1 µM MR807 surface. g.) 40 X magnification of the well containing preadipocytes in binding buffer using 1 µM MR807

SAM to bind cells to the well surface. h.) 40 X magnification of the well containing both preadipocytes in binding buffer using MA-33 SAM surface.

For all the treated samples in there is variety of morphological differences between the preadipocytes seeded with different samples. Preadipocyte growth during the 92 hour xCELLigence assay was confirmed in Figure 5.14, for all samples with preadipocytes seeded within them, especially the samples that had an aptamer modified SAM layer on the surface. Except in the sample control with only preadipocytes, in the binding buffer, added directly to the gold electrode surface of the E-plate (Figure 5.14.b.).

There appears to be lower numbers of preadipocytes from the 500 seeded cells that could adhere directly onto the electrode surface during the 2 hour binding time (Figure 5.11.a.) that the cells were given. This confirms the low CI value of the sample over the duration of the xCELLigence assay. The CI of the preadipocytes directly on the electrode surface began to decrease after 33 hours into the assay, possibly a combination of cells undergoing both apoptosis and initiating differentiation. Figure 5.14.b, confirmed these results showing cells that are undergoing apoptosis or differentiation.

For all the sample wells that were initially treated with a SAM layer, demonstrated much higher levels of 3T3-L1 preadipocytes binding to the electrode surface. There was a distinct difference between the levels of preadipocyte growth on the electrode surface from both the DCI index shown in Figure 5.13 and Figure 5.14.

It is apparent that there was binding of cells to the surface of the β-Mercaptohexanoic acid spacer sample (Figure 5.14.c.) like the preadipocytes binding to the surface of the C27 SAM (Figure 5.14.d.). Although the cell numbers appear to contain a lower number of preadipocytes than the other cells with the developed aptamers and the reference MA-33 aptamer sequence as seen in Figure 5.14.e-h. The DCI values in Figure 5.13, suggests that during the course of cell growth (Figure 5.12) and differentiation (Figure 5.13) there is little to no proliferation from the preadipocytes within these sample wells.

The preadipocytes binding to the surface of the 0.5 μM and 1 μM MR807 SAM layer (Figure 5.14.e. and Figure 5.14.g. respectively) demonstrate higher levels of cell binding to that of the β-Mercaptohexanoic acid spacer only and C27 aptamer SAM layers.

The selection of preadipocytes onto the surface of the 1 μM MR807 SAM layer in the preadipocyte nutrient media (Figure 5.14.f.), show high levels of healthy preadipocyte

growth. From the rapid growth phase that the preadipocytes undergo in the Figure 5.13, from the cells that bound to the MR807 SAM layer in nutrient media and the visual morphology of the preadipocytes in Figure 5.14.f, suggests that the aptamer is able to bind to the cells in nutrient media at 37 ˚C. Furthermore, there appears to be little to no adipogenesis occurring in the preadipocyte samples.

The results presented in the chapter demonstrate though confocal microscopic analysis there was preferable binding of the developed aptamer developed (MR807 and MR801), when presented to preadipocytes opposed mature adipocytes derived from the 3T3-L1 preadipocytes. Interestingly enough the control C27 aptamer sequence (developed to target human CD4) demonstrated a binding towards an unknown, fibular, ECM expressed target in 3T3-L1 preadipocytes.

Additionally, real time xCELLigence Impedimetric cell binding assay, demonstrated a positive upregulation in the binding of 3T3-L1 preadipocytes to the surface of a generated SAM layer comprised of the MR807 aptamer with a β-Mercaptohexanoic acid spacer. Although the binding of the C27 aptamer/ β-Mercaptohexanoic acid SAM demonstrated an initial higher binding of 3T3-L1 preadipocytes. After the preadipocytes were allowed to grow overnight, the preadipocytes were encouraged to undergo differentiation for 68 hours. The MR807/ β-Mercaptohexanoic acid SAM demonstrated a more positive binding affinity towards the binding of the preadipocytes (as the binding of the C27 SAM to the cells seemed to be reduced).

This could be the result of a change in the expression of the ECM, resulting in the release of the aptamer-preadipocyte interactions.

5.5. Conclusions

Following *in silico* analysis of the developed aptamers in Chapter 4, two representative sequences (MR807 and MR810) from each subfamily were evaluated for their binding affinity and selectivity toward the target 3T3-L1 preadipocytes using both a fluorescent (confocal microscopy) and electrochemical (xCELLigence real time analysis) binding assays.

The confocal assays demonstrated that the MR801 aptamer bound to the 3T3-L1 preadipocytes more readily than the MR807 aptamer. However, the MR807 aptamer demonstrated to be more specific toward the 3T3-L1 preadipocytes to that of the mature

adipocytes, when compared with that of the MR801 aptamer. Confocal microscopy further demonstrated specific regions of high fluorescence on the outer regions of the 3T3-L1 preadipocytes (especially between cell – cell interaction sites) where the aptamers could possibly have bound to the surface of the preadipocytes. Judging between differences in the fluorescence patterning of the micrographs, and variation in both the levels of aptamer binding to the surface of both the preadipocytes and mature adipocytes, between the MR801 and MR807 aptamers, most likely bound to different targets ligands on the cell surface.

A combination between the MR807 and MR801 aptamers demonstrated a reduced binding to the 3T3-L1 preadipocytes, the combination retained a binding preference towards the 3T3-L1 preadipocytes when compared to that of the mature adipocytes. This could possibly be the result of hybridisation between the MR801 and MR807 aptamers, decreasing the affinity of the aptamers toward the target sequences. An in-house control sequence (C27, developed to target human CD4) interestingly demonstrated a binding preference to what appeared to be a fibrous ligand expressed in the ECM of the preadipocytes, that showed down regulated expression in the ECM of mature adipocytes.

Taken together, the xCELLigence study provided preliminary indications that the different aptamer-modified surfaces may be influencing the attachment, propagation and subsequent differentiation of the attached cells. To investigate this further, additional studies are warranted to conclusively validate this. These studies are suggested to include varying the number of seeded cells to improve the DCI signals and optimising the lateral density of the aptamers by varying the concentration of thiolated aptamers to the β-mercaptoethanol making up the SAM layer.

Chapter 6 : Summary and final Discussion to the Research Project

6.1 Discussion

The aim of the work in this thesis was for the development and validation of novel aptamer sequences that demonstrated preferable binding to the surface of murine 3T3-L1 preadipocytes. This was achieved using an adapted SELEX protocol targeting living *in vitro* cells. To enhance the aptamers' specificity of binding, mature adipocytes derived from the same cell line were used as a negative selection during SELEX. The project was designed as a starting point to evaluate the ability of aptamers to assist with the selective binding of stem cells to solid surfaces, and the subsequent differentiation of bound cells. Through control of the seeding patterns of the stem cells onto surfaces, a tuneable control mechanism for cellular differentiation can be realised. Additionally, aptamers developed in this manner could assist in supporting future research into these cell lines, through their facile modification to produce fluorescent biosensors.

Chapter 3 reports on the optimisation of several aspects of cell-SELEX performed prior to aptamer generation. Several techniques used within the separate phases of the cell-SELEX cycle were evaluated separately, and their performance optimised, to optimise the overall process. These included: a method of amplifying ssDNA (asymmetric PCR, compared to conventional PCR amplification and exonuclease digestion of the antisense strand), the means of detecting and quantifying the bound aptamer sequences (though both fluorescent spectroscopy and near UV/ VIS ssDNA quantification), and the method of detaching bound sequences from the target cells (Using Phenol: Chloroform: Isoamyl alcohol, Trypsin digestion, and the heating of the cellular material).

A comparison of asymmetric PCR and exonuclease digestion as means of amplifying a cycle selection library, to optimise the generation of a given ssDNA library for following SELEX cycles was evaluated at a variety of asymmetric PCR conditions. This investigation concluded that exonuclease digestion produced both higher yields of ssDNA, where different methods of ssDNA amplification varied between 230 ± 23.2 ng and 876 ± 87.2 ng of ssDNA amplified per 200 µl PCR reaction using a dsDNA template. As expected following the asymmetric PCR amplification of the library, the dsDNA contamination in the reaction varied between 7.31 ± 1.2 and 19.8 ± 5.8 ng/ 200 µl of dsDNA, as seen in Figure 3.7.

The lambda exonuclease digestion exhibited higher levels of 564 ± 27.7 ng per 200 µl ssDNA produced and simultaneously lower levels of dsDNA contamination, of 1.9 ± 1.2 ng per 200 µl, in comparison to the asymmetric PCR reaction. This is despite the increased time required for successful exonuclease digestion, due to challenges noted when retrieving sufficient dsDNA amounts for lambda exonuclease digestion.

Investigations into the most efficient means of detaching bound aptamers from cell exteriors indicated that, by heating the cell lysate to 95 °C removes lower levels of ssDNA off the cell surface, when compared to that of trypsin digestion of the preadipocytes. Although the heating of the cells recovers a lower final yield of ssDNA eluted off the surface of the cells (compared to that of other methods evaluated) to use as a method to remove bound ssDNA from the surface of the target cell, and allow for other surface moieties other than proteins to be included as possible SELEX targets in the selection process. This would introduce greater variety into possible aptamer binding target sites on the surface of the target cell line.

The quantification of detached ssDNA aptamer candidates through UV/ Vis spectrophotometry was not found to provide accurate quantitation, due to interference by the presence of genomic DNA, RNA and other contaminants arising from the presence of cells and cellular debris within the sample matrix. Fluorimetric quantification, using a 5' 6-FAM labelled library provided a more satisfactory means of accurately identifying and monitoring the presence of candidate aptamers binding to the surface of both the preadipocytes and adipocytes for binding quantification during SELEX.

In addition, the accuracy of SELEX relies on the consistent, successful production of differentiated adipocytes to act as samples for the negative-SELEX stage. The production of differentiated adipocytes from 3T3-L1 preadipocytes was trialled and the differentiating ability determined through Oil Red O staining after 13 days of initiating differentiation. Differentiation trials revealed that, after 13 days of preadipocyte differentiation, true adipogenesis that had occurred in the 3T3-L1 preadipocytes. This correlated somewhat to reports by Saito *et al.*, 2007 and Pantoja *et al.*, 2008, who demonstrated that preadipocyte differentiation occurs between 8 – 10 days into cellular differentiation.

In Chapter 4, an adapted cell-SELEX protocol was applied to generate a pool of aptamer sequences that would bind selectively to the surface of 3T3-L1 preadipocytes, using mature adipocytes derived from the 3T3-L1 preadipocytes as the negative target cell line, to remove

sequences capable of binding to both mature adipocytes and preadipocytes. Cell-SELEX took place over eleven selection cycles, using 5' fluorescently-tagged aptamers and measuring the subsequent fluorescent intensity of bound sequences as an indication of the yield.

After eight cycles of cell-SELEX, fluorimetric analysis demonstrated that 74 % of the applied aptamers bound positively (i.e. to their intended preadipocyte targets) and 0.69 % negatively bound (i.e. to adipose counterpart cells). There was a noticeable decline in the specificity of the ssDNA aptamers binding to the target preadipocytes vs. the non-target mature adipocytes for cycles of cell-SELEX following nine selection cycles. The yield of the negatively bound sequences increased upon subsequent SELEX cycles. After 11 cell-SELEX cycles 91 % of the library was bound to the positive (preadipocyte) cell line, with an increased binding of 42 % of the selection pool library to the negative (adipocytes) cell line when compared to that of the 8^{th} SELEX cycle.

After sequencing twenty samples from the cycle 11 selection pool, sequence analysis demonstrated predominately primer concatemer sequences incorporated within the selection pool sample. This is a well-noted and undesired side-product of the PCR phase of SELEX. An additional twenty sequences were sequenced and evaluated from the cycle 8 selection pool, seven of these demonstrated non-concatemeric aptamer sequences. Of these sequences, three of them (MR801, MR803, and MR809) showed sequence consensus to each other while the others were all variable from one another at the primary structural level.

These comprise the first such sequence of aptamers generated in literature specifically targeting preadipocytic stem cells – although aptamers targeting mature 3T3-L1 adipocytes have been noted in literature by Liu *et al.* (2012) and Kim *et al.* (2014). The research accomplished here is novel in the identity of the target cell type and the final uses of the aptamer sequences following selection.

In Chapter 5, the binding efficiency and the selectivity of two of the aptamer sequences from different aptamer subfamilies were analysed using both a confocal and epifluorescent binding assay. A baseline (using binding buffer only) assay was established in parallel to account for cell autofluorescence, during fluorescent microscopic analysis of aptamer binding.

The results showed that both of the developed sequences demonstrated a preference for binding to the preadipocytes over mature adipocytes. Preferable binding of the aptamers in both the epifluorescent (of the MR807 and MR810 aptamer sequences) and confocal assays

(MR801 and MR807 aptamer sequences), suggested that the aptamers were binding at regions on the outer surface of the cell. The C27 control sequence, in the confocal assay, unexpectedly demonstrated a preferable binding towards a target ligand within the ECM of the preadipocytes, and to a lesser extent the ECM of the adipocytes where the ligand appeared to be down - regulated *in vitro*.

Following confocal microscopy, a real time electrical impedance assay using the AECA xCELLigence RTCA, was used to generate data on the binding efficiency of the preadipocytes for seeding purposes on the surface of an aptamer (MR807) SAM layer.

As a control for the attachment of the 3T3-L1 preadipocytes on the surface of the SAM layer, a SAM layer using previously developed sequence (MA-33) developed by Kim *et al.*, (2014) specifically targeting mature adipocytes was used in parallel to that of MR807 for xCELLigence analysis.

The aptamer, MR807, was functionalised with a 5‘ thiol group, to use in a SAM layer with a β–Mercaptohexanoic acid spacer with two different concentrations (1 M and a $5x10^{-1}$ M) of the MR807 aptamer making up the SAM layer.

The results preliminarily indicate preferable binding to the SAM layer with $5x10^{-1}$ M aptamer sequence. There was a noticeable increase in DCI and lower standard error in the $5.x10^{-1}$ M aptamer SAM layer than the binding of the preadipocytes to other control sequences. There was little to no binding of the preadipocytes directly to the surface of the gold electrode.

Interestingly, proliferation of the preadipocytes on the surface of the SAM layer appeared to be inhibited. After approximately 54 hours, after 30 hours post initiation of adipogenesis in the wells, there was a general decrease in the DCI across the control sample wells.

This suggests that the cells were either potentially lifting off the surface of the wells as described by Kramer *et al.*, (2014), or there was degradation of the SAM layer. Although the DCI in the sample wells with the MR807 SAM layer began to demonstrate an increase in the DCI the preadipocytes started to proliferate at this point.

In addition, the SAM is potentially inhibiting cellular proliferation and the cells were able to restart proliferating following the degradation of the cell bound aptamers making up the SAM layer. In order for this to happen the DCI would plateau after 18 – 30 hours (~54 hours) into the xCELLigence assay, as research done by Rosen and MacDougald, 2006 suggest that

preadipocytes proliferate one or two more times before they undergo irreversible differentiation.

The consistent increase in the DCI suggests that the MR807 aptamer potentially could further be interfering with the differentiation pathways of the preadipocytes causing them to maintain a state of consistent proliferation. Taken together, the xCELLigence study demonstrated preliminary indications that aptamer-modified surfaces could be influencing the attachment, propagation and subsequent differentiation of the cells attached to the aptamer SAM.

To investigate this further, additional studies are required to conclusively validate the effect that the aptamer SAM has on the cell proliferation and differentiation. These studies include varying the number of cells seeded in the study to improve on the output DCI signals in the assay and to optimise the lateral density of the aptamers by varying the concentration of thiolated aptamers to the β-mercaptoethanol.

6.2 Future Research

Taken together, this research has shown the generation of a series of aptamer sequences using a cell-SELEX based method targeting murine 3T3-L1 preadipocytes. The binding capabilities of these aptamers were successfully validated using fluorimetry and fluorescent microscopy. From the research presented above, there is opportunity for more research that can go into streamlining and shortening the cell-SELEX protocol and investigation into the binding capabilities of the generated aptamers.

Several aptamer sequences were gathered and analysed, following cell-SELEX. An investigation into the ligand type and potentially the specific ligand would be an interesting experiment to go further into; secondary structural analysis of the gathered sequences demonstrates tertiary structural variability between the sequence families and most likely different target ligands on the surface of the preadipocytes. Additionally, the binding capabilities of the aptamer sequences could determine the affinity of the aptamer for the specific target ligand. This would include an investigation into the cell target affinity of the target cell type, and the binding capabilities of the developed aptamers at a variety temperatures ranging between 4 ˚C and 40 ˚C.

The binding buffer of the aptamer was designed to mimic that of the nutrient growth medium of the preadipocytes furthermore the preliminary ability of the aptamers to bind to cells in

cell media, and subsequent improvements in the DCI and cell numbers observed indicate that a repetition of this study. A further investigation in the selectivity and binding of the aptamer in a substituted complex nutrient media (DMEM nutrient media), opposed to the cell binding buffer used in this study may be warranted for further analysis and would demonstrate the versatility of the aptamer sequences for *in vitro* analysis.

The specific nature of SAM binding the target cell, should be further validated using capture ability of mature adipocytes via xCELLigence should also be validated, in an equivalent manner that proceeded for preadipocytes in Chapter 5.

The use of a CD4 targeting aptamer, C27 (Cromhout *et al.*, 2015) was used as a "negative" control to evaluate the binding of a "random sequence" to the surface of the 3T3-L1 preadipocyte cell surface. Although confocal microscopy suggested that the C27 aptamer was not binding to the cell surface of the preadipocytes, the evidence suggests that this aptamer binds to a high degree to a target that is expressed on the surface of the ECM of the preadipocytes, but which is downregulated in mature adipocytes. An additional investigation into the C27 target in the ECM of the 3T3-L1 preadipocytes could possibly give insight into extracellular scaffolds and changes in the cellular expression of molecules into the extracellular space during adipogenic differentiation.

References

Albrektsen, T., Frederiksen, K.S., Holmes, W.E., Boel, E., Taylor, K., Fleckner, J. (2002) 'Novel genes regulated by the insulin sensitizer rosiglitazone during adipocyte differentiation', *Diabetes*, 51(4), 1042–1051.

Amariglio, N., Hirshberg, A., Scheithauer, B.W., Cohen, Y., Loewenthal, R., Trakhtenbrot, L., Paz, N., Koren-Michowitz, M., Waldman, D., Leider-Trejo, L., Toren, A., Constantini, S., Rechavi, G. (2009) 'Donor-derived brain tumor following neural stem cell transplantation in an ataxia telangiectasia patient', *PLoS Medicine*, 6(2), 0221–0231.

Aquila, R.T.D., Bechtel, L.J., Videler, J. a, Eron, J.J., Gorczyca, P., Kaplan, J.C. (1991) 'Maximizing sensitivity and specificity of PCR by amplification heating', *Nucleic Acids Research*, 19(13), 3749.

Avci-Adali, M., Metzger, M., Perle, N., Ziemer, G., Wendel, H.P. (2010) 'Pitfalls of cell-systematic evolution of ligands by exponential enrichment (SELEX): existing dead cells during in vitro selection anticipate the enrichment of specific aptamers.', *Oligonucleotides*, 20(6), 317–323.

Avci-Adali, M., Paul, A., Wilhelm, N., Ziemer, G., Wendel, H.P. (2010) 'Upgrading SELEX technology by using lambda exonuclease digestion for single-stranded DNA generation', *Molecules*, 15(1), 1–11.

Baer, P.C., Kuçi, S., Krause, M., Kuçi, Z., Zielen, S., Geiger, H., Bader, P., Schubert, R. (2012) 'Comprehensive Phenotypic Characterization of Human Adipose-Derived Stromal/Stem Cells and Their Subsets by a High Throughput Technology', *Stem Cells and Development*, 22(2), 121004062301006.

Baharvand, H., Fathi, A., van Hoof, D., Salekdeh, G.H. (2007) 'Concise review: trends in stem cell proteomics.', *Stem cells*, 25(8), 1888–1903.

Baret, P., Septembre-Malaterre, A., Rigoulet, M., Lefebvre D'Hellencourt, C., Priault, M., Gonthier, M.P., Devin, A. (2013) 'Dietary polyphenols preconditioning protects 3T3-L1 preadipocytes from mitochondrial alterations induced by oxidative stress', *International Journal of Biochemistry and Cell Biology*, 45(1), 167–174.

Barlow, C., Hirotsune, S., Paylor, R., Liyanage, M., Eckhaus, M., Collins, F., Shiloh, Y., Crawley, J.N., Ried, T., Tagle, D., Wynshaw-boris, A. (1996) 'Atm - Deficient Mice : A Paradigm of Ataxia Telangiectasia', *Cell*, 86, 159–171.

Batey, R.T., Rambo, R.P., Doudna, J. a. (1999) 'Tertiary motifs in RNA structure and folding', *Angewandte Chemie - International Edition*, 38, 2326–2343.

Berezovski, M., Musheev, M., Drabovich, A., Krylov, S.N. (2006) 'Non-SELEX selection of aptamers', *Journal of the American Chemical Society*, 128(5), 1410–1411.

Billen, A., Madrigal, J.A., Shaw, B.E. (2014) 'A review of the haematopoietic stem cell donation experience: is there room for improvement?', *Bone marrow transplantation*, 49(6), 729–36.

Biosciences, A. (2013) *Real-Time and Dynamic Monitoring of Cell Proliferation and Viability for Adherent Cells Real-Time and Dynamic Monitoring of Cell Proliferation and Viability for Adherent Cells*.

Blank, M., Weinschenk, T., Priemer, M., Schluesener, H. (2001) 'Systematic evolution of a DNA aptamer binding to rat brain tumor microvessels: Selective targeting of endothelial

regulatory protein pigpen', *Journal of Biological Chemistry*, 276(19), 16464–16468.

Blind, M., Blank, M. (2015) 'Aptamer Selection Technology and Recent Advances', *Molecular Therapy—Nucleic Acids*, 4(1), e223.

Brody, E.N., Gold, L. (2000) 'Aptamers as therapeutic and diagnostic agents.', *Journal of biotechnology*, 74(1), 5–13.

Cadwell, R.C., Joyce, G.F. (1992) 'Randomization of genes by PCR mutagenesis', *PCR Methods and Aplications*, 2(1), 28–34.

Camp, H.S., Ren, D., Leff, T. (2002) 'Adipogenesis and fat-cell function in obesity and diabetes', *Trends in Molecular Medicine*, 8(9), 442–447.

Carson, S.A., Eschenbach, D.A., Lomax, G., Rice, V.M., Sauer, M. V., Taylor, R.N. (2010) 'Proposed oocyte donation guidelines for stem cell research', *Fertility and Sterility*, 94(7), 2503–2506.

Castillo, J., Gáspár, S., Leth, S., Niculescu, M., Mortari, a., Bontidean, I., Soukharev, V., Dorneanu, S. a., Ryabov, a. D., Csöregi, E. (2004) 'Biosensors for life quality - Design, development and applications', *Sensors and Actuators, B: Chemical*, 102(2), 179–194.

Cerchia, L., Ducongé, F., Pestourie, C., Boulay, J., Aissouni, Y., Gombert, K., Tavitian, B., De Franciscis, V., Libri, D. (2005) 'Neutralizing aptamers from whole-cell SELEX inhibit the RET receptor tyrosine kinase', *PLoS Biology*, 3(4), 0697–0704.

Chamberlain, G., Fox, J., Ashton, B., Middleton, J. (2007) 'Concise review: mesenchymal stem cells: their phenotype, differentiation capacity, immunological features, and potential for homing.', *Stem cells*, 25(11), 2739–2749.

Chen, A., Yang, S. (2015) 'Replacing Antibodies With Aptamers In Lateral Flow Immunoassay', *Biosensors and Bioelectronics*, 71, 230–242.

Citartan, M., Tang, T.H., Tan, S.C., Gopinath, S.C.B. (2011) 'Conditions optimized for the preparation of single-stranded DNA (ssDNA) employing lambda exonuclease digestion in generating DNA aptamer', *World Journal of Microbiology and Biotechnology*, 27(5), 1167–1173.

Citartan, M., Tang, T.H., Tan, S.C., Hoe, C.H., Saini, R., Tominaga, J., Gopinath, S.C.B. (2012) 'Asymmetric PCR for good quality ssDNA generation towards DNA aptamer production', *Songklanakarin Journal of Science and Technology*, 34(2), 125–131.

Conget, P. a (1999) 'Phenotypical and Functional Properties of', 73(January), 67–73.

Copelan, E.A. (2006) 'Hematopoietic stem-cell transplantation', *New England Journal of Medicine*, 354(17), 1813–1826.

Cromhout, M., Fogel, R., Frith, K.-A., Limson, J. (2015) 'Analysis of Human Immune Status, South African patent Number: 2015/00933, Aripo patent application Number: AP/P/2015/008263'.

Curran, J.M., Chen, R., Hunt, J. a. (2006) 'The guidance of human mesenchymal stem cell differentiation in vitro by controlled modifications to the cell substrate', *Biomaterials*, 27(27), 4783–4793.

Daar, A.S., Bhatt, A., Court, E., Singer, P.A. (2004) 'Stem cell research and transplantation: Science leading ethics', *Transplantation Proceedings*, 36(8), 2504–2506.

Das, J., Mukherjee, S., Mitra, A., Bhattacharyya, D. (2006) 'Non-Canonical Base Pairs and

Higher Order Structures in Nucleic Acids: Crystal Structure Database Analysis', *Journal of Biomolecular Structure and Dynamics*, 24(2), 149–161.

DeFrancesco, L. (2012) 'Adult stem cell therapies walk the line', *Nature Biotechnology*, 30(8), 739–741.

Dhai, a, Moodley, J., McQuoid-Mason, D.J., Rodeck, C. (2004) 'Ethical and legal controversies in cloning for biomedical research--a South African perspective.', *South African medical journal = Suid-Afrikaanse tydskrif vir geneeskunde*, 94(11), 906–909.

Ding, D.-C., Chang, Y.-H., Shyu, W.-C., Lin, S.-Z. (2015) 'Human umbilical cord mesenchymal stem cells: a new era for stem cell therapy.', *Cell transplantation*, 24(3), 339–47.

Ding, F., Yuan, C., Wu, F., Peng, S., Tian, S., Zhang, X.-L., Zhou, X. (2014) 'Diagnosis applications of new hepatoma carcinoma cell aptamers in vitro', *Anal. Methods*, 6(20), 8110–8114.

Drexler, H., Uphoff, C. (2002) 'Mycoplasma contamination of cell cultures: Incidence, sources, effects, detection, elimination, prevention', *Cytotechnology*, 39(2), 75–90.

Dwivedi, H.P., Smiley, R.D., Jaykus, L.A. (2013) 'Selection of DNA aptamers for capture and detection of Salmonella Typhimurium using a whole-cell SELEX approach in conjunction with cell sorting', *Applied Microbiology and Biotechnology*, 97(8), 3677–3686.

Dyson, N. (1998) 'The regulation of E2F by pRB-family?proteins', *Genes & Development*, 12(617), 2245–2262.

Eberli, D., Atala, A. (2006) 'Tissue Engineering Using Adult Stem Cells', *Methods in Enzymology*, 420(6), 287–302.

Eckert, K.A., Kunkel, T.A. (1990) 'High fidelity DNA synthesis by the Thermus aquaticus DNA polymerase.', *Nucleic acids research*, 18(13), 3739–44.

Edgar, R.C., Batzoglou, S. (2006) 'Multiple sequence alignment', *Current Opinion in Structural Biology*, 16(3), 368–373.

Ehnert, S., Glanemann, M., Schmitt, A., Vogt, S., Shanny, N., Nussler, N.C., Stöckle, U., Nussler, A. (2009) 'The possible use of stem cells in regenerative medicine: Dream or reality?', *Langenbeck's Archives of Surgery*, 394(6), 985–997.

Ellington, A., Szostak, J. (1990) 'In vitro selection of RNA molecules that bind specific ligands', *Nature*, 346, 818–822.

Elnifro, E.M., Ashshi, A.M., Cooper, R.J., Klapper, P.E. (2000) 'Multiplex PCR : Optimization and Application in Diagnostic Virology Multiplex PCR : Optimization and Application in Diagnostic Virology', *Clinical microbiology reviews*, 13(4), 559–570.

English, C.A., Merson, S., Keer, J.T. (2006) 'Use of elemental analysis to determine comparative performance of established DNA quantification methods', *Anal Chem*, 78(13), 4630–4633.

FluoProbes (n.d.) *Protocols: GelRed™ Nucleic Acid Gel Stain*, Interchem.

Fowler, S., Greenspan, P. (1985) 'Application of Nile red, a fluorescent hydrophobic probe, for the detection of neutral lipid deposits in tissue sections: comparison with oil red O.', *The Journal of Histochemistry and Cytochemistry*, 33(8), 833–836.

Frith, J.E., Mills, R.J., Hudson, J.E., Cooper-White, J.J. (2012) 'Tailored Integrin–Extracellular Matrix Interactions to Direct Human Mesenchymal Stem Cell Differentiation', *Stem Cells and Development*, 21(13), 2442–2456.

Fu, X., Toh, W.S., Liu, H., Lu, K., Li, M., Cao, T. (2011) 'Establishment of clinically compliant human embryonic stem cells in an autologous feeder-free system.', *Tissue engineering Part C Methods*, 17(9), 927–937.

Fuchs, E., Tumbar, T., Guasch, G. (2004) 'Socializing with the neighbors: Stem cells and their niche', *Cell*, 116, 769–778.

Gomillion, C.T., Burg, K.J.L. (2006) 'Stem cells and adipose tissue engineering', *Biomaterials*, 27, 6052–6063.

Gordeladze, J.O., Hovik, K.E., Merendino, J.J., Hermouet, S., Gutkind, S., Accili, D. (1997) 'Effect of activating and inactivating mutations of G s - and G i2 -alpha protein subunits on growth and differentiation of 3T3-L1 preadipocytes', *Journal of Cellular Biochemistry*, 64(2), 242–257.

Green, J. V, Murthy, S.K. (2009) 'Microfluidic enrichment of a target cell type from a heterogenous suspension by adhesion-based negative selection.', *Lab on a chip*, 9(15), 2245–2248.

Greene, M. (2006) 'To Restore Fath and Trust: Justice and Biological Access to Cellular Therapies', *The Hastings Center Report*, 36(1), 57–63.

Gregoire, F.M., Smas, C.M., Sul, H.S. (1998) 'Understanding adipocyte differentiation.', *Physiological reviews*, 78(3), 783–809.

Guo, K.-T., SchAfer, R., Paul, A., Gerber, A., Ziemer, G., Wendel, H.P. (2006) 'A new technique for the isolation and surface immobilization of mesenchymal stem cells from whole bone marrow using high-specific DNA aptamers.', *Stem cells*, 24, 2220–2231.

Guo, K.-T., Schäfer, R., Paul, A., Ziemer, G., Wendel, H.P. (2007) 'Aptamer-based strategies for stem cell research.', *Mini reviews in medicinal chemistry*, 7, 701–705.

Guo, K.T., Paul, A., Schichor, C., Ziemer, G., Wendel, H.P. (2008) 'Cell-SELEX: Novel perspectives of aptamer-based therapeutics', *International Journal of Molecular Sciences*, 9(4), 668–678.

Haller, A., Altman, R.B., Soulière, M.F., Blanchard, S.C., Micura, R. (2013) 'Folding and ligand recognition of the TPP riboswitch aptamer at single-molecule resolution.', *Proceedings of the National Academy of Sciences of the United States of America*, 110, 4188–93.

Hicke, B.J., Marion, C., Chang, Y.F., Gould, T., Lynott, C.K., Parma, D., Schmidt, P.G., Warren, S. (2001) 'Tenascin-C Aptamers Are Generated Using Tumor Cells and Purified Protein', *Journal of Biological Chemistry*, 276(52), 48644–48654.

Iliuk, A.B., Hu, L., Tao, W.A. (2011) 'Aptamer in bioanalytical applications', *Analytical Chemistry*, 83(12), 4440–4452.

Ishikawa-Ankerhold, H.C., Ankerhold, R., Drummen, G.P.C. (2012) 'Advanced fluorescence microscopy techniques-FRAP, FLIP, FLAP, FRET and FLIM', *Molecules*, 17(4), 4047–4132.

Jaenisch, R., Young, R. (2008) 'Stem Cells, the Molecular Circuitry of Pluripotency and Nuclear Reprogramming', *Cell*, 132(4), 567–582.

James, A.W. (2013) 'Review of Signaling Pathways Governing MSC Osteogenic and Adipogenic Differentiation.', *Scientifica*, 2013, 684736.

James, W. (2001) 'Nucleic acid and polypeptide aptamers: A powerful approach to ligand discovery', *Current Opinion in Pharmacology*, 1, 540–546.

Kaiden Student, A., Hsu, R., Lane, M.D. (1980) 'Induction of Fatty Acid Synthetase Synthesis in Differentiating 3T3-Ll Preadipocytes', *The Journal of Biological Chemistry*, 255(10), 4745–4750.

Kalle, E., Kubista, M., Rensing, C. (2014) 'Multi-template polymerase chain reaction', *Biomolecular Detection and Quantification*, 2, 11–29.

Katoh, K., Misawa, K., Kuma, K., Miyata, T. (2002) 'MAFFT: a novel method for rapid multiple sequence alignment based on fast Fourier transform.', *Nucleic acids research*, 30(14), 3059–3066.

Katoh, K., Standley, D.M. (2013) 'MAFFT multiple sequence alignment software version 7: Improvements in performance and usability', *Molecular Biology and Evolution*, 30(4), 772–780.

Khow, O., Suntrarachun, S. (2012) 'Strategies for production of active eukaryotic proteins in bacterial expression system', *Asian Pacific Journal of Tropical Biomedicine*, 2(2), 159–162.

Kim, E.Y., Kim, J.W., Kim, W.K., Han, B.S., Park, S.G., Chung, B.H., Lee, S.C., Bae, K.-H. (2014) 'Selection of aptamers for mature white adipocytes by cell SELEX using flow cytometry.', *PloS one*, 9(5), e97747.

Kim, S., Moustaid-moussa, N. (2000) 'Symposium : Adipocyte Function , Differentiation and Metabolism Secretory , Endocrine and Autocrine / Paracrine Function of the Adipocyte 1', *The Journal of nutrition*, (Tartaglia 1997), 3110–3115.

Kim, Y.S., Hyun, C.J., Kim, I.A., Gu, M.B. (2010) 'Isolation and characterization of enantioselective DNA aptamers for ibuprofen', *Bioorganic and Medicinal Chemistry*, 18(10), 3467–3473.

Klemm, D.J., Leitner, J.W., Watson, P., Nesterova, A., Reusch, J.E.B., Goalstone, M.L., Draznin, B. (2001) 'Insulin-induced adipocyte differentiation: Activation of CREB rescues adipogenesis from the arrest caused by inhibition of prenylation', *Journal of Biological Chemistry*, 276(30), 28430–28435.

Kolind, K., Leong, K.W., Besenbacher, F., Foss, M. (2012) 'Guidance of stem cell fate on 2D patterned surfaces', *Biomaterials*, 33(28), 6626–6633.

Korbie, D.J., Mattick, J.S. (2008) 'Touchdown PCR for increased specificity and sensitivity in PCR amplification', *Nature protocols*, 3(9), 13–15.

Kramer, A.H., Joos-Vandewalle, J., Edkins, A.L., Frost, C.L., Prinsloo, E. (2014) 'Real-time monitoring of 3T3-L1 preadipocyte differentiation using a commercially available electric cell-substrate impedance sensor system', *Biochemical and Biophysical Research Communications*, 443(4), 1245–1250.

Krauss, M., Jensen, J.O., Hameka, H.F. (1994) 'Electronic Structure of the Excited States and Phenol Fluorescence', *Journal of Physical Chemistry*, 98(June), 9955–9959.

Kustermann, S., Boess, F., Buness, A., Schmitz, M., Watzele, M., Weiser, T., Singer, T., Suter, L., Roth, A. (2013) 'A label-free, impedance-based real time assay to identify

drug-induced toxicities and differentiate cytostatic from cytotoxic effects', *Toxicology in Vitro*, 27(5), 1589–1595.

Laurent, L.C., Nievergelt, C.M., Lynch, C., Fakunle, E., Harness, J. V, Schmidt, U., Galat, V., Laslett, A.L., Otonkoski, T., Keirstead, H.S., Schork, A., Park, H., Loring, J.F. (2010) 'Restricted ethnic diversity in human embryonic stem cell lines', *Nature Methods*, 7(1), 5–6.

Lemieux, S., Major, F. (2002) 'RNA canonical and non-canonical base pairing types: a recognition method and complete repertoire.', *Nucleic acids research*, 30(19), 4250–4263.

Li, M., Ikehara, S. (2013) 'Autoimmune Disease Treatment with Stem Cell Transplantation', *Journal of Genetic Syndromes & Gene Therapy*, 4(8), 174.

Lichtman, J.W., Conchello, J. (2005) 'Fluorescence microscopy', *Nature Methods*, 2(12), 910–919.

Lindvall, O., Hyun, I. (2009) 'Medical Innovation Versus Stem Cell Tourism', *Science*, 324(5935), 1664–1665.

Liu, J., DeYoung, S.M., Zhang, M., Dold, L.H., Saltiel, A.R. (2005) 'The stomatin/prohibitin/flotillin/HflK/C domain of flotillin-1 contains distinct sequences that direct plasma membrane localization and protein interactions in 3T3-L1 adipocytes', *Journal of Biological Chemistry*, 280(16), 16125–16134.

Liu, J., Liu, H., Sefah, K., Liu, B., Pu, Y., van Simaeys, D., Tan, W. (2012) 'Selection of aptamers specific for adipose tissue', *PLoS ONE*, 7(5), 1–10.

Lucarelli, F., Marrazza, G., Turner, A.P.F., Mascini, M. (2004) 'Carbon and gold electrodes as electrochemical transducers for DNA hybridisation sensors', *Biosensors and Bioelectronics*, 19(6), 515–530.

Luzi, E., Minunni, M., Tombelli, S., Mascini, M. (2003) 'New trends in affinity sensing: Aptamers for ligand binding', *Trends in Analytical Chemistry*, 22(11), 810–818.

Lyu, Y., Chen, G., Shangguan, D., Zhang, L., Wan, S., Wu, Y., Zhang, H., Duan, L., Liu, C., You, M., Wang, J., Tan, W. (2016) 'Generating Cell Targeting Aptamers for Nanotheranostics Using Cell-SELEX', *Theranostics*, 6(9), 1440–1452.

Mackay, A.M., Beck, S.C., Murphy, J.M., Barry, F.P., Chichester, C.O., Pittenger, M.F. (1998) 'Chondrogenic Differentiation of Cultured Human Mesenchymal Stem Cells from Marrow', *Tissue Engineering*, 4(4), 415–428.

Mariman, E.C.M., Wang, P. (2010) 'Adipocyte extracellular matrix composition, dynamics and role in obesity.', *Cellular and molecular life sciences : CMLS*, 67(8), 1277–1292.

Markham, N., Zuker, M. (2008) 'Chapter 1 Software for Nucleic Acid Folding and Hybridization', *Springer Protocols*, 453(1), 3–31.

Marshak, D., Gardner, R., Gottlieb, D. (2001) *Stem Cell Biology*, Cold Spring Harbor Laboratory Press.

Martinez-Serra, J., Ggutierrez, A., Muñoz-Ccapó, S., Nnavarro-Palou, M., Rros, T., Aamat, J.C., Lopez, B., Marcus, T.F., Fueyo, L., Suquia, A.G., Gines, J., Rrubio, F., Rramos, R., Besalduch, J. (2014) 'xCELLcelligence system for real-time label-free monitoring of growth and viability of cell lines from hematological malignancies', *OncoTargets and Therapy*, 7, 985–994.

Mascini, M., Palchetti, I., Tombelli, S. (2012) 'Nucleic acid and peptide aptamers: Fundamentals and bioanalytical aspects', *Angewandte Chemie - International Edition*, 51, 1316–1332.

Master, Z., Resnik, D.B. (2011) 'Stem-cell tourism and scientific responsibility', *EMBO reports*, 12(10), 992–995.

Mayer, G., Ahmed, M.-S.L., Dolf, A., Endl, E., Knolle, P. a, Famulok, M. (2010) 'Fluorescence-activated cell sorting for aptamer SELEX with cell mixtures.', *Nature protocols*, 5(12), 1993–2004.

Mazia, D., Schatten, G., Sale, W. (1975) 'Adhesion of Cells to Surfaces Coated with PolyLysine', *Journal of Cell Biology*, 66(3), 198–200.

McBeath, R., Pirone, D.M., Nelson, C.M., Bhadriraju, K., Chen, C.S. (2004) 'Cell shape, cytoskeletal tension, and RhoA regulate stem cell lineage commitment', *Developmental Cell*, 6(4), 483–495.

McKeague, M., DeRosa, M.C. (2014) 'Aptamers and SELEX: Tools for the Development of Transformative Molecular Recognition Technology', *Aptamers and Synthetic Antibodies*, 1(1), 12–16.

McLean, A.K., Stewart, C., Kerridge, I. (2015) 'Untested, unproven, and unethical: the promotion and provision of autologous stem cell therapies in Australia', *Stem Cell Research & Therapy*, 6(1), 33.

Meissner-Roloff, M., Pepper, M.S. (2013) 'Curbing stem cell tourism in south africa', *Applied and Translational Genomics*, 2(1), 22–27.

Mendonsa, S.D., Mendonsa, S.D., Bowser, M.T., Bowser, M.T. (2004) 'In Vitro Selection of High-Affinity DNA Ligands for Human IgE Using Capillary Electrophoresis', *Analytical Chemistry*, 76(18), 5387–5392.

Murphy, M.B., Fuller, S.T., Richardson, P.M., Doyle, S. a (2003) 'An improved method for the in vitro evolution of aptamers and applications in protein detection and purification.', *Nucleic acids research*, 31(18), e110.

New England Biolabs (n.d.) 'Lambda Exonuclease'.

Newton, L., Slater, T., Clark, N., Vijayaraghavan, A. (2013) 'Self assembled monolayers (SAMs) on metallic surfaces (gold and graphene) for electronic applications', *Journal of Materials Chemistry C*, 1(3).

Nikfarjam, L., Farzaneh, P. (2012) 'Prevention and detection of mycoplasma contamination in cell culture', *Cell Journal*, 13(4), 203–212.

Notredame, C., Higgins, D.G., Heringa, J. (2000) 'T-Coffee: A novel method for fast and accurate multiple sequence alignment.', *J. Mol. Biol.*, 302(1), 205–217.

Ojima, K., Oe, M., Nakajima, I., Muroya, S., Nishimura, T. (2016) 'Dynamics of protein secretion during adipocyte differentiation', *FEBS Open Bio*, 6, 816–826.

Ossewaarde, J.M., De Vries, A., Bestebroer, T., Angulo, a. F. (1996) 'Application of a Mycoplasma group-specific PCR for monitoring decontamination of Mycoplasma - infected Chlamydia sp. strains', *Applied and Environmental Microbiology*, 62(2), 328–331.

Pajvani, U.B. (2003) 'Structure-Function Studies of the Adipocyte-secreted Hormone Acrp30/Adiponectin. IMPLICATIONS FOR METABOLIC REGULATION AND

BIOACTIVITY', *Journal of Biological Chemistry*, 278(11), 9073–9085.

Pantoja, C., Huff, J., Yamamoto, K. (2008) 'Glucocorticoid Signaling Defines a Novel Commitment State during Adipogenesis Glucocorticoid Signaling Defines a Novel Commitment State during Adipogenesis In Vitro', *Seikagaku*, 19, 4032–4041.

Parish, C.R. (1999) 'Fluorescent dyes for lymphocyte migration and proliferation studies', *Immunology and Cell Biology*, 77(6), 499–508.

Peng, R., Yao, X., Ding, J. (2011) 'Effect of cell anisotropy on differentiation of stem cells on micropatterned surfaces through the controlled single cell adhesion', *Biomaterials*, 32(32), 8048–8057.

Phillips, J.E., Petrie, T.A., Creighton, F.P., García, A.J. (2010) 'Human mesenchymal stem cell differentiation on self-assembled monolayers presenting different surface chemistries', *Acta Biomaterialia*, 6(1), 12–20.

Pittenger, M.F., Mackay, A.M., Beck, S.C., Jaiswal, R.K., Douglas, R., Mosca, J.D., Moorman, M. a, Simonetti, D.W., Craig, S., Marshak, D.R. (1999) 'Multilineage potential of adult human mesenchymal stem cells.', *Science (New York, N.Y.)*, 284(April), 143–147.

Popenda, M., Bielecki, L., Adamiak, R.W. (2006) 'High-throughput method for the prediction of low-resolution, three-dimensional RNA structures.', *Nucleic acids symposium series (2004)*, 50, 67–68.

Poulos, S.P., Dodson, M. V, Hausman, G.J. (2010) 'Cell line models for differentiation: preadipocytes and adipocytes.', *Experimental biology and medicine*, 235(10), 1185–1193.

Ramírez-Zacarías, J.L., Castro-Muñozledo, F., Kuri-Harcuch, W. (1992) 'Quantitation of adipose conversion and triglycerides by staining intracytoplasmic lipids with oil red O', *Histochemistry*, 97(6), 493–497.

Reblova, K., Spackova, N., Stefl, R., Csaszar, K., Koca, J., Leontis, N., Jirı, S. (2003) 'Non-Watson-Crick Basepairing and Hydration in RNA Motifs: Molecular Dynamics of 5S rRNA Loop E', *Biophysical journal*, 84(6), 3564–3582.

Reusch, J.E., Colton, L.A., Klemm, D.J. (2000) 'CREB activation induces adipogenesis in 3T3-L1 cells.', *Molecular and cellular biology*, 20(3), 1008–20.

Robertson, J. (2010) 'Embryo Stem cell Research: Ten Years of Controversy', *Journal of Law, Medicine & Ethics*, 13(1), 191–203.

Rosen, E.D., MacDougald, O. a (2006) 'Adipocyte differentiation from the inside out.', *Nature reviews. Molecular cell biology*, 7(12), 885–96.

Ruiz-Ojeda, F., Rupérez, A., Gomez-Llorente, C., Gil, A., Aguilera, C. (2016) 'Cell Models and Their Application for Studying Adipogenic Differentiation in Relation to Obesity: A Review', *International Journal of Molecular Sciences 2016, Vol. 17, Page 1040*, 17(7), 1040.

Russell, T., Ho, R. (1976) 'Conversion of 3T3 fibroblasts into adipose cells: triggering of differentiation by prostaglandin F2alpha and 1-methyl-3-isobutyl xanthine.', *Proceedings of the National Academy of Sciences of the United States of America*, 73(12), 4516–4520.

SA, S. (2012) 'SA Census Statistical realease 2011'.

Saito, T., Abe, D., Sekiya, K. (2007) 'Nobiletin enhances differentiation and lipolysis of 3T3-L1 adipocytes', *Biochemical and Biophysical Research Communications*, 357(2), 371–376.

Salomatina, E., Jiang, B., Novak, J., Yaroslavsky, A.N. (2011) 'Optical properties of normal and cancerous human skin in the visible and near-infrared spectral range.', *Journal of biomedical optics*, 11(6), 64026-64026–9.

SantaLucia, J., Hicks, D. (2004) 'The thermodynamics of DNA structural motifs.', *Annual review of biophysics and biomolecular structure*, 33, 415–440.

Schäfer, R., Wiskirchen, J., Guo, K., Neumann, B., Kehlbach, R., Pintaske, J., Voth, V., Walker, T., Scheule, a. M., Greiner, T.O., Hermanutz-Klein, U., Claussen, C.D., Northoff, H., Ziemer, G., Wendel, H.P. (2007) 'Aptamer-based isolation and subsequent imaging of mesenchymal stem cells in ischemic myocard by magnetic resonance imaging', *Rapid Communication*, 179, 1009–1015.

Schönichen, A., Webb, B.A., Jacobson, M.P., Barber, D.L. (2013) 'Considering Protonation as a Posttranslational Modification Regulating Protein Structure and Function', *Annual Review of Biophysics*, 42(1), 289–314.

Schütze, T., Arndt, P.F., Menger, M., Wochner, A., Vingron, M., Erdmann, V.A., Lehrach, H., Kaps, C., Glökler, J. (2009) 'A calibrated diversity assay for nucleic acid libraries using DiStRO-a Diversity Standard of Random Oligonucleotides', *Nucleic Acids Research*, 38(4).

Scott, M.A., Nguyen, V.T., Levi, B., James, A.W. (2011) 'Current methods of adipogenic differentiation of mesenchymal stem cells', *Stem cells and development*, 20(10), 1793–1804.

Sefah, K., Shangguan, D., Xiong, X., O'Donoghue, M.B., Tan, W. (2010) 'Development of DNA aptamers using Cell-SELEX.', *Nature protocols*, 5(6), 1169–1185.

Shangguan, D., Bing, T., Zhang, N. (2015) *Aptamers Selected by Cell-SELEX for Theranostics*.

Shangguan, D., Li, Y., Tang, Z., Cao, Z.C., Chen, H.W., Mallikaratchy, P., Sefah, K., Yang, C.J., Tan, W. (2006) 'Aptamers evolved from live cells as effective molecular probes for cancer study.', *Proceedings of the National Academy of Sciences of the United States of America*, 103(32), 11838–11843.

Shao, K., Ding, W., Wang, F., Li, H., Ma, D., Wang, H. (2011) 'Emulsion PCR: A high efficient way of PCR amplification of random DNA libraries in aptamer selection', *PLoS ONE*, 6(9), 1–7.

da Silva Meirelles, L., Chagastelles, P.C., Nardi, N.B. (2006) 'Mesenchymal stem cells reside in virtually all post-natal organs and tissues.', *Journal of cell science*, 119(Pt 11), 2204–13.

Song, K.M., Lee, S., Ban, C. (2012) 'Aptamers and their biological applications', *Sensors*, 12, 612–631.

Stellwagen, N.C., Stellwagen, E. (2008) 'Effect of the matrix on DNA electrophoretic mobility', *Journal of Chromatography*, 1216(10), 1917–1929.

Stephens, D., Allan, V. (2003) 'Light Microscopy Techniques for Live Cell Imaging', *Science*, 300, 82–86.

Stoltenburg, R., Reinemann, C., Strehlitz, B. (2007) 'SELEX-A (r)evolutionary method to generate high-affinity nucleic acid ligands', *Biomolecular Engineering*, 24(4), 381–403.

Storch, J., Thumser, A.E.. (2000) 'The fatty acid transport function of fatty acid-binding proteins', *Biochimica et Biophysica Acta (BBA) - Molecular and Cell Biology of Lipids*, 1486(1), 28–44.

Strehlitz, B., Nikolaus, N., Stoltenburg, R. (2008) 'Protein detection with aptamer biosensors', *Sensors*, 8, 4296–4307.

Sun, L., Åkerman, B. (2014) 'Characterization of self-assembled DNA concatemers from synthetic oligonucleotides', *Computational and Structural Biotechnology Journal*, 11(18), 66–72.

Sviatopolk-Mirsky Pais, F., de Cássia Ruy, P., Oliveira, G., Santos Coimbra, R. (2014) 'Assessing the efficiency of multiple sequence alignment programs', *Algorithms for Molecular Biology*, 9(1), 18.

Tabarzad, M., Kazemi, B., Vahidi, H., Aboofazeli, R., Shahhosseini, S., Nafissi-Varcheh, N. (2014) 'Challenges to design and develop of DNA aptamers for protein targets. I. optimization of asymmetric PCR for generation of a single stranded DNA library', *Iranian Journal of Pharmaceutical Research*, 13(November 2013), 133–141.

Tan, L., Gee Neoh, K., Kang, E.-T., Choe, W.-S., Su, X. (2012) 'Designer Tridentate Mucin 1 Aptamer for Targeted Drug Delivery', *Journal of pharmaceutical sciences*, 101, 1672–1677.

Tan, W., Wang, H., Chen, Y., Zhang, X., Zhu, H., Yang, C., Yang, R., Liu, C. (2011) 'Molecular aptamers for drug delivery', *Trends in Biotechnology*, 29(12), 634–640.

Tan, Z.-J., Chen, S.-J. (2006) 'Nucleic acid helix stability: effects of salt concentration, cation valence and size, and chain length.', *Biophysical journal*, 90(4), 1175–90.

Tang, J., Peng, R., Ding, J. (2010) 'The regulation of stem cell differentiation by cell-cell contact on micropatterned material surfaces', *Biomaterials*, 31(9), 2470–2476.

Tang, J., Xie, J., Shao, N., Yan, Y. (2006) 'The DNA aptamers that specifically recognize ricin toxin are selected by two in vitro selection methods', *Electrophoresis*, 27(7), 1303–1311.

Tang, Z., Shangguan, D., Wang, K., Shi, H., Sefah, K., Mallikratchy, P., Chen, H.W., Li, Y., Tan, W. (2007) 'Selection of aptamers for molecular recognition and characterization of cancer cells', *Analytical Chemistry*, 79(13), 4900–4907.

Thévenot, D.R., Toth, K., Durst, R. a., Wilson, G.S. (2001) 'Electrochemical biosensors: Recommended definitions and classification', *Biosensors and Bioelectronics*, 16, 121–131.

Thompson, J.D., Higgins, D.G., Gibson, T.J. (1994) 'CLUSTAL W: Improving the sensitivity of progressive multiple sequence alignment through sequence weighting, position-specific gap penalties and weight matrix choice', *Nucleic Acids Research*, 22(22), 4673–4680.

Tombelli, S., Minunni, M., Mascini, M. (2005) 'Analytical applications of aptamers', *Biosensors and Bioelectronics*, 20(12), 2424–2434.

Tong, G.J., Hsiao, S.C., Carrico, Z.M., Francis, M.B. (2009) 'Viral capsid DNA aptamer conjugates as multivalent cell-targeting vehicles', *Journal of the American Chemical*

Society, 131(31), 11174–11178.

Tontonoz, P., Hu, E., Devine, J., Beale, E.G., Spiegelman, B.M. (1995) 'PPAR gamma 2 regulates adipose expression of the phosphoenolpyruvate carboxykinase gene.', *Mol. Cell. Biol.*, 15(1), 351–357.

Trimarchi, J.M., Lees, J.A. (2002) 'Sibling Rivalry in the E2F Family', *Nature Reviews Molecular Cell Biology*, 3(1), 11–20.

Tuerk, C., Gold, L. (1990) 'Systematic Evolution of Ligands by Exponential Enrichment: RNA Ligands to Bacteriophage T4 DNA Polymerase', *Science*, 249, 505–510.

Ulrich, H., Trujillo, C. a, Nery, A. a, Alves, J.M., Majumder, P., Resende, R.R., Martins, A.H. (2006) 'DNA and RNA aptamers: from tools for basic research towards therapeutic applications.', *Combinatorial chemistry & high throughput screening*, 9(8), 619–632.

Urak, K.T., Shore, S., Rockey, W.M., Chen, S.J., McCaffrey, A.P., Giangrande, P.H. (2016) 'In vitro RNA SELEX for the generation of chemically-optimized therapeutic RNA drugs', *Methods*, 103, 167–174.

Villa-Diaz, L.G., Ross, a. M., Lahann, J., Krebsbach, P.H. (2013) 'Concise review: The evolution of human pluripotent stem cell culture: From feeder cells to synthetic coatings', *Stem Cells*, 31(1), 1–7.

Wang, C., Zhang, M., Yang, G., Zhang, D., Ding, H., Wang, H., Fan, M., Shen, B., Shao, N. (2003) 'Single-stranded DNA aptamers that bind differentiated but not parental cells: Subtractive systematic evolution of ligands by exponential enrichment', *Journal of Biotechnology*, 102(1), 15–22.

Wang, Y., Liu, Y., Maye, P., Rowe, D.W. (2008) 'Examination of Mineralized Nodule Formation in Living Osteoblastic Cultures Using Fluorescent Dyes', *Biotechnology progress*, 22(6), 1697–1701.

Wei, G., Schubiger, G., Harder, F., Müller, a M. (2000) 'Stem cell plasticity in mammals and transdetermination in Drosophila: common themes?', *Stem cells*, 18, 409–414.

Wendel, H.-P., Guo, K., Schaefer, R. (2008) 'Device and Substance for the Immobilization of Mesenchymal Stem Cells (MSCs)'.

de Wert, G., Mummery, C. (2003) 'Human embryonic stem cells: research, ethics and policy', *Human Reproduction*, 18(4), 672–682.

Williams, K.P., Bartel, D.P. (1995) 'PCR product with strands of unequal length.', *Nucleic acids research*, 23(20), 4220–4221.

Wilson, D., Szostak, J. (1999) 'In Vitro Selection of Functional Nucleic Acids', *Annual Review of BioChemistry*, 68, 611–647.

Wink, T., van Zuilen, S.J., Bult, a, van Bennkom, W.P. (1997) 'Self-assembled monolayers for biosensors.', *The Analyst*, 122(4), 43r–50r.

Wong, R.S.Y. (2011) 'Mesenchymal stem cells: Angels or demons?', *Journal of Biomedicine and Biotechnology*, 2011, 1–8.

Woodbury, D., Schwarz, E.J., Prockop, D.J., Black, I.B. (2000) 'Adult rat and human bone marrow stromal cells differentiate into neurons.', *Journal of neuroscience research*, 61(4), 364–370.

Wu, W., Yu, L., Fang, Z., Lie, P., Zeng, L. (2013) 'A lateral flow biosensor for the detection

of human pluripotent stem cells.', *Analytical biochemistry*, 436(2), 160–4.

Xi, Z., Huang, R., Deng, Y., He, N. (2014) 'Progress in Selection and Biomedical Applications of Aptamers', *Journal of Biomedical Nanotechnology*, 10(10), 3043–3062.

Xu, W., Zhang, X., Qian, H., Zhu, W., Sun, X., Hu, J., Zhou, H., Chen, Y. (2004) 'Mesenchymal stem cells from adult human bone marrow differentiate into a cardiomyocyte phenotype in vitro.', *Experimental biology and medicine (Maywood, N.J.)*, 229(7), 623–631.

Zeng, X., Shen, Z., Mernaugh, R. (2012) 'Recombinant antibodies and their use in biosensors', *Analytical and Bioanalytical Chemistry*, 402, 3027–3038.

Zhang, J.D. (2014) *Introduction to the Data Analysis of the Roche xCELLigence ™ System with RTCA Package*, Stand.

Zuk, P., Zhu, M., Ashjian, P., De Ugarte, D., Huang, J., Mizuno, H., Alfonso, Z., Fraser, J., Benhaim, P., Henrick, M. (2002) 'Human Adipose Tissue Is a Sourse of Multipotent Stem Cells', *Molecular biology of the cell*, 13, 4279–4295.

Zuker, M. (2003) 'Mfold web server for nucleic acid folding and hybridization prediction', *Nucleic Acids Research*, 31(13), 3406–3415.

Appendices

Appendix A, Raw data gathered for the binding efficiencies of aptamer to both preadipocytes and adipocytes during cell-SELEX

Cell-SELEX Cycle Number	Binding buffer (RFU)	Preadipocyte binding (RFU)	Adipocyte binding (RFU)	Preadipocyte binding (%)	Adipocyte binding (%)	Negative / positive binding %
3	42973	778.00	539.00	1.81	1.25	0.693
4	5736	190.00	-138.00	3.31	-2.41	-0.726
5	16975	-258.00	378.00	-1.52	2.23	-1.465
6	7073	3470.00	NA	49.06	NA	NA
7	8524	NA	5178.00	NA	60.75	NA
6 and 7	7798.5	3470	5178	44.50	66.40	1.492
8	27554	20419.00	189.00	74.11	0.69	0.009
9	4339	NA	393.70	NA	9.07	NA
10	15290	7360.00	490.00	48.14	3.20	0.067
11	14004	12804.00	6064.00	91.43	43.30	0.474

*RFU values evaluated at 669 nm emission with 640 nm excitation, NA values represent fluorescent reading that was not recorded.

*RFU values were set to a standard reference concentration of 1 μM 5'-labelled forward primer in binding buffer, Standard fluorescent at an RFU value of 90 000

Appendix B, MUSCLE Sequence Alignment of cycle 8 and cycle 11 gathered aptamer sequences

MUSCLE Multiple sequence alignment of sequences from cycle 8, chosen sequences are in darkened columns

Sequence ID	MUSCLE Sequence Alignment
MR810	--GCCTGTT- -GTGAGCCTC CTAACC---- -CTAGTTGAA AATTA---CG ATTACCATTA TCCTTT---- TTCCTCGAGA TCG------- ----- GGTCA TGCTTATTCT TGTCTCCC
MR807	--GCCTGTT- -GTGAGCCTC CTAACAAGGA GCAGCGCACG TATTAATTTG -----TGGTA GGTTCG---- GGGTTCGTAC GTA------- ----- ---CA TGCTTATTCT TGTCTCCC
MR806	--GCCTGTT- -GTGAGCCTC CTAACT---- ---ATGTATA CAACGTCCTG -----CGGAA TCCGGT---- CAGTAATTTT GCACTTGGT- ------- TCA TGCTTATTCT TGTCTCCC
MR801	--GCCTGTT- -GTGAGCCTC CTAACT---- -ATATATTAT CACGT---GG -----ACATA ---------- -CATTTACGG ACACTTAGTC TCGGATAGCA TGCTTATTCT TGTCTCCC
MR803	--GCCTGTT- -GTGAGCCTC CTAACT---- -ATATATTAT CACGT---GG -----ACATA ---------- -CATTTACGG ACACTTAGTC TCGGATAGCA TGCTTATTCT TGTCTCCC
MR809	--GCCTGTT- -GTGAGCCTC CTAACT---- -ATATATTAT CACGT---GG -----ACATA ---------- -CATTTACGG ACACTTAGTC TCGGATAGCA TGCTTATTCT TGTCTCCC
MR802	--GCCTGTT- -GTGAGCCTC CTAACTTGCT CGTATATGGC GACAG---AG -----CGA-A CATTGG---- TCGTTTATTG ACTATC---- ------- -CA TGCTTATTCT TGTCTCCC
MR808	--GCGGGACT CAAGAATAAT CATGGTCGGT AGTAGCTATG GAATA---AG -----CAATA TCTCGCGCAA TTATTCAGCG TCA------- ---------- -GCTTATTCT TGTCTCCC
MR820	--GCCAGTT- -AAGA-TCTC CTGCCC---- ---CTGCGCT CACCA---CG -----CCACA TCTTGT---- CTATTCCCCC TCACTCCCC- ------ AGCA CGATTATTCT TGACTCCC
MR804	--GCCTGAC- -AAGAATAAG CATGTG---- -CTAAGTGTT C-TTG---CG -----CCATA TCAGGT---- CTATTCAGGT GGAACTACC- ----- GAGCA TGATGATTTA TGACTCCC
MR813	--GCCTGAC- -AAGAATAAG CTGACG---- ---ATGTGTT CATGG---AG -----CGACA TCTTGT---- CTATTCAGGT GCTACTACC- ----- GAGCA TGATGATTCT TGACTCTC
MR814	CCGCCTGACG CATAAGCTGC CTTGTG---- ---------T TCTTG---CG -----CGATA TCTTGT---- CTATTCAGGT GCTACTACC- ----- GACCA TGATGATTCT TGTCTCCC
MR817	--GCCTGAC- -GT-AATAAG CTGCCC---- ---TTGTGTT CATTG---CG -----CGATA TCTTGA---- CTATTGAGCT GCTACTACC- ----- GACCA TGATGATTCT TGACTCCC

MR819	--GCCTGAC- -AAGAATAAG CATGTC---- --GCTGTGTT CATTG---CG -
	GAGCA TGATGATTCT TGACTCCC
MR812	--GCCTGAC- -GTGAACCTC CTGCCG---- ---TCGTAAT CATTG---CG --
	GACCA TGATGATTCT TGACTCCC
MR816	--GCCAGAC- -AAAAGCCTC ATGCCG---- ---TTGTGTT CATTG---CG --
	GACCA TGATGATTCT TGACTCCC
MR811	--GCCTGAC- -AAGAGCCTC ATGCCG---- ---CTGTGTT CATTG---CG --
	GACCA TGATGATTCT TGACTCCC
MR805	--GCCTGAC- -GTGAGCCTC ATGCCG---- ---CTGTGTT CATGG---CG --
	GACCA TGATGATTCT TGACTCCC
MR815	--GCCTGAC- -GTGAGCCTC CTGCCC---- ---TTGTGTT CATTG---CG ---
	GACCA TGATGATTCT TGACTCCC
MR818	--GCCTGAC- -GTGAGCCTC CTGCCG---- ---CTGTGTT CATTG---CG ---
	GACCA TGATGATTCT TGACTCCC

-----CGATA TATTGT---- CTATTGAGGT GCTACTACC- -----

---CGATA TCTTGT---- CTATTCCGCT GCTACTACC- -----

----CGACA TCTTGT---- CTATTCAGGA GCTACTACC- -----

---CGATA TCTTGT---- CTATTCAGGT GCTACTACC- -----

---CGATA TCTTGA---- CTATTCAGGT GCTACTACC- -----

---CGATA TCTTGT---- CTATTCAGGT GCTACTACC- -----

---CGATA TCTTGT---- CTATTCAGGT GCTACTACC- -----

MUSCLE Multiple sequence alignment of sequences from cycle 11 chosen sequences are in darkened columns

Sequence	MUSCLE Sequence alignment
	GCCAGACGAGAAT-AAGCATG-
MR18	AGCTTGTGTTCATTGCGCGATATATTGTATATTGAAGTGCTACTACCGAGCATGATGATTCTTGTCTCCC
	GCCA----AGAAT-AAGCATG---
MR01	ATTGTGTTCATGGCGCGATATCTTGAATATTGAGCTGCTACTACCGAGCATGATGATTCTTGACTCCC
	GCCAGACGTGAG--CCTCATG-CCGCTGTGTTCATT-
MR14	CGCGATATCTTGACTATTCAGGTGCTACTACCGACCATGATGATTCTTGTCTCCC
	GCCAGACGAGAA--CCTCCTG-
MR06	CCGCTGTGTTCATTGCGCGATATCTTGTCTATTCAGGTGCTACTACCGACCATGATGATTCTTGACTCCC
	GCCAGACGAGAGTACTGCATGACCCCTGTGTTCATTGCGCGATATCTTGTCTATTCAGGTGCTACTACCGAGCATGATGATTCTT
MR15	GACTCCC
	GCCAGACGAGAG--CCTCATG-CC-
MR19	TTGTGTTCATTGCGCGATATCTTGTCTATTCAGGTGCTACTACCGACCATGATGATTCTTGACTCCC
	GCCAGACGAGAG--CCTCATG-
MR02	CCGCTGTGTTCATTGCGCGATATCTTGTCTATTCAGGTGCTACTACCGAGCATGATGATTCTTGACTCCC
	GCCAGACGTGAG--CCTCATG-
MR10	CCGCTGTGTTCATTGCGCGATATCTTGTCTATTCAGGTGCTACTACCGACCATGATGATTCTTGACTCCC
	GCCAGACGAGAG--CCTCATG-
MR05	CCGCTGTGTTCATTGCGCGATATCTTGTCTATTCAGGTGCTACTACCGACCATGATGATTCTTGACTCCC
	GCCAGACGAGAG--CCTCATG-
MR07	CCGCTGTGTTCATTGCGCGATATCTTGTCTATTCAGGTGCTACTACCGACCATGATGATTCTTGACTCCC
	GCCAGACGAGAG--CCTCATG-
MR11	AGCTTGTGTTCATTGCGCGATATCTTGTCTATTGAGGTGCTACTACCGACCATGATGATTCTTGACTCCC
	GCCAGACGTGAG--CCTCATG-
MR13	TGCTTGTGTTCATTGCGCGATATCTTGTCTATTCAGGTGCTACTACCGACCATGATGATTCTTGACTCCC
	GCCAGACGTGAAT-AAGC-TG-
MR16	CCGCTGTGTTCATGGCGCGATATCTTGTCTATTGAGGTGCTACTACCGACCATGATGATTCTTGACTCCC
	GCCAGACGTGAAT-AAGCATG-
MR20	CCGCTGTGTTCATTGCGCGATATCTTGACTATTCAGGAGCTACTACCGACCATGATGATTCTTGACTCCC
	GCCAGACGAGAAT-AAGCATG-
MR03	CCGCTGTGTTCATGGCGCGATATCTTGTCTATTCAGGTGCTACTACCGAGCATGATGATTCTTGACTCCC

	GCCAGACGTGAAT-AAGC-TG-
MR04	CCGCTGTGTTCATTGCGCGATATCTTGTCTATTCAGGTGCTACTACCGACCATGATGATTCTTGACTCCC
	GCCAGACGAGAAT-AAGCATG-
MR12	CCGCTGTGTTCATTGCGCGATATCTTGCCTATTCAGGTGCTACTACCGACCATGATGATTCTTGACTCCC
	GCCAGACGAGAAT-AAGCATG-
MR17	CCGCTGTGTTCATTGCGCGATATCTTGTCTATTCAGGTGCTACTACCGACCATGATGATTCTTGACTCCC
	GCCA-ACGAGAAT-AAGC-TG-
MR08	CCCTTGTGTTCATTGCGCGATATCTTGTCTATTGAGGTGCTACTACCGAGCATGATGATTCTTGACTCCC
	GCCAGACGAGAAT-AAGC-TG-
MR09	AACTTGTGTTCATGGCGCGATATCTTGTCTATTGAGGTGCTACTACCGACCATGATGATTCTTGACTCCC